UNIVERSITY OF THE
WITWATERSRAND,
JOHANNESBURG

Redescription and new material of the Triassic cynodont *Cistecynodon parvus* and reassessment of its phylogeny

Erin S. Lund (2281922) (ORCID number: 0000-0002-6290-6081)

A research proposal submitted in fulfilment of Master of Science in Palaeontology to the Faculty of Science at the University of the Witwatersrand, Johannesburg.

Supervisors: Assoc. Prof. Julien Benoit, Dr. Frederik Wolvaardt and Prof. Roger Smith

Acknowledgments: PAST Africa, National Research Foundation (NRF), Evolutionary Studies Institute (University of the Witwatersrand)

PLAGIARISM DECLARATION

SENATE PLAGIARISM POLICY: APPENDIX ONE

I, Erin Shawn Lund (Student number: 228 1922) am a student registered for the degree of Master of Science in Palaeontology in the academic year 2023-2024. I hereby declare the following:

1. I am aware that plagiarism (the use of someone else's work without their permission and/or without acknowledging the original source) is wrong.
2. I confirm that the work submitted for assessment for the above degree is my own unaided work except where I have explicitly indicated otherwise.
3. I have followed the required conventions in referencing the thoughts and ideas of others.
4. I understand that the University of the Witwatersrand may take disciplinary action against me if there is a belief that this is not my own unaided work or that I have failed to acknowledge the source of the ideas or words in my writing.
5. I have included as an appendix a report from "Turnitin" (or other approved plagiarism detection) software indicating the level of plagiarism in my research document.

Signature:  **Date: ___13/01/2025_____**

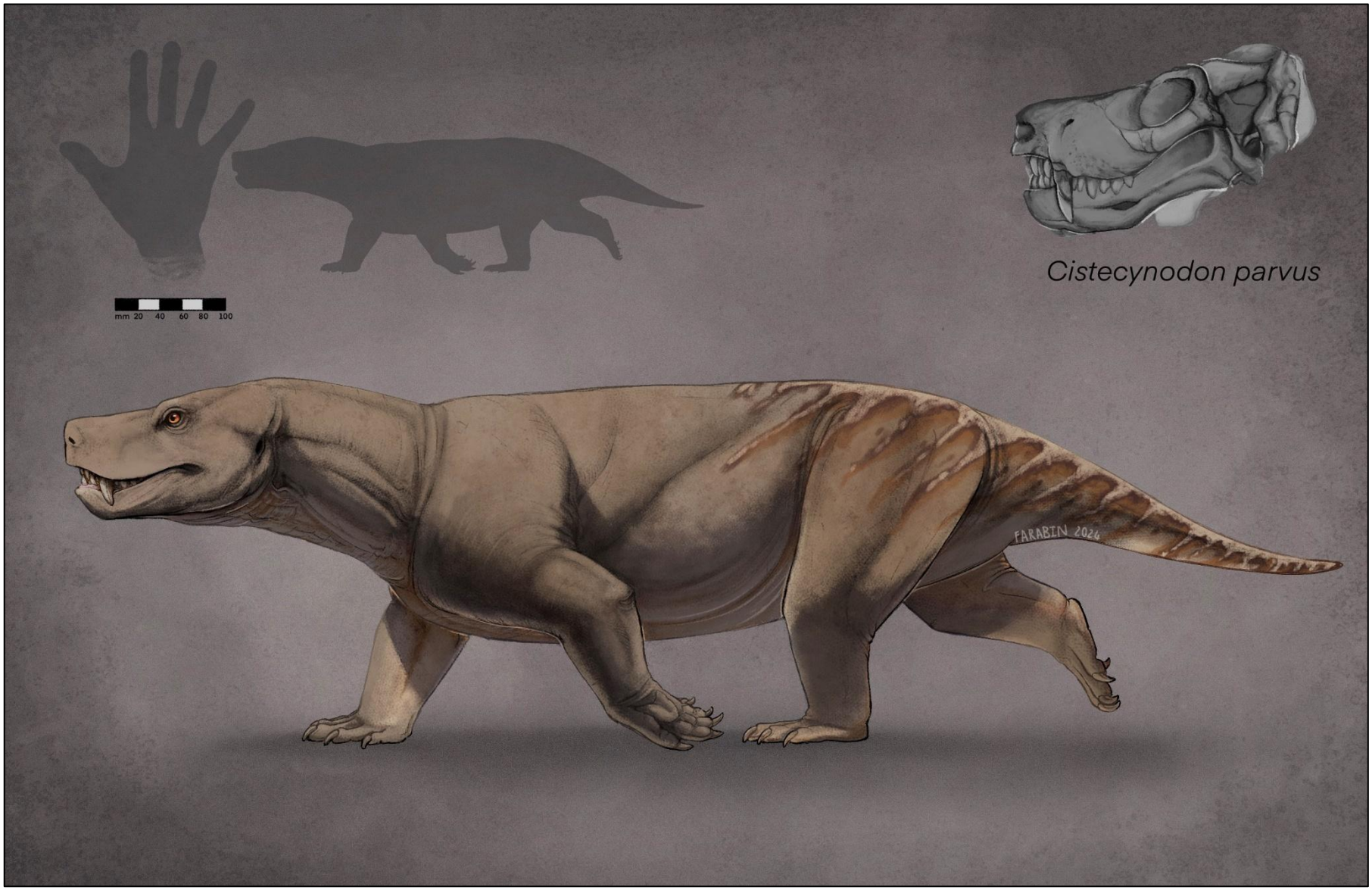

Palaeoartist reconstruction of *Cistecynodon parvus*. Artist: Morgan Hopf.

Table of Contents

Abstract

Cynodonts are an important clade of non-mammaliaform therapsid that first occur in the late Permian and include the subclade Mammaliaformes, the latter ultimately giving rise to modern mammals. The systematics of non-mammaliaform cynodonts has been extensively studied and is relatively well-resolved, however, there are still many problematic taxa that are difficult to identify and place confidently into the cynodont phylogenetic tree. *Cistecynodon parvus* is one such taxon, known only from a single specimen, the holotype skull, which was found in the Middle Triassic Burgersdorp Formation of South Africa, in strata assigned to the *Trirachodon – Kannemeyeria* Subzone of the *Cynognathus* Assemblage Zone. Over the past century *Cistecynodon* has been variously referred to the Probainognathia, Cynognathia, and non-eucynodont cynodonts, without any emerging consensus. Recently, a new specimen possibly referrable to this genus has been discovered on the farm Lemoenfontein, within the same subzone. Here the holotype of *Cistecynodon parvus* and the new specimen are described using CT scans of the skulls to produce 3D models. This new data is used to score a phylogenetic matrix which supports that *Cistecynodon parvus* is a basal, non-eucynodont. This basal position reflects on the anatomy of its secondary palate, which is not closed despite the specimen being a subadult. The inner ear, trigeminal canal, parietal foramen and carotid foramina are uniquely derived, likely as adaptations to an obligate fossorial lifestyle, confirming the validity of the taxon and its subterranean ecology. The new specimen from Lemoenfontein is found to be closely related, but clearly distinct from *Cistecynodon*, and thus likely represents a new species of early Middle Triassic cynodont.

Introduction

Cynodontia is a major clade of non-mammalian therapsids that appeared during the late Permian and comprised a substantial and diverse quantity of the tetrapod fauna during the Triassic (Kemp 1982; Battail 2001; Abdala & Ribeiro 2010). Cynodontia includes the subclade Mammaliaformes (Kemp 1982; Rubidge & Sidor 2001; Botha *et al.* 2007) making this order crucial for evaluating the origin of mammals. Triassic cynodonts are divided into two suborders: the Cynognathia and Probainognathia (Martinelli & Soares 2016). Cynognathia is the most diverse of the two suborders in Triassic rocks, but they decline in number and diversity by the end of the Middle Triassic and eventually become extinct during the Norian, 227 to 208.5 million years ago (Gradstein *et al.* 2004; Brack *et al.* 2005; Lukic-Walther *et al.* 2019). The Probainognathia is the clade that gave rise to the Mammaliaformes (Martinelli & Soares 2016; Abdala 2019).

The systematics of non-mammaliaform cynodonts is one of the best studied among early therapsids and their phylogeny is well resolved and supported (Ruta *et al.* 2013; Benoit *et al.* 2022a; Gaetano *et al.* 2022; Fonseca *et al.* 2024; Pusch *et al.* 2024). Despite this, some controversial taxa such as *Cistecynodon parvus* (Fig. 1) have been overlooked by recent researchers, in most part because they are rare and notoriously difficult to classify. *Cistecynodon* is known from a single specimen, the holotype skull (BP/1/2520), which was found at Luiperdkop in the Joe Gqabi District, Eastern Cape, South Africa, in strata of the Burgersdorp Formation (Tarkastad Subgroup, Karoo Supergroup) (Brink & Kitching 1953). The specimen was discovered in a grey horizon which Brink and Kitching (1953) identified as the middle of the *Cynognathus* Zone. This is suggestive of its position in the middle Burgersdorp Formation, in the Middle Triassic *Cynognathus* Assemblage Zone (Abdala & Ribeiro 2010; Smith *et al.* 2020), which dates to roughly 247.2 - 243.53 million years ago (Liu *et al.* 2017; Hancox *et al.* 2020).

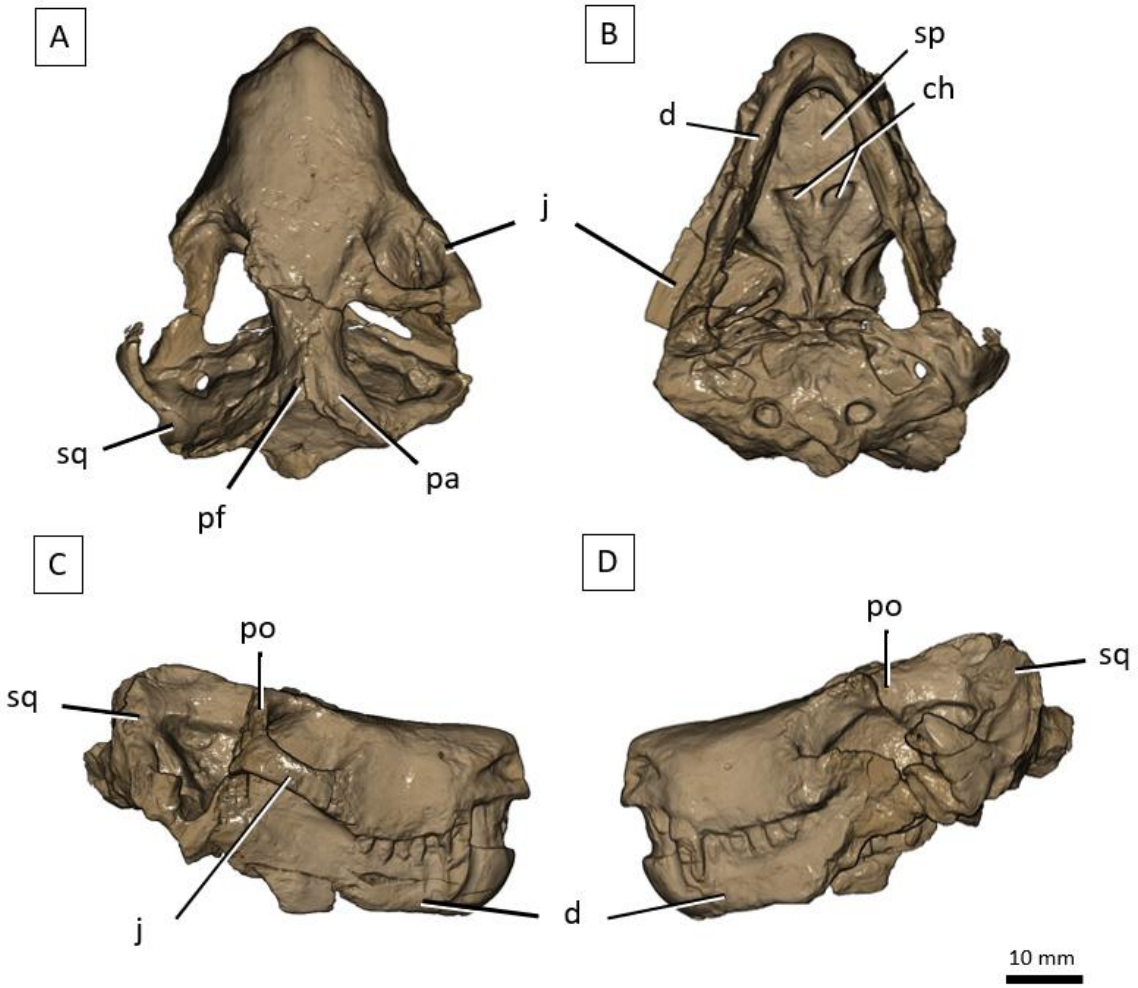

Figure 1: 3D reconstruction of the skull of specimen BP/1/2520 in dorsal (A), ventral (B), right lateral (C) and left lateral (D) view. Abbreviations: ch, choanae; d, dentary; j, jugal; pa, parietal; pf, parietal foramen; po, postorbital; sp, secondary palate; sq, squamosal.

The specimen was originally considered by Brink and Kitching (1953) to represent a new family of cynodonts. Since its discovery, *Cistecynodon* has been referred to Chiniquodontidae (a family of the Probainognathia) (Battail 1991a), juvenile *Cynognathus* (a genus of Cynognathia) (Hopson & Kitching 1972), and a non-eucynodont (neither a cynognathian nor a probainognathian) (Tatarinov 1974; Abdala 1995, 1996). Brink and Kitching (1953) hypothesised *Cistecynodon* to be a new family among cynodonts because the palatine does not contribute to the secondary bony palate at its posterior end. The palatine bone not contributing to the secondary palate suggests that *Cistecynodon* is more likely to be a non-eucynodont (following Tatarinov 1974; Abdala 1995, 1996). Battail (1991a, 1991b)

referred *Cistecynodon* to chiniquodontids because of the presence of a 'long' secondary palate and the dorsal position of the zygomatic arch compared to the position of the alveolar edge of the maxilla. This classification has been challenged by Hopson (1991), noting that the secondary palate is not as long as in other chiniquodontids. Abdala (1996) notes the absence of a parietal foramen and used this trait, among others (presence of a descending jugal arch, well-developed squamosal groove, and a thin postorbital bar), to exclude *Cistecynodon* from the cynognathians. The presence of a parietal foramen was later noted in *Cistecynodon* using CT scanning (Benoit *et al.* 2022a). These differing conclusions are just some of the many made over the years (see Table 1), illustrating how notoriously difficult it has been to classify *Cistecynodon*.

Table 1: Differing hypotheses about the classification of *Cistecynodon* by various authors during the 20th century.

Publications	Family (and subfamily)	Genus
Brink & Kitching (1953)	New family of cynodonts	*Cistecynodon*
Watson & Romer (1956)	Bauriamorpha	*Cistecynodon*
Lehman (1961)	Cynognathidae	*Cistecynodon*
Hopson & Kitching (1972)	Cynognathidae	Juvenile *Cynognathus* Synonymous with *Cynognathus crateronotus*
Tatarinov (1974)	Galesauridae Subfamily: Cistecynodontinae	*Cistecynodon* (Subfamily includes *Sinognathus*)
Battail (1991a)	Chiniquodontidae	*Cistecynodon*
Abdala (1995, 1996)	Neither a cynognathid nor probainognathid (non-eucynodont cynodont)	*Cistecynodon*

Additionally, a new cynodont specimen (SAM-PK-K11655) (Fig. 2) was recently discovered at roughly the same stratigraphic level as the holotype of *Cistecynodon* on the farm Lemoenfontein 44 in the Free State of South Africa (Wolvaardt *et al.* 2023). Wolvaardt *et al.* (2023) compare the new cynodont specimen with *Lumkuia fuzzi* (the most primitive probainognathian cynodont), *Bolotridon* and *Cistecynodon*, but they could not identify it with confidence. The specimen differs from *Lumkuia* by the presence of a shorter secondary palate, the presence of a parietal foramen and non-hooked cusps on the postcanine teeth, and from *Bolotridon* by its significantly smaller size and the fewer number of postcanine teeth (Wolvaardt *et al.* 2023). An identification as *Cistecynodon* thus remains open pending digital preparation using CT scanning to assess this possibility.

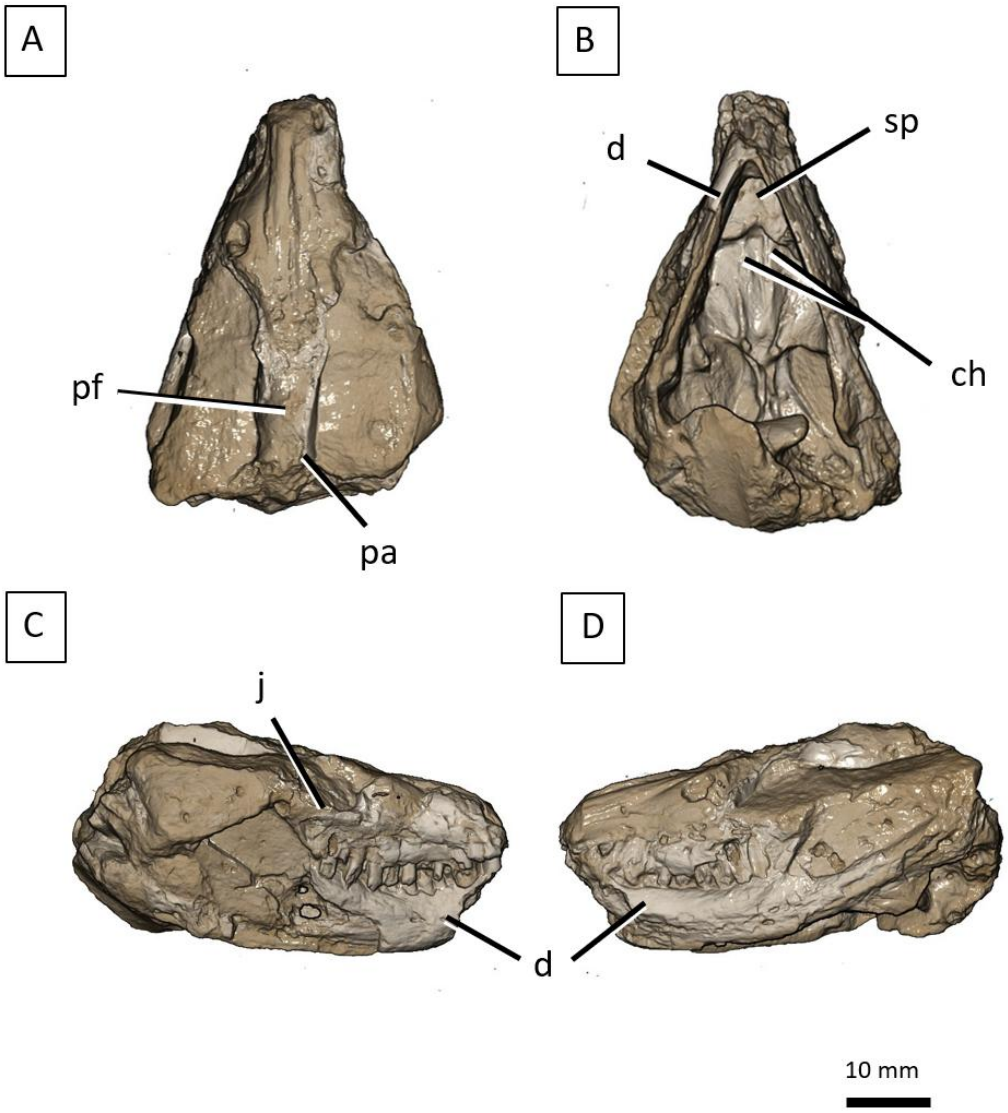

Figure 2: Preliminary CT scan images of the skull of specimen SAM-PK-K11655 in dorsal (A), ventral (B), right lateral (C) and left lateral (D) view. Abbreviations: ch, choanae; d, dentary; j, jugal; pa, parietal; pf, parietal foramen; sp, secondary palate.

Since the original description of the holotype specimen, there has been no formal reassessment of the morphology and anatomy of *Cistecynodon parvus*. The literature is tenuous (Brink & Kitching 1953; Watson & Romer 1956; Lehman 1961; Hopson & Kitching 1972; Tatarinov 1974; Battail 1991a; Abdala 1995, 1996), often anecdotally mentioning *Cistecynodon* without placing it at the centre of the research. Moreover, none of the above have been included in a phylogenetic analysis. A proper re-

assessment of the anatomy and systematic positioning using state-of-the-art scanning technology and including the two specimens in a phylogenetic analysis is warranted.

Recently, micro-computed tomography (CT) scanning and bone-by-bone three-dimensional reconstructions of the skulls and post-crania of various cynodonts have allowed for more in-depth observations of their anatomy and morphology, thereby providing crucial information to clarify the phylogenetic positioning of taxa (e.g., Pusch *et al.* 2021; Benoit *et al.* 2022a). CT scanning enables access to the internal anatomy of fossils which are now being used to add new characters into current cynodont phylogenetic analyses (i.e., Benoit *et al.* 2022a; Fonseca *et al.* 2024; Pusch *et al.* 2024) to improve upon the knowledge of the relationships between cynodonts and the evolution toward the mammalian condition.

Here I present a re-description of the holotype specimen of *Cistecynodon parvus* and assess the new cynodont specimen from Lemoenfontein 44 (SAM-PK-K11655) using CT scans to produce highly detailed three-dimensional models of the skull and lower jaw. This has enabled proper identification of the new specimen and has provided access to previously “out-of-reach” internal cranial characters (inner ear, trigeminal canals, endocranial cast etc.) that are used to update pre-existing phylogenetic matrices in order to re-assess the systematic and phylogenetic position of *Cistecynodon parvus.*

Material and Methods

Institutional abbreviations

BP, Evolutionary Studies Institute (formerly Bernhard Price Institute for Palaeontological Research), of the University of the Witwatersrand, Johannesburg, South Africa; SAM, Iziko South African Museum, Cape Town, South Africa.

Geological setting

Both specimens come from the Early Anisian, middle Burgersdorp Formation (Beaufort Group) of South Africa.

Specimen BP/1/2520

Specimen BP/1/2520 (museum reference number BP/1/318) was found in 1952 at Luiperdkop (or Luiperdskop) (Fig. 3C), located west of the town Maletswai (formerly Aliwal North) in the Joe Gqabi District of the Eastern Cape Province of South Africa (Brink & Kitching 1953). Brink and Kitching (1953) and Kitching (1977) assigned the locality to the *Cynognathus* Zone based on the discovery of *Diademodon* and supposed stratigraphic correlation with the middle Burgersdorp Formation, which is Early to Middle Triassic (Hancox 1998). Based on Brink and Kitching's (1953) description of the Luiperdkop site as the "middle" Burgersdorp Formation, the holotype was inferred to have come from the *Trirachodon-Kannemeyeria* Subzone of the *Cynognathus* Assemblage Zone (AZ) (Hancox *et al.* 2020; Smith *et al.* 2020); however, the definitive chronostratigraphic age of this specimen has not been properly addressed.

In March 2024, fieldwork was conducted at Luiperdkop to reassess the geological age of the locality. Fieldwork consisted of surface collecting of fossils and logging the relevant information. The collected fauna includes cranial and postcranial material of kannemeyeriiform dicynodonts and of a possible specimen of *Cynognathus*, partial skulls of

trirachodontids and two bauriamorphs, a new and complete skull of *Kombuisia frerensis*, the large tibia of an erythrosuchid archosauromorph and fragments of amphibian skulls. The abundance and combination of the above-mentioned tetrapods supports that Luiperdkop exposes solely the *Trirachodon-Kannemeyeria* Subzone of the *Cynognathus* AZ. Additionally, the holotype of *Kombuisia* is from the lower-most part of the *Trirachodon-Kannemeyeria* Subzone (Fröbisch 2007; Hancox *et al.* 2020), therefore the discovery of a specimen of *Kombuisia* on Luiperdkop further confines the age of *Cistecynodon* to the oldest part of the *Trirachodon-Kannemeyeria* Subzone. To date there is no radiometric date for this subzone, but a Middle Triassic (Early Anisian) age of approximately 247.2 million years is generally accepted (Miller & Baranyi 2021).

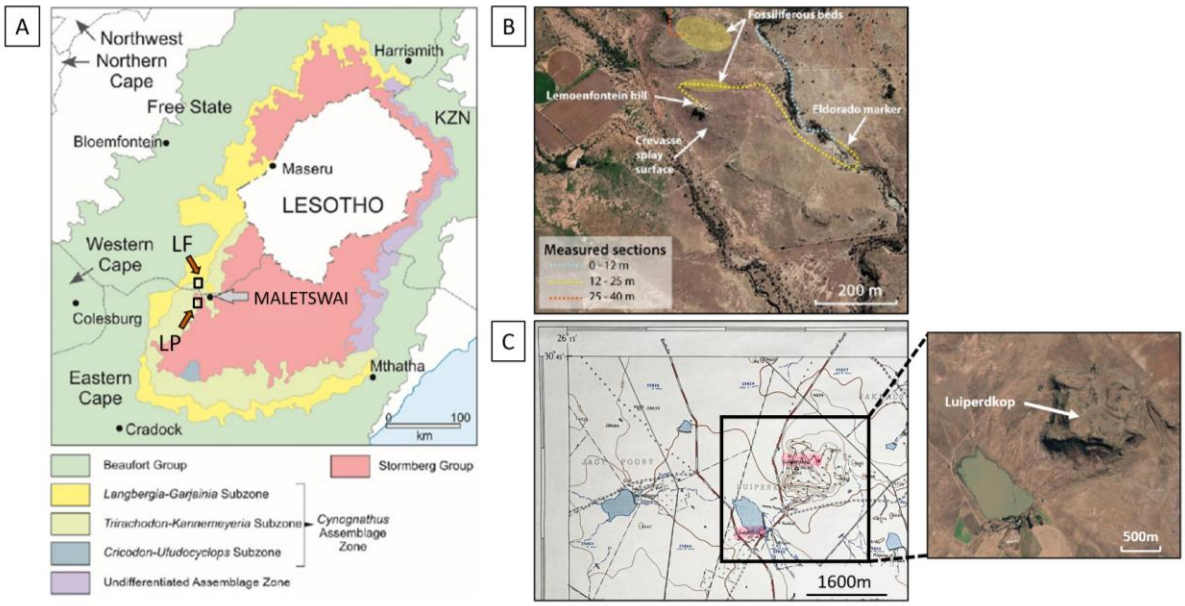

Figure 3: (A) Geographic location of Lemoenfontein 44 farm (LF) and Luiperdkop (LP) relative to the location of the Maletswai (Aliwal North) District in the Eastern Cape Province. (B) Satellite image of the Lemoenfontein 44 site (bone accumulation site marked in yellow). (C) Topographic map of the Luiperdkop site with enlarged satellite image (right). Image A and B modified from Wolvaardt, *et al*. (2023).

Specimen SAM-PK-K11655

Specimen SAM-PK-K11655 was discovered at Lemoenfontein 44 farm (Figs. 3B and 4) in the Xhariep (Rouxville) District of the Free State Province. Lemoenfontein 44 is roughly 14km north-west of the town of Maletswai, along the road to the town of Bethulie (Wolvaardt *et al.* 2023). This site is also located in the "middle" Burgersdorp Formation (Brink & Kitching 1953; Wolvaardt *et al.* 2023) in the same lower *Trirachodon-Kannemeyeria* Subzone as the Luiperdkop site (Hancox *et al.* 2020; Smith *et al.* 2020).

The Burgersdorp Formation is Early to Middle Triassic in age, with a thickness of up to 1000m in the southern-most areas (Johnson *et al.* 2006). This region consists of horizontally stratified mudrocks inter-bedded with layers of sandstone (Hancox 1998). An extensive study of the Burgersdorp Formation is reported in (Hancox 1998). Most of the Burgersdorp Formation was deposited by meandering rivers flowing in a northwesterly direction under a warm, arid to semi-arid climate (Hancox 1998). Suspension-load deposition on the floodplains during flood events is the primary accumulation method of the mudrocks in this formation. These depositional episodes resulted in a succession of ribbon-shaped channel sandstone bodies, tabular crevasse splay sandstone sheets and thick vertically accreted beds of pedogenically-modified overbank mudrocks (Hancox 1998; Neveling 2004). The overbank mudrocks consist primarily of siltstones and mudstones with a few sand-filled mudcracks and contain vertebrate and invertebrate burrows and other traces as well as numerous vertebrate body fossils.

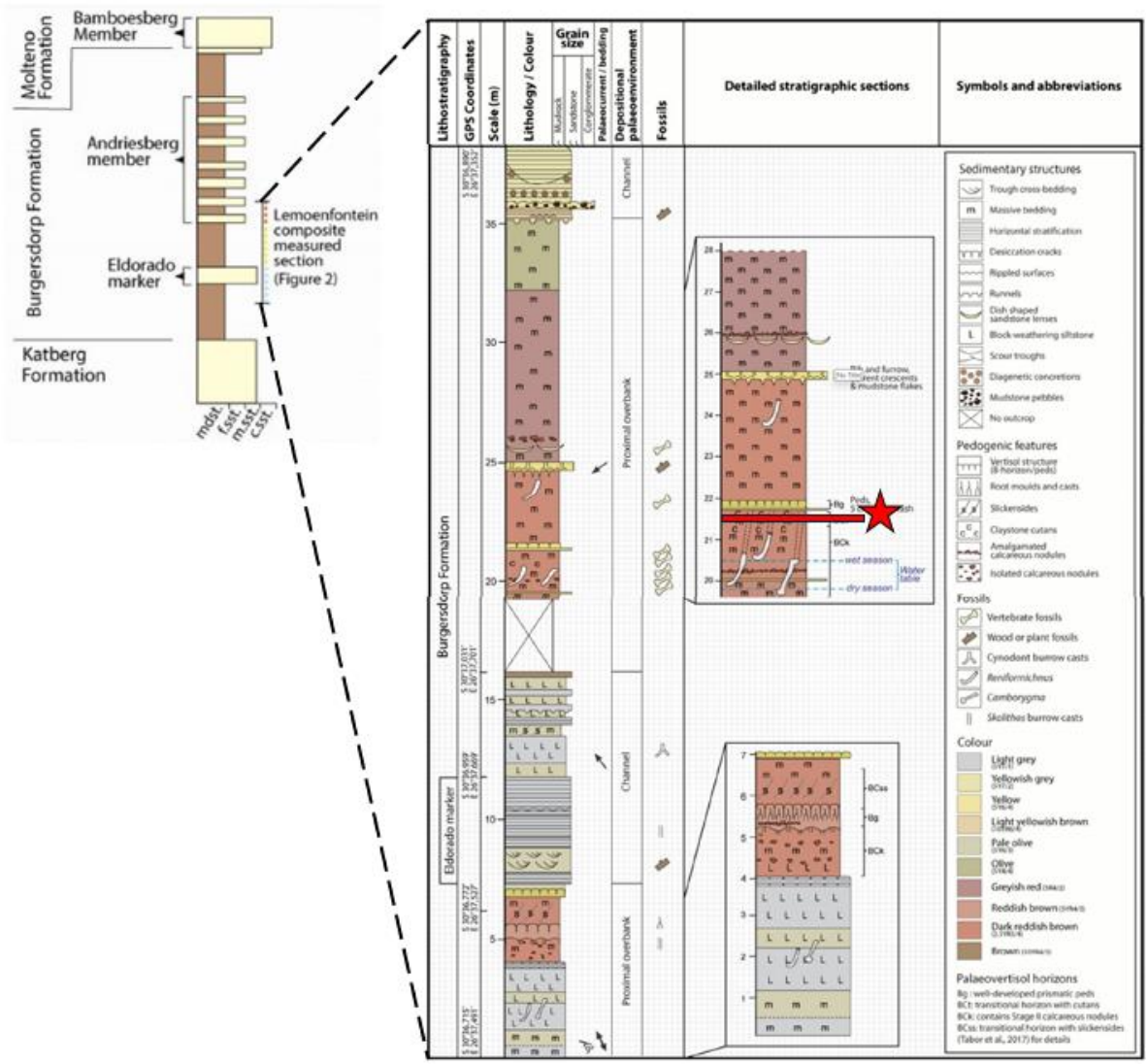

Figure 4: Diagrams of the geological structure and faunal content of the stratigraphical column at the Lemoenfontein 44 locality (modified from Wolvaardt, *et al.* 2023). The red line and star indicate the stratigraphic level (21.5 m) in which SAM-PK-K11655 was discovered on Lemoenfontein.

Computed Tomography scanning

The holotype skull (BP/1/2520) was CT scanned using the micro PET/CT scanner at NECSA and the new specimen SAM-PK-K11655 was scanned at the Evolutionary Studies Institute (ESI) at the University of the Witwatersrand. The NECSA scanner is a Nikon XTH 225 ST micro-focus X-ray tomography system

(Hoffman & De Beer 2012), and the ESI scanner is a Nikon Metrology XTH 225/320 LC dual source micro-CT system. Specimen BP/1/2520 was scanned with parameters for the isotopic voxel size (in mm) of 0.0562 and SAM-PK-K11655 with size of 0.0308. The postcranial elements of SAM-PK-K11655 are disarticulated beneath the posterior end of the cranium, therefore these bones have been digitally reorganised using the software programme Blender 3.6 to their approximate hypothesised anatomical positions for description.

The programme Avizo Lite 9.0.0 (Hillsboro, FEI SAS 2015) was used to segment out the skulls of both specimens and create 3D models from the CT images. Avizo Lite 9.0.0 was also used to reconstruct the brain endocast and inner ear and take measurements of various anatomical features in both specimens. The anatomical and morphological characteristics of these elements was described bone-by-bone following the example of Pusch *et al.* (2019, 2021, 2024). Anatomical comparisons with other cynodonts with sectorial teeth (i.e., *Cynognathus*, *Thrinaxodon*, *Nythosaurus*, *Procynosuchus*, *Lumkuia*, *Platycraniellus*, and *Galesaurus*, from the literature (Seeley 1895; Estes 1961; Fourie 1974; Kemp 1979; Hopson & Kitching 2001; Botha *et al.* 2007; Pusch *et al.* 2019, 2023; Norton *et al.* 2020; Benoit *et al.* 2022a) are used to address the validity and taxonomy of *Cistecynodon parvus*.

Phylogenetic analyses

The following non-mammalian cynodonts consisting of basal cynodonts, cynognathians and probainognathians are used for comparison. For this research, cynodonts are considered as the clade including *Charassognathus gracilis* (Botha *et al.* 2007), *Dvinia prima* (Ivakhnenko 2013) and *Procynosuchus delaharpeae* (Kemp 1979) and the epicynodonts. The epicynodonts included for comparison are: *Thrinaxodon liorhinus* (Parrington 1934; Estes 1961; Fourie 1974; Abdala *et al.* 2013; Crompton *et al.* 2015; Jasinoski *et al.* 2015), *Nanictosaurus kitchingi* (van Heerden & Rubidge, 1990), *Galesaurus planiceps* (Jenkins 1971; Butler *et al.* 2019; Pusch *et al.* 2019; Norton *et al.* 2020), *Progalesaurus lootsbergensis* (Sidor & Smith 2004), *Nythosaurus larvatus* (Pusch *et al.* 2023),

Cynosaurus suppostus (Van den Brand and Abdala 2018; Norton *et al*. 2021), *Vetusodon elikhulu* (Abdala *et al.* 2019), *Platycraniellus elegans* (Abdala 2007) and *Bolotridon frerensis* (Pusch *et al.* 2021). Eucynodonts included in the study are the cynognathians *Cynognathus crateronotus* (Seeley 1895; Abdala 1995, 1996; Abdala & Ribeiro 2010) and *Boreogomphodon jeffersoni* (Pusch *et al.* 2024), and the basal probainognathian *Lumkuia fuzzi* (Hopson & Kitching 2001; Benoit *et al.* 2022a).

New observations of *Cistecynodon* (BP/1/2520) and SAM-PK-K11655 are scored in the two most recent character matrices using the software Mesquite to assess the phylogenetic placement of these specimens: Pusch *et al.* (2024) and Fonseca *et al.* (2024). Pusch *et al.* (2024) used a matrix obtained from Huttenlocker & Sidor (2020) and added characters from other matrices (see Pusch *et al.* 2024). The matrix includes five therocephalian taxa (used as the outgroup) and seventeen cynodont taxa, with most of the dataset focused on early cynodonts. The null hypothesis for the phylogenetic position of BP/1/2520 and SAM-PK-K11655 is that both specimens are possibly basal cynodonts based on their palatal and simple dental morphology, therefore making the matrix of Pusch *et al.* (2024) appropriate. Furthermore, the matrix from Pusch *et al.* (2024) contains more endocranial characters than other matrices available in the literature. Some changes to this matrix were made for this research project. These include the addition of *Cynognathus crateronotus*, as BP/1/2520 was referred to *Cynognathus* by previous researchers (Lehman 1961; Hopson & Kitching 1972) and the addition of one new character: the presence or absence of carotid foramina on the ventral surface of the basisphenoid, as their loss is an important synapomorphy of the Cynognathia (Hopson & Kitching 2001). The Fonseca *et al.* (2024) matrix was updated by scoring BP/1/2520 and SAM-PK-K11655, with no further additions. Twenty four cynodont taxa were removed from the original Fonseca *et al*. (2024) matrix because they are not part of the focus group. The taxa that remain were selected as representatives of the different clades within Cynodontia for phylogenetic comparison with BP/1/2520 and SAM-PK-K11655. The taxa that were removed are as follows: *Pascualgnathus polanskii*, *Luangwa drysdalli*, *Massetognathus pascuali*, *Exaeretodon argentinus*, *Scalenodon angustifrons*, *Mandagomphodon hirschoni*, *Riojanodon nenoi*, specimen 'CRILAR Pv 567', *Cromptodon mamiferoides*, *Trucidocynodon riograndensis*,

Prozostrodon brasiliensis, *'Bonacynodon schultzi'*, *'Protheriodon estudianti'*, *'Agudotherium gassenae'*, *Therioherpeton cargnini*, *Riograndia guaibensis*, *Irajatherium hernandezi*, *Diarthrognathus broomi*, *Pachygenelus monus*, *Botucaraitherium belarminoi*, *Oligokyphus major*, *Bienotherium yunnanense*, *Adelobasileus cromptoni* and *Sinoconodon rigneyi*. Following the character scoring of the specimens in Mesquite, the nexus files were exported to TNT to conduct phylogenetic analyses. For each character matrix a traditional search was conducted with the parameters set as follows: the analysis was set for one hundred replicates, with one tree from each replication saved using the tree bisection reconnection (TBR) method. Following this, a consensus tree was constructed from the trees produced by the traditional search. A Bremer support analysis was then conducted on the consensus tree. Specimens BP/1/2520 and SAM-PK-K11655 were also scored in the matrix used in Benoit *et al.* (2022a), which is an updated version of the matrix by Gaetano *et al.* (2022). However, the result was a complete irresolution across Cynodontia, so it is not included in this research.

Results: Anatomical Descriptions

BP/1/2520 – *Cistecynodon* holotype

Overall preservation

Specimen BP/1/2520 preserves an almost complete skull with articulated lower jaw (Fig. 5). The skull length is 57.20 mm, measured from the anterior most point of the premaxilla to the posterior most point of the basioccipital. This differs from the length given by Brink and Kitching (1953) of 55 mm. The entire snout and complete secondary palate (including the premaxilla, palatal region of the maxilla and palatine, and the vomer) are well preserved. The secondary palate of *Cistecynodon* is 20.26 mm long and extends posteriorly to the level of the fifth postcanine. This differs from the description in Abdala (1996) in which the secondary palate is said to extend to the level of the fourth postcanine only. The secondary palate is not closed medially, as in *Nanictosaurus* (van Heerden & Rubidge (1990) but see Pusch *et al*. 2024), *Galesaurus* (Pusch *et al.* 2019), *Nythosaurus* (Pusch *et al.* 2023), and the Permian cynodonts *Dvinia*, *Procynosuchus* and *Abdalodon* (Tatarinov 1974; Kemp 1979; Hopson & Kitching 2001; Ivakhnenko 2013; Kammerer 2016; Pusch *et al.* 2019). The most stemward presence of a definite complete secondary palate in Cynodontia remains that of *Thrinaxodon* (Fourie 1974; Hopson 1991; Crompton *et al*. 2015, 2017) and is retained in all crownward cynodonts (Hopson & Kitching 2001).

The anterior most region of the top of the snout is damaged due to post-burial weathering; however, most of the left septomaxilla and a fragment of the right one are preserved. The frontal, nasal, prefrontal, and lacrimal are almost entirely preserved on both sides. Most of the right jugal is

preserved but only a fragment of the left one remains. The pterygoid bones are completely preserved. Only the ventral half of the left and right epipterygoid are present. Small ectopterygoids are preserved ventrolaterally to the palatine, like in *Galesaurus*, *Thrinaxodon*, *Nythosaurus* (Parrington 1934; Pusch *et al.* 2019, 2023). Both parietal bones are preserved, and a small parietal foramen is visible. Both postorbital bones are present, however the lateral projection of the postorbital is damaged on the right side and missing on the left side (Fig. 5). The parabasisphenoid, basioccipital (including exoccipitals), prootic and opisthotic bones are mostly complete. The squamosal bones are present, with the left squamosal being better preserved than the right one. The occipital region including the tabular, supraoccipital and interparietal bones are preserved but due to weathering the suture lines between the interparietal and supraoccipital are difficult to assess. The complete dentary and fragments of the other postdentary bones of the lower jaw on both sides are preserved. On the right side, the right articular, surangular and right quadrate are well preserved in anatomical position.

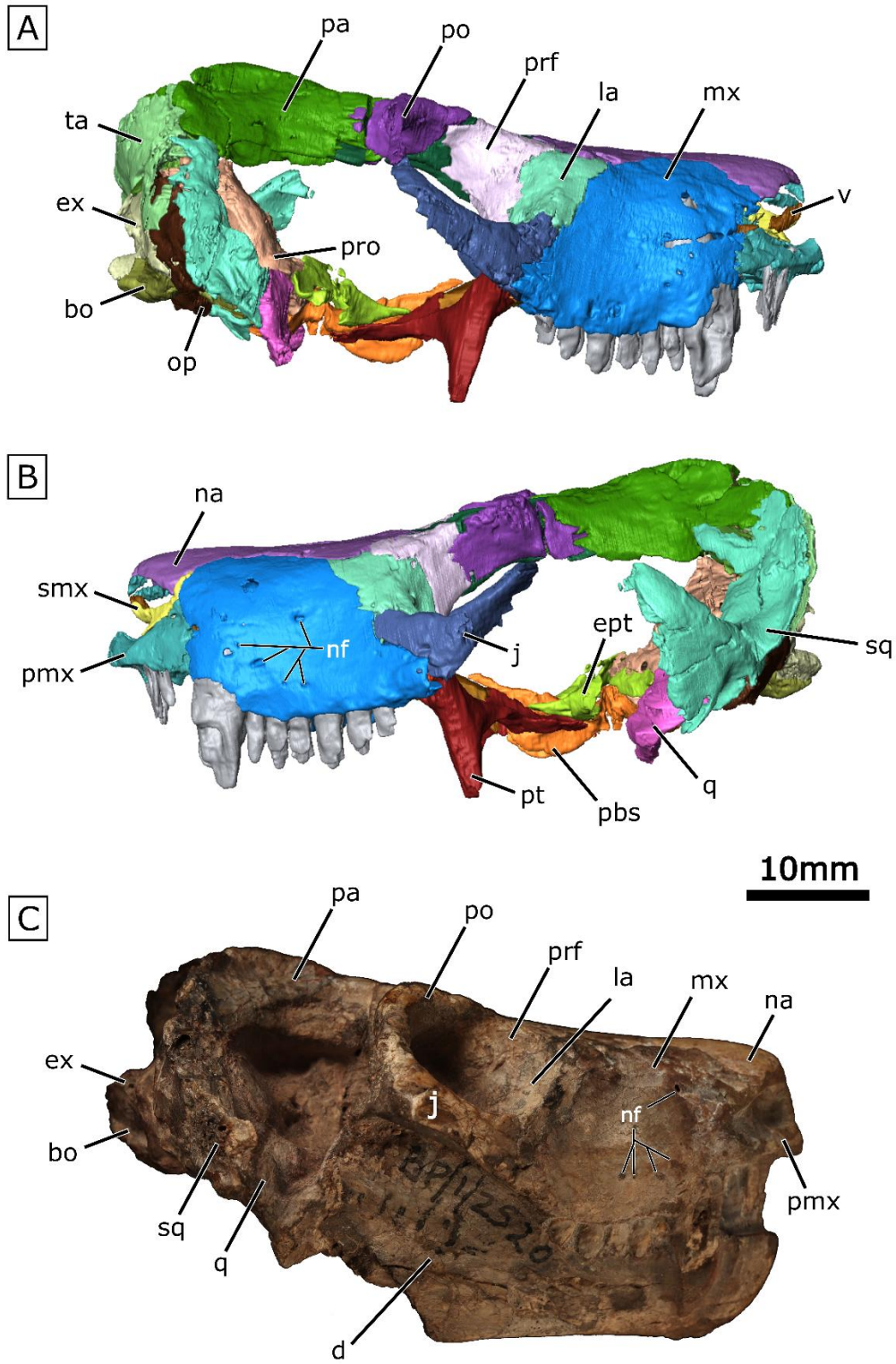

Figure 5: 3D digital reconstructions of the cranium of BP/1/2520 in (A) right lateral, (B) left lateral view. (C) specimen BP/1/2520 in right lateral view. Abbreviations: bo, basioccipital; d, dentary; ept, epipterygoid; ex, exoccipital; d, dentary; j, jugal; la, lacrimal; mx, maxilla; na, nasal; nf, nutrient

foramina; op, opisthotic; pa, parietal; pbs, parabasisphenoid; pmx, premaxilla; po, postorbital; prf, prefrontal; pro, prootic; pt, pterygoid; q, quadrate; smx, septomaxilla; sq, squamosal; ta, tabular; v, vomer.

Snout and secondary palate

The septomaxilla is a small bone of irregular outline situated anterodorsally to the premaxilla and on the anterolateral end of the snout (Fig. 6A). In BP/1/2520, the left septomaxilla is well preserved, but only a fragment of the lateral region of the right septomaxilla is preserved. The posterior most point of the septomaxilla contacts the anteromedial surface of the maxilla. In BP/1/2520, the septomaxilla does not appear to contact the nasal bone; however, at the anterior end of each bone there is a clear gap between the lateral margin of the nasal and medial margin of the maxilla, where the lateral process of the septomaxilla would have extended (Fig. 5B). This morphology is also seen in *Galesaurus* (Pusch *et al.* 2019). The footplate of the septomaxilla connects to the dorsolateral surface of the premaxilla. This footplate is fully preserved in the left septomaxilla and only a fragment of the right one is preserved. The footplate of the septomaxilla forms the inside wall of the nasal passage and floor of the external naris, as described in *Cynosaurus* (Van den Brandt & Abdala 2018). At the anterior most point, the septomaxillary footplate diverges into two narrow processes, assuming a V shape in dorsal view (Fig. 6A). There is a robust intranarial process septomaxilla which extends anteromedially. On the lateral surface of the snout the small septomaxillary foramen is located along the suture between the premaxilla and maxilla.

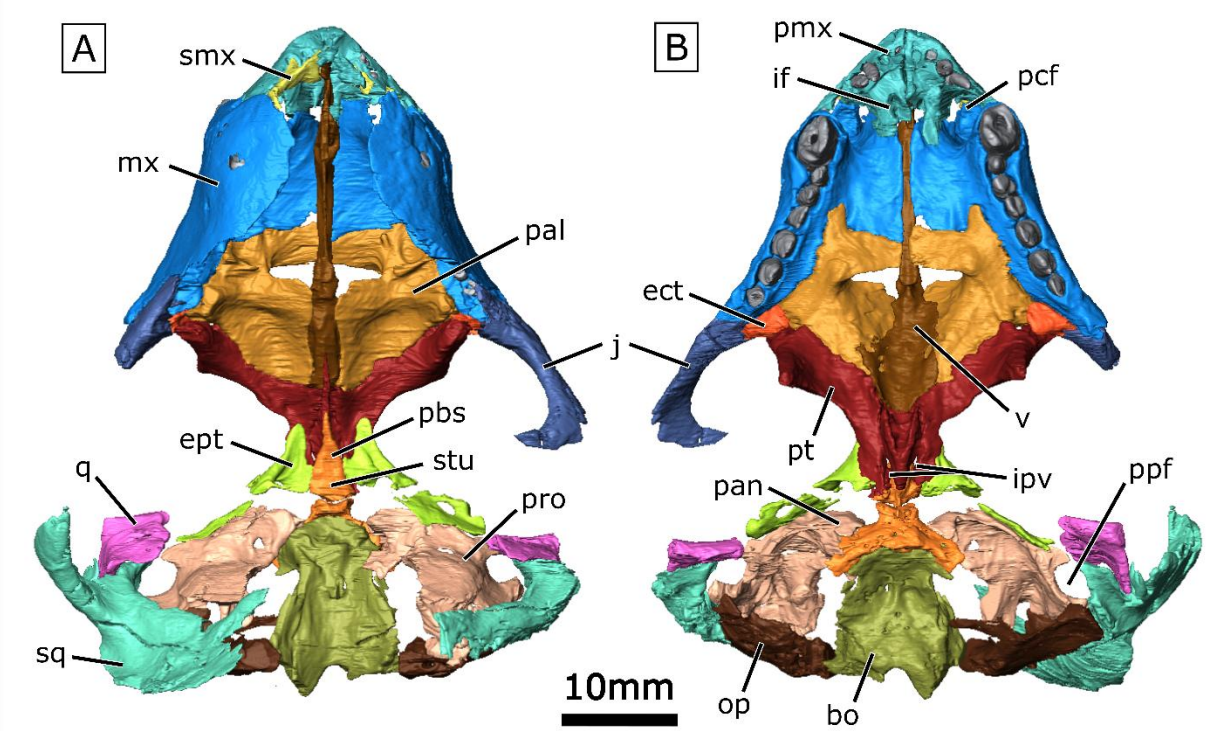

Figure 6: segmented palate and basicranium of BP/1/2520 in dorsal (left) and ventral (right) views. Abbreviations: bo, basioccipital; ect, ectopterygoid; ept, epipterygoid; if, incisive foramen; ipv, interpterygoid vacuity; j, jugal; mx, maxilla; op, opisthotic; pcf, paracanine fossa; pal, palatine; pan, pila antotica; pbs, parabasisphenoid; ppf, pterygoparoccipital foramen; pmx, premaxilla; pro, prootic; pt, pterygoid; q, quadrate; smx, septomaxilla; sq, squamosal; stu, sella turcica; v, vomer.

The premaxilla is a small, medially elongated bone at the anterior-most point of the snout. In BP/1/2520, it is damaged anteriorly and dorsally. Damage to the dorsal region of the premaxilla prevents observations of the morphology of the external nares, as only the anterior-most point of the prenasal processes of the premaxilla is preserved (Fig. 5). In other cynodonts, the dorsal extension of the premaxilla separates the two external nares from one another medially (Brink & Kitching 1953). In ventral view, the premaxilla of BP/1/2520 is 5.86 mm long in anteroposterior length. This accounts for 28,92% of the length of the secondary palate. An incisive foramen is located at the suture with the maxilla and premaxilla, medially. The two incisive foramina are fused, forming a heart shaped opening

in the secondary palate. The incisive foramina split the posterior end of premaxilla along the midline of the secondary palate (Fig. 6B). An incisive foramen is present in *Procynosuchus* (Kemp 1979), *Thrinaxodon* (Estes 1961), *Platycraniellus* (Abdala 2007), *Cynosaurus* (Van den Brandt & Abdala 2018), *Lumkuia* (Hopson & Kitching 2001). The posteromedial margin of the incisive foramen is not enclosed by the maxilla or premaxilla, thus resulting in an incomplete (posteriorly open) foramen. The premaxilla contributes the anterior and anterolateral margin of the paracanine fossa for the lower canines, with the posterior margin of the paracanine fossa formed by the maxilla. The paracanine fossa is large (3.31 mm wide and 4.41 mm in anteroposterior length) and located medially to the upper canine. There are four alveoli in the premaxilla on each side, housing narrow, elongated incisors. There is a small diastema between the last incisor and the canine (Fig. 6). This morphology is also seen in *Charassognathus*, *Dvinia* and *Procynosuchus* but is commonly absent in most cynodonts more crownward than these taxa (Botha *et al.* 2007).

The nasal bone is hourglass shaped in dorsal view. The anterior half of the nasal is narrower than the posterior half. Posteriorly, the nasal expands laterally until it contacts the lacrimal posterolaterally and the frontal and prefrontal posteromedially (Fig. 7A). There are no foramina on the dorsal surface of the nasal (Fig. 7A). There are nutrient foramina are present on the nasal of *Cynosaurus* (Van den Brandt & Abdala 2018). In ventral view the nasal is concave and smooth. A shallow fossa is visible ventrally, just posterior to the level of the paracanine fossa (Fig. 7B). A low median ridge runs along the midline of the ventral surface of the nasal. On either side of the median ridge there are weak lateral ridges that run parallel to it. The depressions between the median and lateral ridges would have housed the nasal turbinates, if present or cartilaginous. This morphology is also seen in a number of basal cynodonts including *Procynosuchus* (Kemp 1979), *Thrinaxodon* (Crompton *et al.* 2015), *Galesaurus* (Pusch *et al.* 2019) and *Bolotridon* (Pusch *et al.* 2021). The morphology differs in *Procynosuchus*, where the lateral ridges are prominent and sharp (Kemp 1979).

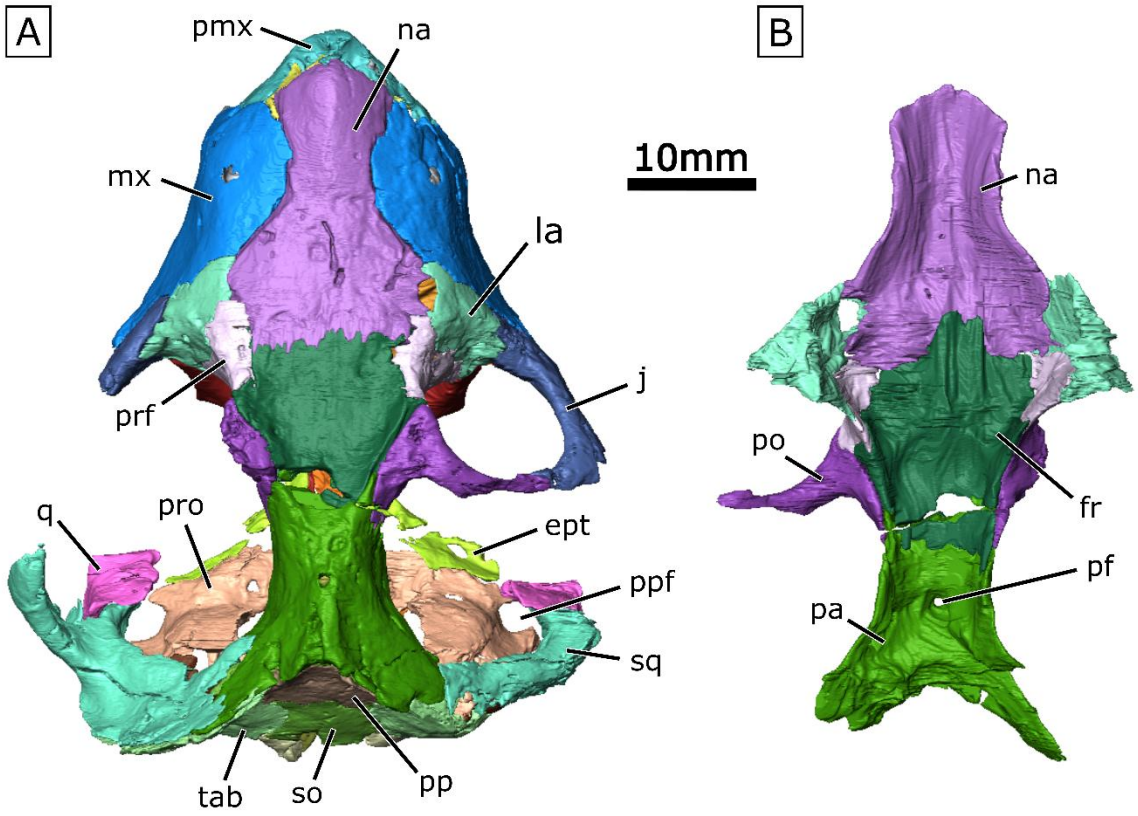

Figure 7: segmented skull of BP/1/2520 in (A) dorsal view and (B) skull roof in ventral view. Abbreviations: ept, epipterygoid; fr, frontal; j, jugal; la, lacrimal; mx, maxilla; na, nasal; pa, parietal; pf, parietal foramen; prf, prefrontal; po, post orbital; pmx, premaxilla; pp, postparietal; ppf, pterygoparoccipital foramen; pro, prootic; q, quadrate; so, supraoccipital; sq, squamosal; tab, tabular.

The maxilla of BP/1/2520 forms the majority of the lateral wall of the snout and extends posteriorly to level of the anterior margin of the orbit. The total length of the snout measures 18.46 mm from the anterior most point of the maxilla to the posterior contact with the jugal. At the level of the paracanine fossa, the snout is 20.96 mm wide. Posteriorly, at the level of the posterior margin of the secondary palate, it broadens further to 27.33 mm. The snout is short and wide, similar to *Cynosaurus* (Van den Brandt & Abdala 2018), but different compared to the laterally compressed snout of other basal cynodonts (i.e., *Platycraniellus* (Abdala 2007), *Thrinaxodon* (Brink 1954); *Galesaurus* (Pusch *et al.* 2019); *Cynognathus* (Abdala & Ribeiro 2010)). Ventrally, the maxilla sutures with the premaxilla

anteriorly and palatine posteriorly and posterolaterally to form the secondary palate (Fig. 6B). The palatal process of the maxilla is 11.82 mm long, which contributes 58,34% of the total length of the secondary palate. The palatal process is concave in dorsal view. As seen for the premaxillae, the paired processes do not meet medially. There are six postcanine teeth within the maxilla. There is no diastema present between the canines and postcanines. The palatal processes of the maxilla are convex in ventral view and extend posteriorly to the level of the third post canine (Fig. 6B). In lateral view, the maxilla is convex anteromedially at the level of the canines. The posterolateral surface of the maxilla extends to meet the jugal at the level of the anterior margin of the orbit, posterior to the last postcanine. There are many nutrient foramina present on the lateral surface of the snout. There are five foramina on the left side but only four foramina are preserved on the right side of the maxilla. On the left side, four of the foramina are arranged in a gentle arc, beginning at the level of the canine, and sloping posteroventrally to the level of the third postcanine. The fifth foramen is at the level of the third postcanine, but more dorsal, at the same horizontal level as the septomaxilla. The right maxilla shows the same pattern of foramina, however there are four foramina organised in an arc beginning at the level of the canine, instead of five. Weathering on the right side of the maxilla prevents the observation of any other foramina. A number of cynodonts show nutrient foramina on the maxilla (i.e., *Thrinaxodon* (Estes 1961), *Galesaurus* (Pusch *et al.* 2019), *Cynosaurus* (Van den Brandt & Abdala 2018), *Lumkuia* (Hopson & Kitching 2001) and *Cynognathus* (Seeley 1895)). The maxillary canal that connects these foramina internally is a relatively simple bony tube that runs parallel to the tooth row in the maxilla (Benoit *et al.* 2016a). The maxillary canal of BP/1/2520 has been extensively described in Benoit *et al*. (2024a) and thus will not be re-described in this analysis. However, it is important to note that the maxillary canal morphology in *Cistecynodon* is unique among cynodonts as there is a combination of plesiomorphic and derived features (see Benoit *et al.* 2024a). The maxillary canal extends posteriorly to meet the maxillary sinus (maxillary antrum); however, the shape and size of this sinus is difficult to delineate as there are no distinct ridges on the medial surface of the maxilla

that define its margins (Fig. 8). Overall, this sinus is rather shallow compared to other cynodonts (see Pusch *et al.* 2024).

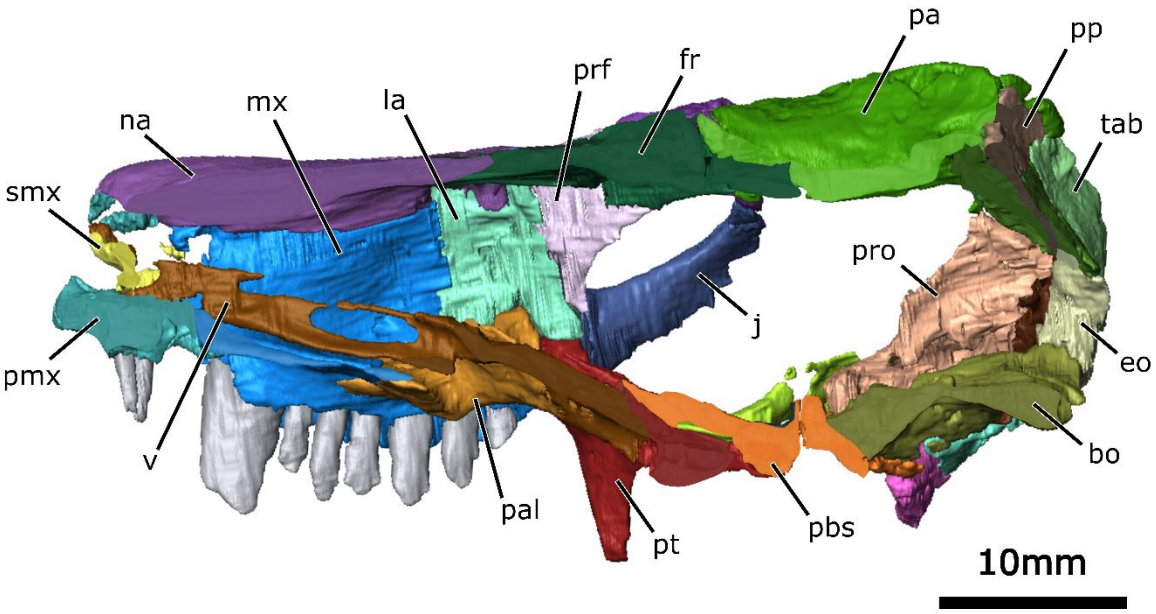

Figure 8: cross section of the palate of BP/1/2520 in right lateromedial view. Abbreviations: bo, basioccipital; ex, exoccipital; fr, frontal; j, jugal; la, lacrimal; mx, maxilla, na, nasal; pa, parietal; pal, palatine; pbs, parabasisphenoid; pmx, premaxilla; pp, postparietal; prf, prefrontal; pro, prootic; pt, pterygoid; mx, septomaxilla; tab, tabular; v, vomer.

The palatine of BP/1/2520 is a paired bone forming the posterior end of the secondary palate. It sutures posteriorly with the pterygoid, posterolaterally with the ectopterygoid, anteriorly and anterolaterally with the maxilla. In dorsal view, the medial palatal processes of the palatines are concave and do not contact each other along the midline. The palatal process of the palatine is 2.58 mm long, contributing only 12,73% of the secondary palate. This is contrary to the description by Brink and Kitching (1953) who argued that the palatine did not contribute at all to the secondary palate. Along the anterior border of each palatal process of the palatine, the bone extends a small triangular process anteriorly that separates the dental margin from the palatal process of the maxilla (Fig. 6).

There is no palatine foramen. The palatal process of the palatine extends anteroposteriorly from the level of the second to fourth postcanines. The palatine sutures with the small triangular ectopterygoid posterolaterally. Dorsally, the paired palatines suture medially with the posterior end of the vomer, to form the transverse lamina and form the roof of the primary choana. The secondary choana is dorsoventrally compressed, resulting in an elongated, narrow kidney bean shape.

The vomer is an anteroposteriorly elongated bone that runs along the midline of the snout. Anteriorly, the vomer is situated dorsally to the premaxillae, the palatal processes of the maxilla and the palatal processes of the palatine. Its anterior half is mediolaterally compressed, forming a vertical lamina. This vertical ridge extends dorsally toward the ventral surface of the nasal, thereby dividing the nasal cavity into two passages. Anteriorly, the lamina is rather tall as it occupies half the height of the nasal cavity while it gently slopes posteriorly, ultimately reaching only a quarter of the height of the cavity. In lateral view, there is a large ovoid foramen in the vertical process of the vomer, at the level of the second to fourth postcanines (Fig. 8). However, this structure is not seen in other cynodonts and is likely the result of erosion or taphonomical processes. Posteriorly, the posterior half of the vomer is horizontally flat, and mediolaterally expanded, and forms the roof of the posterior end of the nasal cavity and choanae (Figs. 6 and 8).

The pterygoid is an irregularly shaped bone, often described as somewhat butterfly-shaped in ventral view. In BP/1/2520, the pterygoid lacks this shape, as in dorsal view it is anteroposteriorly narrow, appearing as a widened U-shape (Fig. 6A). In lateral view, the transverse flange of the pterygoid is almost completely vertically oriented and dorsoventrally salient in lateral view (Figs. 5 and 8). In ventral view, the vertical orientation of the transverse flange means that it does not project slightly posteriorly, as in some other cynodonts, which would have given the butterfly shape (Fig. 6B). The ventral extension of the transverse flange reaches the ventromedial most margin of the coronoid process of the dentary. The surfaces of the left and right pterygoid are smooth. They are fused in the midline just ventral to the processus cultriformis of the parabasisphenoid. There are two small

interpterygoid vacuities present on either side of the parabasisphenoid in BP/1/2520 and visible in dorsal and ventral view (Fig. 6). In ventral view, the vacuities are visible as mediolaterally narrow openings, with the anterior margin formed by the pterygoid, the lateral and posterior margins formed by the epipterygoid, the medial margin formed by the processus cultriformis of the parabasisphenoid. Interpterygoid vacuities are present in adult specimens of *Dvinia* and *Procynosuchus* (Estes 1961; van Heerden & Rubidge 1990; Hopson & Kitching 2001; Ivakhnenko 2013). They are also present in specimens of *Thrinaxodon* (Estes 1961; Fourie 1974; Jasinoski *et al.* 2015), *Nanictosaurus* (van Heerden & Rubidge 1990), *Cynosaurus* (Van den Brandt & Abdala 2018) and *Lumkuia* (Hopson & Kitching 2001), however the specimens from these taxa are identified as juveniles or sub-adults. Since this structure is absent in adults of these taxa, this suggests an ontogenetic loss of these vacuities (Van den Brandt & Abdala 2018). Interpterygoid vacuities are absent in *Galesaurus* (Jasinoski & Abdala 2017; Butler *et al.* 2019). The quadrate ramus of the pterygoid is absent, a trait seen in eucynodonts rather than the basal cynodonts (Hopson & Kitching 2001).

The ectopterygoid is retained in *Cistecynodon*, as in *Galesaurus*, *Nythosaurus*, *Thrinaxodon, Platycraniellus*, *Cynosaurus* (Parrington 1934; Abdala 2007; Van den Brandt & Abdala 2018; Pusch *et al.* 2019). The ectopterygoid is absent in *Lumkuia* (Hopson & Kitching 2001). The ectopterygoid of BP/1/2520 is located laterally to the palatine at the suture with the maxilla and jugal. It is a small bone that is roughly triangular in dorsal and ventral view and is dorsoventrally compressed. A similar morphology is seen in *Nythosaurus* and *Galesaurus* which also have triangular ectopterygoids (Pusch *et al.* 2019, 2023), but in *Platycraniellus*, the ectopterygoid is quadrangular (Abdala 2007).

Circumorbital region

Only the anterior projection of the left jugal and most of the right jugal are preserved (Fig. 7). The jugal contacts the maxilla anteriorly and anterolaterally, and the lacrimal medially. The posterior projection of the jugal extends medially to contact the postorbital. The jugal is thick in lateral view, resulting in a

robust and prominent zygomatic arch. There is no distinct fossa on the medial surface of the jugal to indicate the attachment point for the master muscle. The zygomaticofacial foramen is present along the anterior margin of the jugal where it sutures with the maxilla. The jugal of BP/1/2520 is oriented quite obliquely in lateral view compared to other cynodonts such as *Thrinaxodon*, *Galesaurus* and *Lumkuia* in which it is more horizontal (Hopson & Kitching 2001; Pusch *et al.* 2019) (Fig. 5). This morphology is similar to that of *Cynognathus* and *Progalesaurus*, which gives the orbit an upward and more forward facing orientation (Seeley 1895; Sidor & Smith 2004).

Most of the left and right squamosal bones are preserved. In the left squamosal, the anterolateral projection which would contact the posterior margin of the jugal is preserved. It appears tubular in dorsal view (Fig. 7) and concave on its medial surface, whereas in lateral view it is triangular (Fig. 5). The right squamosal is damaged due to post burial weathering. The anterodorsolateral projection toward the jugal is not preserved; however, the anterolateral projection is partially preserved. The anterior margin flares out in a dorsoventral expansion. The dorsal point of the projection extends anterodorsally, and it appears that it would have met the jugal at the level halfway along the dorsoventral height of the orbit. In dorsal view, the squamosal sutures mediodorsally with the parietal, posterodorsally with the tabular, the opisthotic ventrally and the prootic anteroventrolaterally. The ventral region of the anterior projection is a relatively flat surface to accommodate articulation with the quadrate. In BP/1/2520 there is a deep groove in the shape of an inverted “V” on the ventrolateral side of the squamosal which accommodates the quadratojugal (Fig. 9). There is a deeply concave fossa on the anterior surface of the lateral projection of the squamosal which accommodates the quadrate.

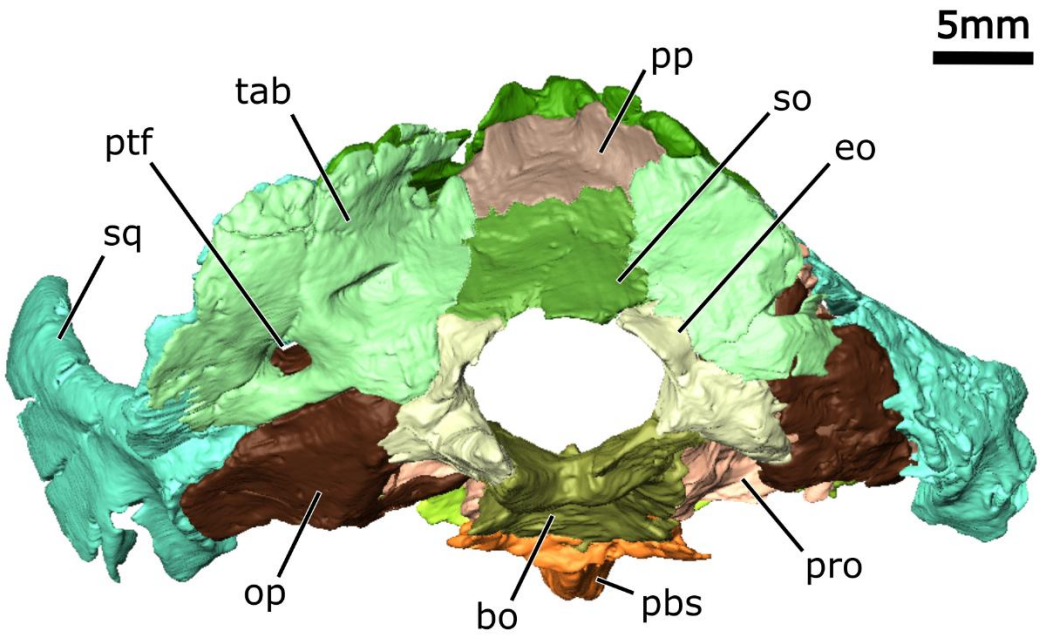

Figure 9: cranium of BP/1/2520 in occipital view. Abbreviations: bo, basioccipital; eo, exoccipital; op, opisthotic; pbs, parabasisphenoid; pp, postparietal; pro, prootic; ptf, post-temporal fenestra; so, supraoccipital; sq, squamosal; t, tabular.

The prefrontals of BP/1/2520 are small. The prefrontal is rhomboid in dorsal view, with the lateral surface of the bone being concave, contributing to the anteromedial margin of the orbit. The prefrontal contacts the nasal anteriorly, lacrimal laterally, frontal medially and postorbital posteriorly. In dorsal view, the prefrontal does not contact the postorbital as it is separated by a narrow triangular process of the frontal (Fig. 6). This process of the frontal which extends between the two bones does not contribute to the orbital rim (Fig. 6). Contribution of the frontal to the orbital wall is a derived trait seen in the probainognathians (except for *Lumkuia*) and crownward taxa (Hopson & Kitching 2001).

The left and right frontal bones of BP/1/2520 are complete. The frontal has a broad suture contact with the nasal anteriorly, prefrontal anterolaterally, postorbital posterolaterally and the parietal posteriorly. It appears as an inverted triangle in dorsal view, with indentations in the anterolateral regions where the prefrontal extends medially. The frontal is dorsoventrally flat but slopes dorsally at its posterolateral margin, where it contacts the postorbital. This results in a prominent diagonal ridge

being formed at the suture between the frontal and postorbital. The suture between the frontal and parietal is damaged by a crack, thus preventing its description; however, it seems that the frontal would have extended posteriorly in a V shape into the anterior margin of the parietal. The frontal extends as a triangular process between the prefrontal and postorbital in dorsal view but does not contribute to the margin of the orbit. In ventral view, the posterior half of the frontal is smooth, and excavated by a pair of shallow depressions located at the level of the suture with the postorbital . These depressions would have housed the olfactory bulbs (Fig. 7). Anteriorly, the frontal expands laterally. It bears a pair of prominent longitudinal ridges, one medial and the other more lateral. The ridges may be slightly offset from the midline due to deformation. These ridges extend onto the nasal bone anteriorly, and thus correspond to what is commonly identified as the ridges for the nasal (or olfactory) turbinates in other cynodonts (Hillenius 1994, 2000).

Both lacrimal bones are preserved. The lacrimal is a pentagonal bone in dorsal view and makes up about one third of the anterior margin of the orbit. The lacrimal contacts the maxilla anteriorly, jugal laterally, and the nasal anterodorsomedially. The lacrimal sutures with the lateral margin of the prefrontal, forming the anteromedial rim of the orbit. The ventral edge of the lacrimal contacts the dorsal surface of the transverse lamina of the pterygoid internally. In dorsal view, the lacrimal is quite large, similar to that seen in *Galesaurus* (Pusch *et al.* 2019), *Bolotridon* (Pusch *et al.* 2021), *Thrinaxodon* (Jasinoski *et al.* 2015) and *Lumkuia* (Hopson & Kitching 2001), and different from other cynodonts (i.e. *Platycraniellus* (Abdala 2007)). In posterior view, the nasolacrimal canal is visible and begins posteriorly as two foramina located intra-orbitally. Both foramina are closed medially. The dorsal lacrimal foramen is smaller in diameter than that of the ventral foramen. The two canals extend anteriorly on the internal surface of the lacrimal and merge, resulting in a single canal. The canal ends as a foramen that opens at the anteromedial margin of the lacrimal, onto the medial aspect of the maxilla, just above the maxillary antrum (Fig. 8). This forms a shallow sulcus on the internal surface of the maxilla. The lacrimal exposure on the rostrum is quite broad relative to *Lumkuia,* where the

lacrimal is only exposed for a short distance (Hopson & Kitching 2001). In *Cynognathus* there is only one lacrimal foramen on the internal surface of the lacrimal (Seeley 1895).

The left postorbital is badly damaged but the right postorbital is quite well-preserved. It is very large, unlike in *Lumkuia* and *Chiniquodon* and is absent in other probainognathians (Hopson & Kitching 2001). The postorbital contacts the frontal on its anteromedial surface and parietal on its posteromedial surface. The lateral process (descending ramus) of the postorbital is damaged but would have formed the posteromedial rim of the postorbital bar. The descending ramus of the postorbital contacts the ascending ramus of the jugal laterally. The posterior side of the postorbital extends posteriorly a short distance where it contacts the dorsolateral surface of the parietal (Figs. 5 and 7).

The parietals of BP/1/2520 are well preserved and broad in dorsal view. However, there is damage to both parietals on the posterior surface. The posterolateral surface curves laterally to meet the squamosal and tabular. The parietals are fused together. The parietal is laterally concave in dorsal view (Fig. 7). It extends anteriorly where it meets the postorbital anterolaterally and frontal anteromedially. In dorsal view, there is an anterolateral projection of the parietal that extends between the posterior margins of the postorbital and frontal resulting in a W-shaped anterior suture (Fig. 7). The ventral surface of the parietal is relatively smooth, with a deep fossa in the midline about halfway along the anteroposterior length of the parietal (Fig. 7). This fossa leads to the parietal foramen dorsally and therefore would have housed the pineal body of the forebrain. The parietal foramen is very small and laterally pinched, measuring 0.28 mm in transverse diameter. This is contrary to the description from Brink and Kitching (1953) who stated that there is no foramen, perhaps because of damages to the bone surface which may have prevented them from observing this feature. Basal cynodonts such as *Platycraniellus*, *Galesaurus*, *Cynosaurus*, and *Thrinaxodon* have a parietal foramen (Fourie 1974; Abdala 2007; Van den Brandt & Abdala 2018). However, in *Cynosaurus*, the 'foramen' is noted in a juvenile and may be a pathology from preparation (Benoit *et*

al. 2016). In both Cynosaurus and Galesaurus, no foramen is noted in adult specimens (Benoit *et al.* 2016; Pusch *et al.* 2019). A parietal foramen is absent in *Lumkuia* (Hopson & Kitching 2001) and *Cynognathus* (Seeley 1895). In BP/1/2520, the ventrolateral margins of the parietal are mediolaterally narrow, forming a ridge for contact with the dorsal margin of the epipterygoids.

The postparietal is a triangular sheet of bone located medially between the two tabular bones on the occiput (Fig. 9). It sutures anteriorly with the parietal, laterally with the tabular and ventrally and anteroventrally with the supraoccipital. The postparietal is concave in dorsal view.

The supraoccipital forms the dorsal margin of the foramen magnum. In occipital view, it sutures ventrolaterally with the exoccipitals and dorsally with the postparietal (Fig. 9). Most of the posterior surface of the supraoccipital is covered by the left and right tabular laterally, and as such this bone is roughly quadrangular. The internal surface is smooth and gently concave, forming the roof of the hind region of the brain cavity. The ventrolateral margin of the supraoccipital contacts the dorsal margin of the opisthotic. The ventral margin of the supraoccipital sutures forms a saddle shaped suture with the dorsal margin of the postparietal (Fig. 9).

Braincase and Occiput

CT scans and 3D reconstruction of the specimens has allowed access to the epipterygoids, which is situated dorsolaterally to the posterior most end of the pterygoid, where the quadrate ramus is located in other cynodonts (Fig. 7). It projects posterolaterally toward the quadrate, but its distal-most end is damaged on both sides in BP/1/2520. The dorsal process of the epipterygoid is broken almost at its base, but it is possible to see that it is thin and sheet-like, fanning out dorsolaterally and covering the anterior surface of the prootic.

The parabasisphenoid is located medially, between the quadrate rami of the pterygoids. It sutures anteriorly with the vomer and extends posteriorly to the basioccipital. The lateral tubera of the parabasisphenoid extend posterolaterally, forming a U-shape around the ventral surface of the basioccipital in ventral view (Fig. 6). The processus cultriformis of BP/1/2520 extends dorsally from the anterior margin of the parabasisphenoid. It sutures laterally with the pterygoid at the level where the quadrate ramus would have been located and comes to lie dorsal to the posterior end of the vomer. In dorsal view, the processus cultriformis extends anteriorly where it contacts the anterior process of the pterygoid (Fig. 6A). In lateral view, the anterior half of the processus cultriformis is a narrow rod with a height of 0.75 mm. This height almost doubles to 1.46 mm posteriorly, where it is more lobe-like (Fig. 8). The sella turcica is located on the dorsal surface of the parabasisphenoid just posterior to the cultriform process. It is a fossa that houses the hypophysis of the brain. The sella turcica of the parabasisphenoid is damaged at its posterior end but is present in BP/1/2520 as a triangular platform with a flat dorsal surface (Fig. 6A). Specimen BP/1/2520 (*Cistecynodon*) does not have carotid foramina or canals, which would normally be visible on the ventral surface of the parabasisphenoid and on CT images respectively (Fig. 6B). This is similar to the condition seen in *Platycraniellus* (Abdala 2007), and in cynognathians, including *Cynognathus* and *Diademodon* (Huttenlocker & Sidor 2020). This is unlike the condition in basal cynodonts (i.e., *Galesaurus* and *Prosynosuchus* (Pusch *et al.* 2019, 2024)) and in *Lumkuia* (Hopson & Kitching 2001). The posterior end of the parabasisphenoid is damaged on its dorsal surface, preventing observation of the dorsum sellae. A narrow unossified zone separates the parabasisphenoid from the basioccipital (Fig. 6B). The orbitosphenoids of BP/1/2520 are not preserved, likely because they were loosely attached to the skull by cartilage, as in most cynodonts (Benoit *et al.* 2017a).

Both quadrates of BP/1/2520 are preserved. The left quadrate is displaced slightly dorsally from its anatomical position whereas the right quadrate is well preserved in anatomical position. The quadrate is anteroposteriorly compressed and almost square in ventral view (Fig. 6B). An anteroposteriorly compressed quadrate is seen in other cynodonts such as *Nanictosaurus* and *Trirachodon* (Pusch *et al.*

2024). The dorsal plate and trochlea of the quadrate are present and fused. The quadrate articulates with the articular anteriorly. On the anterolateral surface of the quadrate, there is a shallow socket, for articulation with a small margin of the posterior end of the surangular. There is no quadrate foramen.

The prootic is located posteriorly to the epipterygoid and contributes to the sidewall of the braincase (Fig. 6). The anterodorsal extension of the prootic is a thin, broad sheet of bone which forms the capsule of the anterior inner ear. In BP/1/2520, due to the inflation of the vestibule of the inner ear, the entire prootic wall is a very thin sheet of bone that partially covers the inner ear vestibule (Fig. 6B). In other cynodonts, this extension contacts the posterodorsal margin of the epipterygoid, however the dorsal process of the epipterygoid of BP/1/2520 is not preserved. The lateral flange of the prootic is anterodorsally wide and would have contacted the squamosal at its lateralmost point. The pterygoparoccipital foramen is located at the suture between the two bones (Fig. 7). In dorsal view this foramen is almost completely circular and has a diameter of 3.48 mm. The pila antotica is an anteromedial projection of the prootic and usually lies posteromedially to the epipterygoid (Pusch *et al.* 2024), but in BP/1/2520, only the base of the pila antotica is preserved (Fig. 6B). The pila antotica would have formed the posterior border of the trigeminal notch (cranial nerve V). At its posterior margin, the suture line between the prootic and opisthotic is difficult to discern, and its position on the 3D reconstruction of BP/1/2520 (Fig. 9) is an approximation. This may be because the prootic and opisthotic have fused to form the periotic. Posteriorly the quadrate articulates with the squamosal and makes a small point of contact medially with the prootic, where the lateral flange of the prootic would extend out towards the squamosal (Fig. 7).

The opisthotic is a large bone at the posterior end of the skull (Fig. 9). It is bordered anteriorly by the prootic, laterally by the squamosal, ventromedially by the basioccipital, dorsomedially by the supraoccipital and posterodorsally by the tabular (Figs. 6 and 9). The ventroposterior surface of the bone is exposed. The opisthotic contributes the posterior wall of the chamber for the inner ear.

Similarly to the prootic, the vertical component of the opisthotic which contacts the prootic laterally, medially and dorsally is very thin due to hyperinflation of the vestibule of the inner ear. The only component of the opisthotic which is slightly more thickened is the lateral process which extends to contact the ventromedial surface of the squamosal. The fenestra ovalis is a relatively large opening present on the ventral surface of the basicranium. The lateral border of the fenestra ovalis is not preserved, thus it is difficult to assess its full extent (Fig. 6B). In ventral view it is bordered anteromedially by the parasphenoid ala, medially by the basioccipital, posteriorly by the opisthotic and anteriorly by the prootic (Fig. 6B). The jugular foramen of BP/1/2520 is a large circular opening in the ventroposterior surface of the basicranium. Its medial and posterior margins are formed by the basioccipital, and the lateral and anterior margins are formed by the opisthotic.

The basioccipital is well preserved. In dorsal view it has a roughly hourglass shape, with the posterior end wider than the anterior end (Fig. 6B). The main body of the basioccipital is concave in dorsal view. On its ventral surface, there are two distinct, ovoid depressions separated along the midline by a small ridge. A similar morphology is seen in most therapsids (Pusch *et al.* 2024). The posteroventral margin is an inverted V-shape in ventral and dorsal views, separating the two occipital condyles (Fig. 6). The bone is thickened along this margin, forming a ridge which allows articulation with the atlas. From the CT scans, it is difficult to assess the exact suture contact between the basioccipital and exoccipitals, thus the segmentation is an approximation of the sutural contact. The exoccipitals are on the laterodorsal sides of the basicranium (Fig. 9). This bone sutures with the supraoccipital dorsomedially, the tabular dorsolaterally, the opisthotic laterally and the basioccipital ventromedially. The exoccipital contributes the lateral margin of the foramen magnum. The foramen magnum is large and circular in occipital view (Fig. 9). This differs from the morphology of *Cynognathus* in which the foramen magnum is mediolaterally compressed and ovoid (Seeley 1895).

The tabular is a large, flat bone on the occipital surface of the skull. It is a paired bone that is separated in the sagittal plane by the supraoccipital ventrally and postparietal dorsally (Fig. 9). The tabular

sutures dorsally with the posterior margin of the parietal, forming a pronounced lambdoid crest in dorsal view. The tabular encloses the entire rim of the post-temporal fenestra (Fig. 9), as is seen in *Charassognathus*, *Procynosuchus*, *Vetusodon*, *Thrinaxodon*, *Nanictosaurus*, *Platycraniellus*, *Trirachodon* and *Lumkuia* (Abdala 2007; Abdala *et al*. 2019; Hopson & Kitching 2001; Pusch *et al.* 2024).

Most of the endocast of BP/1/2520 is preserved, however the ventral and lateral borders of the endocast could not be accurately reconstructed due to the absence of delimiting bony structures (the orbitosphenoid and superior half of the epipterygoid (see Figs. 5 and 6)). The anteroposterior length of the endocast is 27.52 mm from the anterior point of the cast of the olfactory bulbs to the foramen magnum and a height of 13.74 mm (Fig. 10). The volume of the endocast is 1827.84 mm^3. The olfactory bulbs are positioned anteriorly to the endocast. They are broader than the width of the hemispheres (7.52 mm compared to 6.96 mm respectively). The olfactory bulbs are separated from each other along the midline by a very shallow median sulcus like in most Triassic cynodonts (i.e. *Galesaurus*, *Nythosaurus* (Pusch *et al.* 2019, 2023)) (Fig. 10A). The orbitosphenoids of BP/1/2520 are not preserved, therefore the ventral surface of the olfactory bulbs and anterior part of the forebrain cannot be described. The dorsal surface of the olfactory bulbs is slightly convex. The general morphology of the olfactory bulbs matches that of other basal cynodonts (i.e., *Thrinaxodon, Nythosaurus, Galesaurus* (Pusch *et al.* 2024)). The margin between the olfactory bulbs and forebrain is not clearly visible. The forebrain of BP/1/2520 is long and tubular and there does not appear to be a distinct division between the cerebral hemispheres. The small parietal canal houses a narrow pineal body on the dorsal surface of the forebrain. The posterior end of the forebrain is usually encased by the epipterygoids in cynodonts, but as these structures are damaged in BP/1/2520, the width of the posterior end of the forebrain cannot be assessed. Similarly, the extent of the anterior projection of the hypophysis cannot be clearly assessed. The boundary between the forebrain and midbrain is not well defined. Just posterior to the pineal body, there is an unossified zone of the braincase housed in the supraoccipital bone. This unossified zone is noted as a bulge on the endocasts of other cynodonts

(Pusch *et al.* 2019, 2023) rather than as a narrow projection as seen in BP/1/2520. The hindbrain (cerebellum) is shorter than the fore- and midbrain, but wider than both structures (Fig. 10A). The ventral surface of the endocast is defined by the prootic, opisthotic and partially by the supraoccipital. The posteroventral surface of the endocast is defined by the basioccipital. Specimen BP/1/2520 has shallow floccular fossae, and as such, the paraflocculus is not salient. This type of morphology has been considered unique among cynodonts (Kielan-Jaworowska *et al.* 2004; Rodrigues *et al.* 2014; Benoit 2023), however specimens of *Charassognathus*, *Procynosuchus*, *Abdalodon*, *Cynosaurus*, *Trirachodon* and *Boreogomphodon* also have a paraflocculus which is not salient (Pusch *et al*. 2024). It appears only as a slight broadening of the hindbrain between the anterior and lateral semicircular canals of the inner ear.

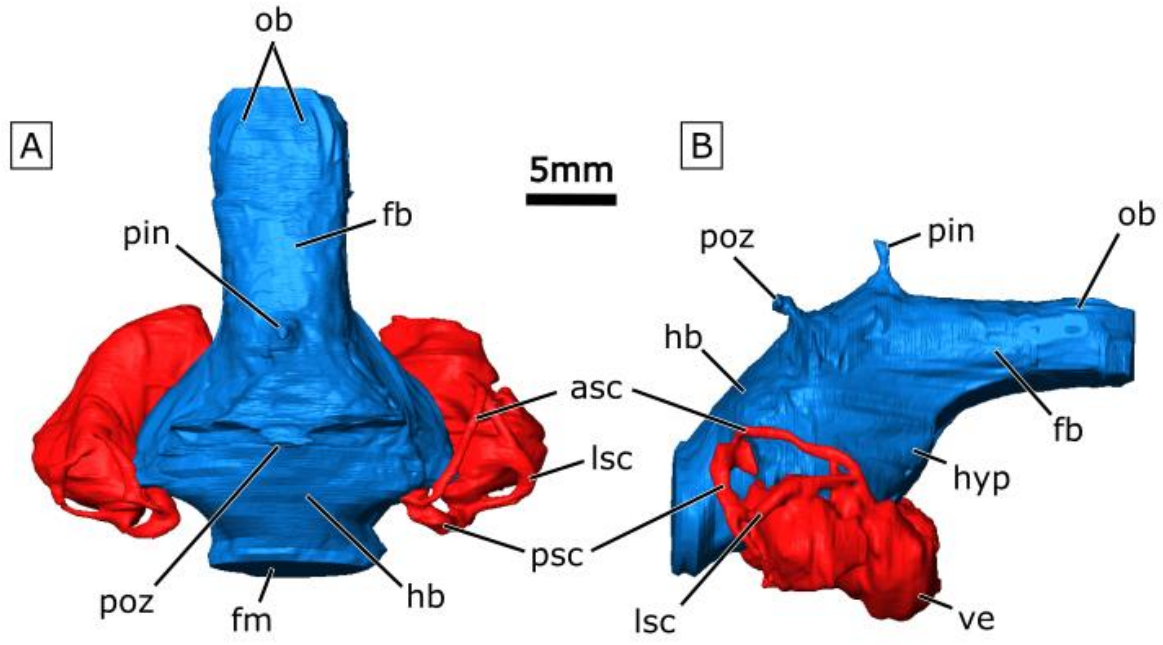

Figure 10: 3D reconstruction of the endocast and inner ear of BP/1/2520 in (A) dorsal and (B) right lateral views. Abbreviations: asc, anterior semicircular canal; fm, foramen magnum; fb, forebrain; hb, hindbrain; hyp, hypophysis; lsc, lateral semicircular canal; ob, olfactory bulb; pf, parietal foramen; poz, projection of the midbrain into the unossified zone; psc, posterior semicircular canal; ve, vestibule.

Both the left and right inner ear of BP/1/2520 are preserved (Fig. 11). In other cynodonts, the inner ear consists of three parts: the semicircular canals, vestibule, and cochlear recess (Pusch *et al.* 2019, 2023, 2024). However, in BP/1/2520, the inner ear is short dorsoventrally, with an enlarged vestibule, but has no visible cochlear recess (Fig. 11A and B). The housing for the inner ear is formed by the opisthotic, prootic, exoccipital, basioccipital and supraoccipital, as in other therapsid taxa (e.g. Luo 1994; Kielan-Jaworowska *et al.* 2004). The semicircular canals are enclosed by the opisthotic, exoccipital, supraoccipital and prootic. The anterior semicircular canal is 9.86 mm long and encircles the floccular fossa, which is shallow in BP/1/2520. The lateral semicircular canal is almost as long as the anterior canal (9.47 mm). The posterior semicircular canal is the shortest of the three canals (6.85 mm long). The anterior and posterior semicircular canals originate from the crus commune, a short, thickened structure located dorsomedially on the inner ear (Fig. 11B). The posterior semicircular canal extends from the posterodorsal apex of the crus commune and is broader at this point than the anterior semicircular canal. The posterior semicircular canal extends posteriorly from the crus commune, curving downwards to the level of the lateral semicircular canal, and joining the posterior ampullar recess. A secondary common crus is present between the descending posterior semicircular canal and posterior arm of the lateral canal (Fig. 11), a common feature seen in most non-mammalian therapsids (e.g. Laaß 2014; Benoit *et al.* 2017b). The presence of a secondary crus commune has been interpreted as a plesiomorphic therapsid feature that is retained in early mammals (e.g. Luo *et al.* 2011). The vestibule of the inner ear is surrounded by the opisthotic and prootic. The vestibule of BP/1/2520 is unusual among cynodonts with reconstructed inner ears, as it is very enlarged, with a volume of 7.06 mm^3. Thus far, a similar morphology has only been noted in the cynognathian cynodont *Boreogomphodon* (Pusch *et al*. 2024). The fenestra vestibuli is an opening at the suture between the prootic, opisthotic, basioccipital and the posterior most point of the parasphenoid ala. Contribution of the parasphenoid ala to the rim of the fenestra vestibuli is a condition shared with other basal cynodonts such as *Thrinaxodon*, *Galesaurus*, *Nanictosaurus* and *Dvinia* (Gaetano *et al.* 2022; Pusch *et*

al. 2024). The fenestra vestibuli accommodates the stapedial footplate but no stapes is preserved here.

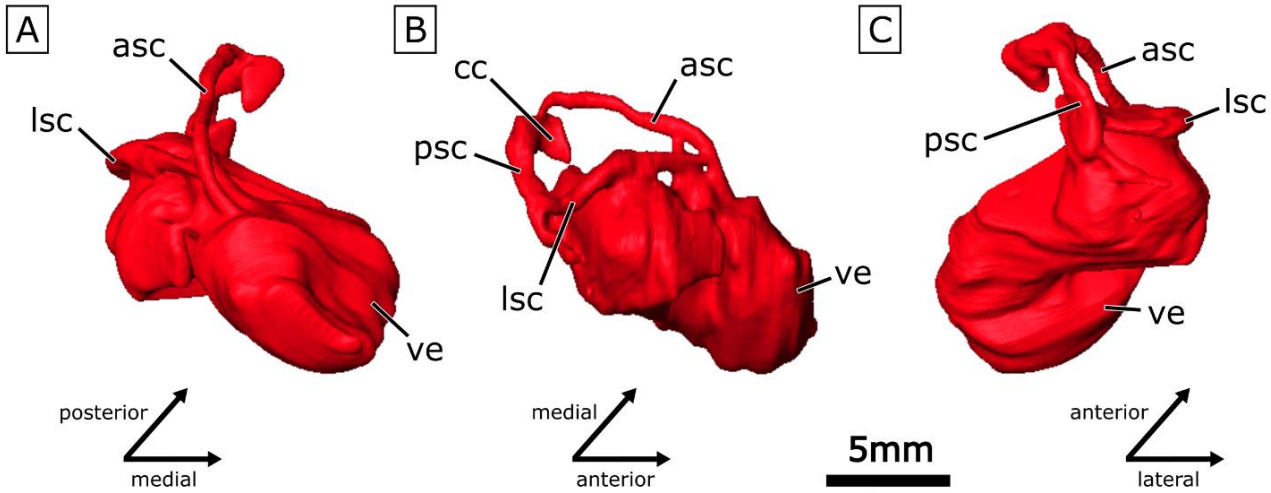

Figure 11: 3D reconstruction of the right inner ear of BP/1/2520 in anterior (A), lateral (B) and posterior (C) view. Abbreviations: asc, anterior semicircular canal; cc, crus commune; lsc, lateral semicircular canal; psc, posterior semicircular canal; v, vestibule.

Lower jaw

The lower jaw of BP/1/2520 is very robust. The dentary measures 28.61 mm from its anterior most point to the base of the coronoid process and is mediolaterally thick (Fig. 12). There are eleven alveoli in each dentary, and all of the dentary teeth are preserved to varying degrees. There are three small alveoli to accommodate the incisors, an enlarged alveolus for the canine, and seven alveoli which house the postcanines. The coronoid process of the dentary is 10.57 mm wide and 22.27 mm tall. The coronoid process angles posterodorsally at a 37.4° angle to the dentary. With the exception of the non-eucynodont *Bolotridon* (Pusch *et al.* 2021), the dentary symphysis is unfused in non-eucynodonts and fused in eucynodonts (Hopson & Kitching 2001). The trough on the medial surface of the dentary

for the postdentary bones is elongate, dorsoventrally broad but shallow. In BP/1/2520 the masseteric fossa is low down on the coronoid process of the dentary, roughly at the level of the tooth row (Fig. 12). This condition is typical of epicynodonts (Hopson & Kitching 2001).

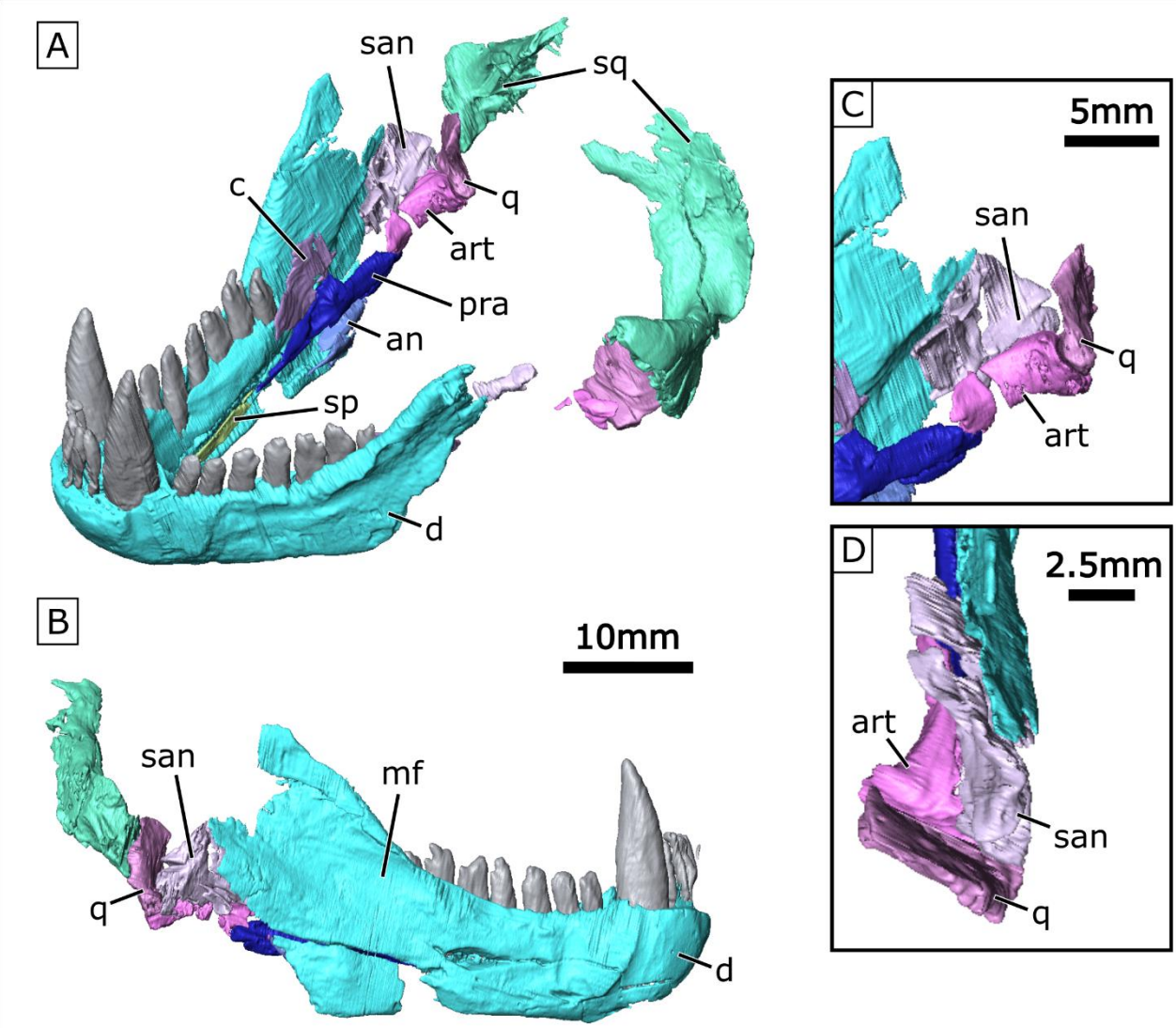

Figure 12: 3D reconstructions of the lower jaw of BP/1/2520 in (A) anterodorsolateral, (B) right lower jaw in lateral view; magnification of the right lower jaw in (C) medial and (D) dorsal view. Abbreviations: an, angular; art, articular; c, coronoid; mf, masseteric fossa; pra, prearticular; q, quadrate; san, surangular; sp, splenial; sq, squamosal.

The anterior half of the left and right splenial and a fragmentary portion of the posterior half of the left splenial are preserved. The splenial is a sheet-like bone that lies in a trough that runs along the dentary medial surface of the horizontal ramus of the dentary (Fig. 12A). The anteroventral margin of the splenial sutures with the ventral most surface of the fused dentary symphysis.

Most of both the left and right coronoid of BP/1/2520 are preserved (Fig. 12A). The coronoid is present as a mediolaterally compressed sheet of bone along the medial surface of the dentary and appears almost triangular in medial view. The coronoid sits dorsally to the prearticular and angular bones of the lower jaw. This bone is located halfway along the anteroposterior length of the prearticular, at the anterior base of the coronoid process, and extends anteriorly to the level of the sixth lower postcanine.

Only a thin fragmentary sheet of bone of both the left and right angular of BP/1/2520 are preserved (Fig. 12A). In medial view, this sheet of bone has a ridge running along its anteroposterior length. The angular is situated medially to the dentary and ventromedially to the prearticular (Fig. 12A).

Only the posterior end of the right surangular of BP/1/2520 is preserved. The posterior end of the surangular is a thickened piece of bone located between the medial surface of the coronoid process of the dentary and the articular. Its ventral surface is aligned with the ventral surface of the articular and becomes concave on its medial surface as it extends dorsally (Fig. 12C and D). The posterior end of the surangular contacts the anterolateral surface of the quadrate via a shallow socket on the quadrate (Fig. 12B and D). This contact is minimal and does not appear to contribute largely towards the articulation of the lower jaw in any significant capacity. However, this morphology still constitutes a double jaw articulation in BP/1/2520, these being the quadrate-articular and quadrate-surangular (Fig 12D).

The right articular of BP/1/2520 is almost completely preserved and there is only a fragment of the left articular preserved (Fig. 12A). At its anterior end, the articular is a narrow and elongated shaft of bone. However, it is possible that the articular and prearticular are fused and have been damaged by

taphonomical processes which makes them appear as separate components (Fig. 12A and C). Posteriorly, the articular expands in mediolateral width to create a broad articulation facet for the quadrate. The articulation facet is concave in posterior and medial view (Fig. 12C and D). Only the posterior ends of the left and right prearticular bones are preserved.

Dentition

Specimen BP/1/2520 preserves an almost complete upper and lower dentition (Fig. 13). The canines and postcanines of the upper and lower dentition are preserved, but the crowns are slightly weathered, making observation of cusp number difficult. The upper and lower incisors are preserved but are weathered anteriorly. There are no replacement teeth and posteriorly there is no space in the posterior region of the tooth row for the development of more teeth. As such, the dentition of BP/1/2520 has completely erupted. There are open roots on both upper and lower canines, as well as open roots on some of the postcanines. There is an open root on both the right and the left PC4 and PC5. There are open roots noted on the right lower pc1, pc4, pc5, pc6 and pc7, and on the lower left pc4, pc6 and pc7. In BP/1/2520, PC4 and PC5 are the largest and the size of the teeth decreases slightly anteriorly and posteriorly. In the lower dentition, pc1 is the smallest and the size of the teeth increase posteriorly, with the exception of pc7 which is smaller.

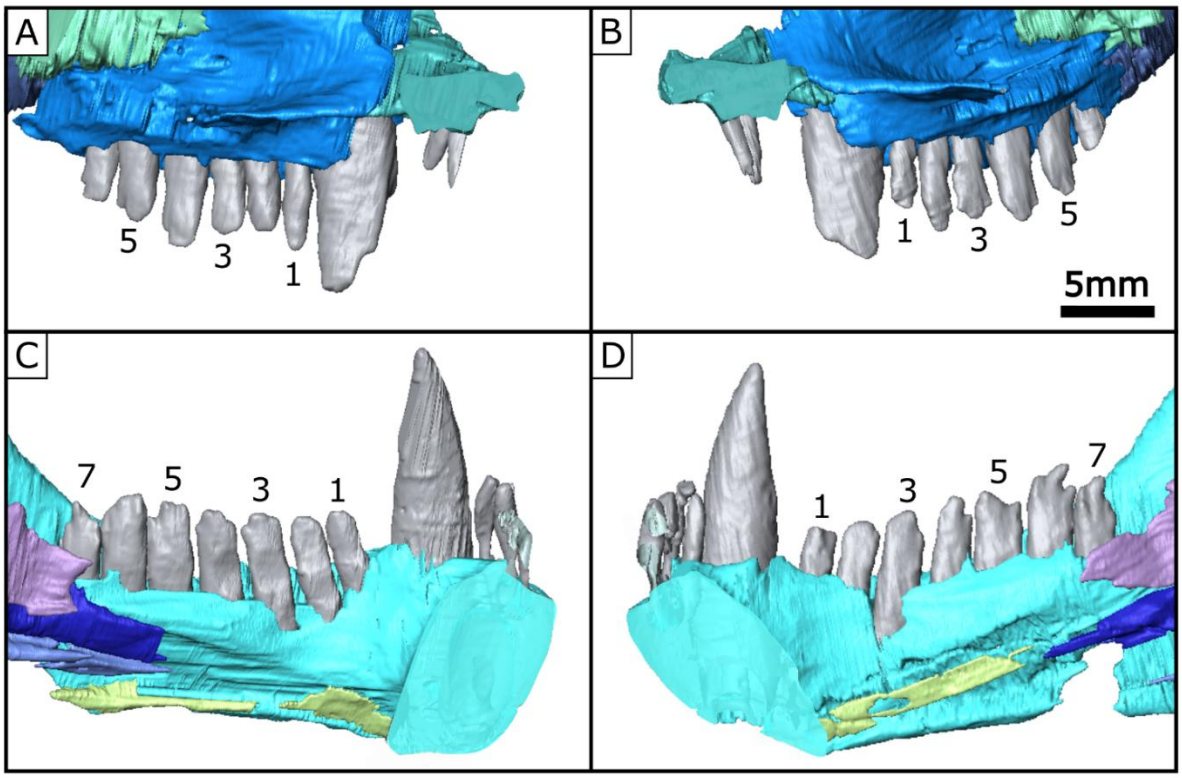

Figure 13: Dentition of BP/1/2520. (A) Left upper dentition, (B) right upper dentition, (C) left lower dentition and (D) right lower dentition in lingual view.

In the upper left and right series, there are four alveoli present in the premaxilla. On the left premaxilla only I2, I3 and I4 are preserved. In the right premaxilla, only I1, I3 and I4 are preserved. The incisors are narrow and tubular. The second incisor in the left series preserves only the root of the tooth; I3 preserves a portion of the root and a small portion of the posterior rim of the crown; I4 preserves the crown of the tooth and a fragmentary piece of the root. In the right series, there is only a very small fragment of the root of the first incisor and there is no I2 present. Incisors I3 and I4 are almost completely preserved, with both root and crown present for each; however, they show weathering on the anterior (labial) surface. All the incisors are roughly the same size. There is a diastema present between the upper incisors (I4) and upper canines (Fig. 13A and B). A similar morphology is seen in *Platycraniellus* (Abdala 2007) and adult specimens of *Cynosaurus* (Van den Brandt & Abdala 2018). The upper right and left dentition each preserve one large canine and six postcanine teeth (Fig. 13A

and B). There is no indication of replacement teeth for the canines or any of the postcanines in the upper dentition. The upper canines are large, conical and smooth, compared to in which the canines are laterally compressed *Lumkuia* (Benoit *et al.* 2022a).

It is difficult to accurately assess cusp count on the postcanine teeth as they show considerable wear (Fig. 13). On the upper left dentition, PC1 has a single cusp and PC2 and PC3 appear tricuspid (Fig. 13A). The main cusp on PC2 seems to be almost vertically oriented. The remaining teeth, PC4, PC5 and PC6 appear bicuspid. On the upper right dentition, PC1 is single-cusped, and PC2, PC3 and PC4 are tricuspid (Fig. 13B). The right PC5 appears tetracuspid, with two small anterior cusps, one main cusp and one small posterior cusp, as seen in PC5 of *Lumkuia* (Hopson & Kitching 2001). Due to weathering, the main cusp of the upper postcanine teeth is not clearly defined and no observations can be made regarding their morphology. The crown of PC6 is damaged and no observations can be made. The general morphology of BP/1/2520 is similar to that of *Thrinaxodon* (Estes 1961; Fourie 1974), *Nanictosaurus* (van Heerden & Rubidge 1990), *Lumkuia* (Hopson & Kitching 2001; Benoit *et al.* 2022a) and *Cynognathus* (Seeley 1895), in which most of the postcanines are tricuspid.

The lower left dentition preserves three incisors, one large canine and seven postcanines. This morphology is reflected in the right lower dentition. For i2, only the crown of the tooth is preserved whereas all other lower incisors preserve almost the entire tooth. There is no indication of replacement teeth for the canines or the postcanines in the lower dentition. The crown of pc1 and pc2 are very weathered, therefore cusp number is difficult to identify (Fig. 13C). The lower pc3, pc4 and pc5 are tricuspid, each with one anterior and posterior accessory cusp surrounding a large main cusp. The crown of pc6 is completely weathered away. The pc7 also appears tricuspid, with one small anterior accessory cusp, the large, slightly recurved main cusp in the middle, and one small posterior accessory cusp (Fig. 13C). In the lower right dentition, the crown of pc1 and pc2 are very weathered, therefore it is not possible to get the cusp number, however the cusps would have been quite straight (Fig. 13D). The third postcanine appears to be tricuspid but pc4 is bicuspid. The crown of pc5 is too

damaged to accurately assess cusp count, though it seems that it has at least two cusps, the main cusp and a small posterior cusp. The main cusp of pc6 is recurved posteriorly, at about 45°, forming a slight hook (Fig. 13D). However, the curvature of the hook on the cusps is not as severe as that seen in *Galesaurus* (Pusch *et al.* 2019). The curvature of the main cusp is more similar to that of *Lumkuia* (Hopson & Kitching 2001) and *Cynognathus* (Seeley 1895) which have a gentle recurve and hook. There are four cusps on pc7, with one main cusp, one small anterior cusp and two small posterior accessory cusps. Overall, the lower dentition of BP/1/2520 is reminiscent of *Cynognathus*, *Thrinaxodon* and *Lumkuia*, which is also mostly tricuspid, with a prominent curved main cusp and less well defined accessory cusps (Seeley 1895; Hopson & Kitching 2001; Abdala *et al.* 2013).

SAM-PK-K11655

Overall preservation

Specimen SAM-PK-K11655 is a relatively well preserved skull with occluded mandible (Fig. 14). The skull length is 55.44 mm, measured from the anterior most point of the maxilla to the posterior-most point of the basioccipital and including the length of the damaged premaxilla situated ventral to the maxilla. The top of the snout and the occipital region have been damaged due to recent, post-burial weathering, as moulds of weathered out bones are still visible on the specimen. A mould of the coronoid process of the right dentary is preserved. Most of the rostral region of the skull is missing, preserving only a small portion the lateral wall of the right maxilla, the alveolar region of the left maxilla, and a fragment of the nasal bone. Fragments of the jugal, prefrontal, frontal, postorbital and parietal bones are present, but are insufficient for providing descriptions. The dorsal surface of the left and right parietal bones is missing; however, a mould of the small parietal foramen is preserved in the rock matrix. The ventral part of the left and right lacrimal are preserved. The secondary palate is well preserved, with the premaxilla, palatal region of the maxilla, palatine, and vomer present (Fig. 14). The secondary palate is not closed medially compared to other cynodonts (see 'Overall

preservation' section of BP/1/2520). Ventrolateral to the palatine, the right and left ectopterygoid are preserved. The left and right pterygoid and epipterygoid are preserved. The parabasisphenoid, basioccipital and prootic bones are mostly complete. There is a fragment of the left opisthotic present, and the lateral regions of the left and right squamosal bones are partially preserved. The medial portion of the squamosal and prootic bones are damaged. There is insufficient bone preservation of the prootic, opisthotic and skull roof to determine the complete morphology of the endocast and inner ear (Fig. 14). Observations of the endocast are made from the moulds preserved on the dorsal aspect of the specimen. Both the left and right quadrate are preserved, but damaged, and posterior pieces of the articulatory bones of the lower jaw are partially preserved. The left dentary is better preserved than the right one. The right upper and lower dentition is preserved almost entirely, whilst the left upper and lower dentition preserves only a few postcanine teeth.

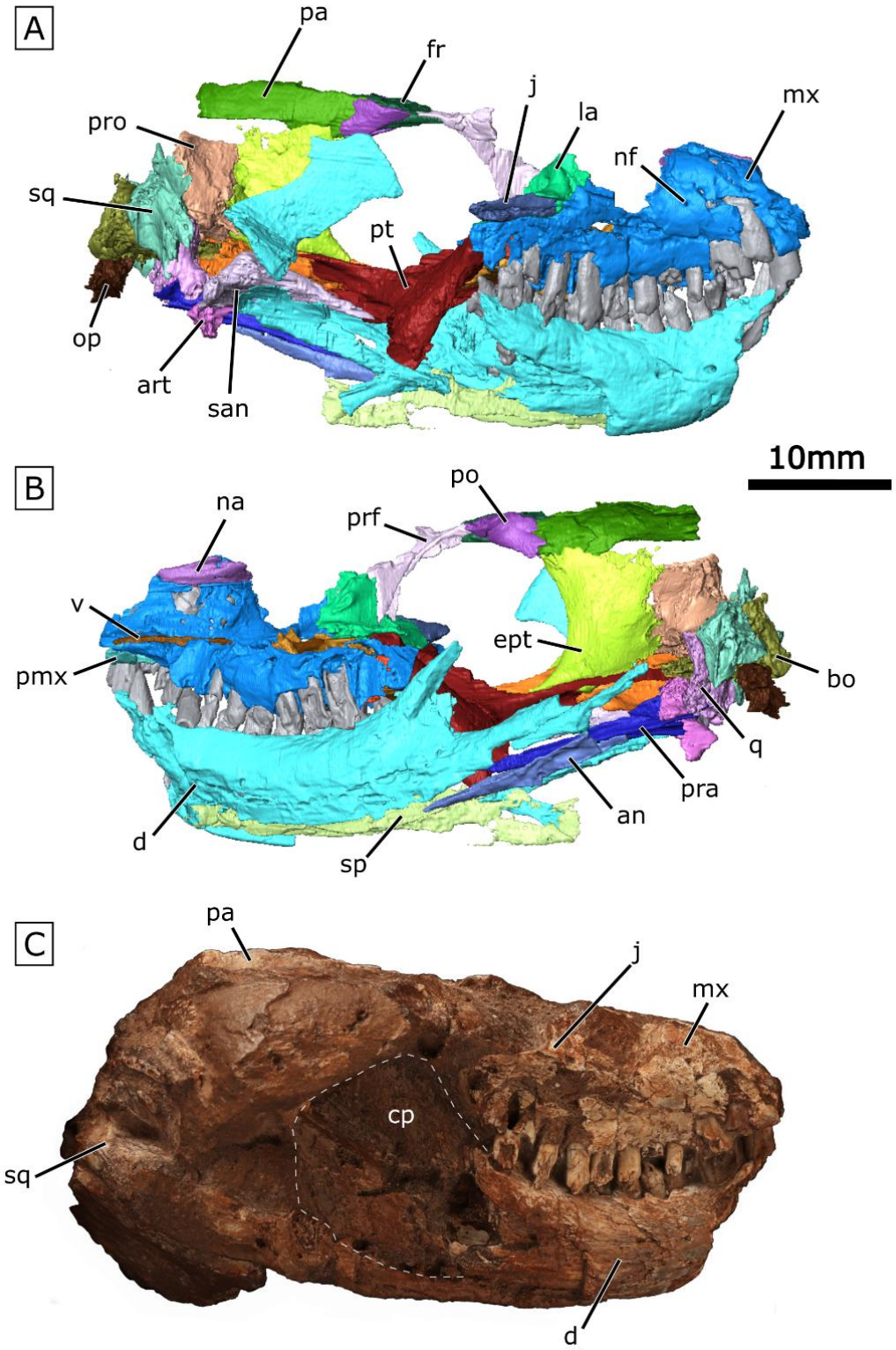

Figure 14: cranium of SAM-PK-K11655 in (A) right lateral, (B) left lateral view. (C) Specimen SAM-PK-K11655 in right lateral view. Abbreviations: art, articular; bo, basioccipital; cp, coronoid process of the dentary; d, dentary; ept, epipterygoid; fr, frontal; j, jugal; la, lacrimal; mx, maxilla; na, nasal; op,

opisthotic; pa, parietal; pmx, premaxilla; po, postorbital; prf, prefrontal; pro, prootic; pt, pterygoid; q, quadrate; sp, splenial; sq, squamosal. Dashed white line indicates the preserved mold of the coronoid process of the dentary.

Snout and secondary palate

The premaxilla forms the anterior region of the snout; however, in SAM-PK-K11655 the anterior most part of the snout is laterally crushed, and the premaxilla is displaced from its anatomical position (Fig. 15). Only two small slivers of the medial region of each premaxilla are preserved and sit ventral to the maxilla. The overall preservation of the specimen, including moulds of bones, suggests that damage to the skull by weathering took place post-burial. It is not possible to determine whether the pieces of premaxilla that are preserved represent the entire premaxilla. Although not in anatomical position, an antero-posterior length of 5.13 mm is estimated for the premaxilla. This length, added to the length of the maxilla and palatine gives a secondary palate that is 20.86 mm long. Thus, the premaxilla contributes 24,5 % of the total length of the secondary palate. No incisive foramen is preserved. The premaxilla sutures with the maxilla laterally and posteriorly and would have contacted the septomaxilla anterodorsally, but it is not preserved here. The premaxillae do not contact each other on the midline but are separated by the anterodorsal extension of the anterior process of the vomer (Fig. 15A). The septomaxilla of SAM-PK-K11655 is not preserved and only a very small fragment of the right nasal is present, lying flush with the ventromedial surface of the maxilla (Fig. 15B).

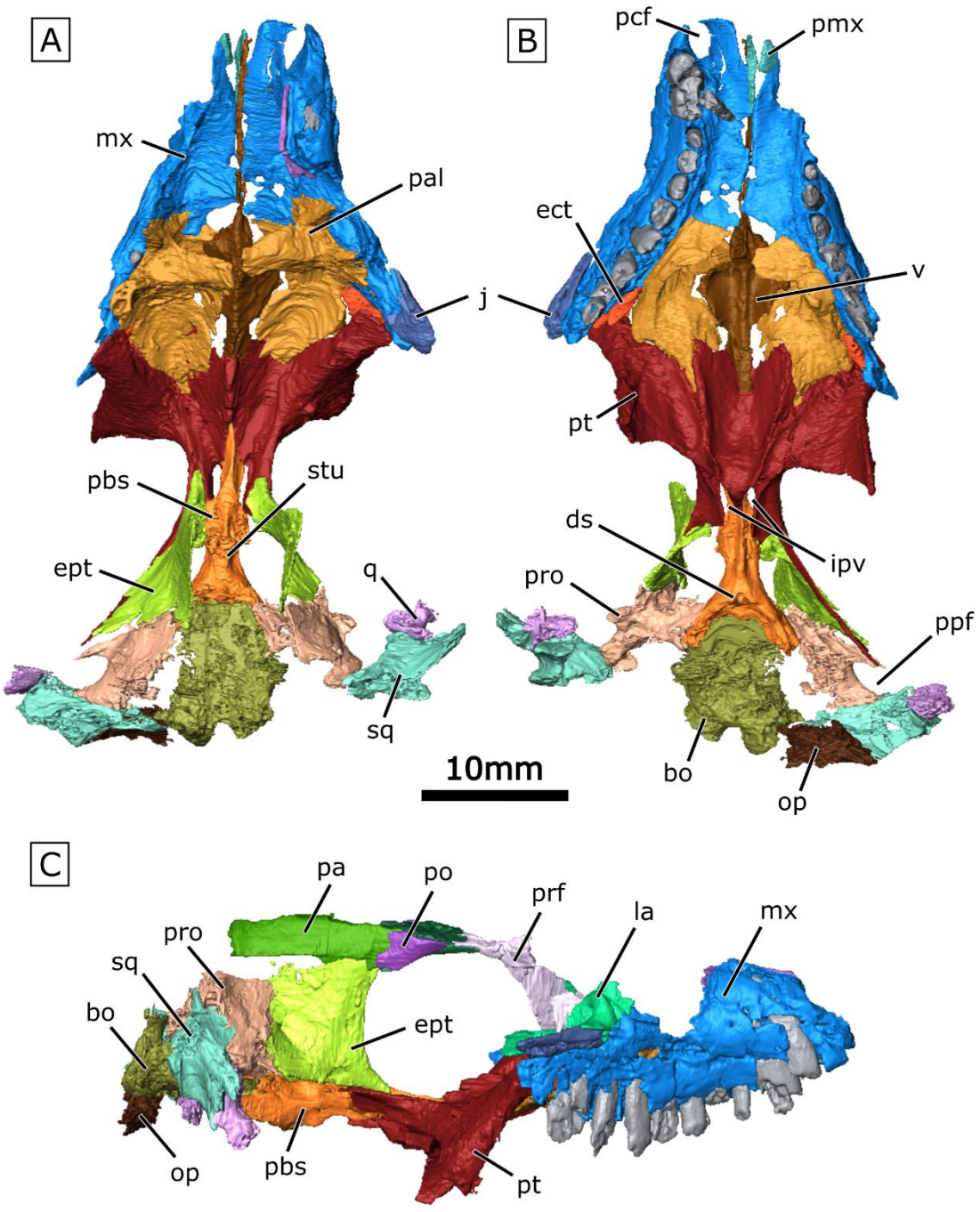

Figure 15: basicranium and palate of SAM-PK-K11655 in (A) dorsal, (B) ventral and (C) right lateral views. Abbreviations: bo, basioccipital; cf, carotid foramen; ds, dorsum sellae; ept, epipterygoid; ect, ectopterygoid; ipv, interpterygoid vacuity; j, jugal; la, lacrimal; mx, maxilla; na, nasal; op, opisthotic; pa, parietal; pal, palatine; pbs, parabasisphenoid; pcf, paracanine fossa; pmx, premaxilla; prf, prefrontal; pro, prootic; pt, pterygoid; q, quadrate; sq, squamosal; stu, sella turcica; v, vomer.

A cast of the left and right nasal turbinals of SAM-PK-K11655 is preserved on the dorsal surface of the specimen (Fig. 16). The turbinal ridges run parallel and longitudinally on each side of the midline. They are long and narrow in dorsal view. The cast of a cartilaginous nasal septum runs sagittally. The cast of the nasal cavity extends posteriorly to the level of the anterior margin of the orbit.

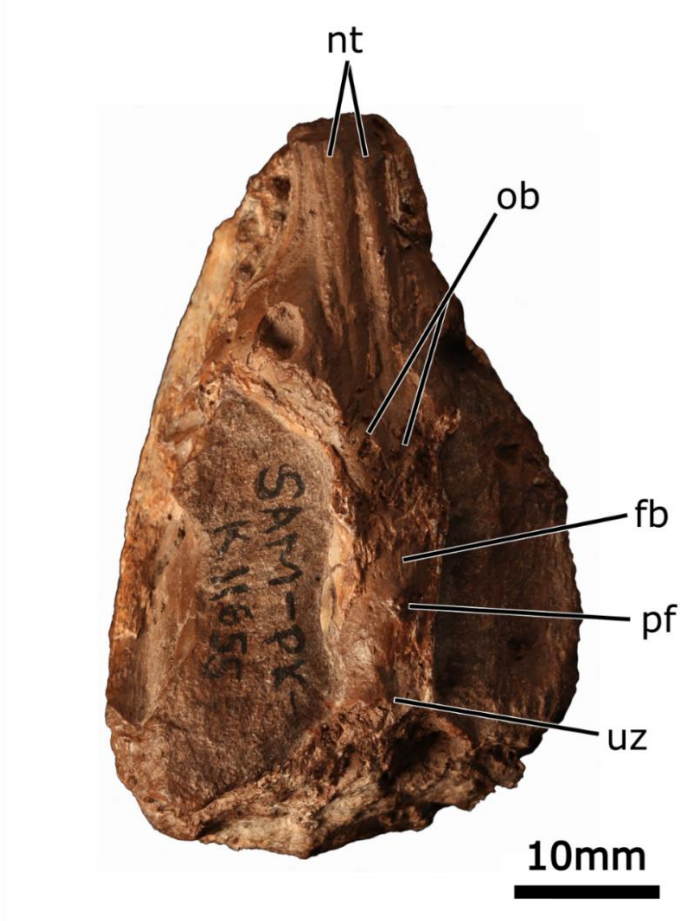

Figure 16: Images of SAM-PK-K11655 in (A) enlarged dorsal view of the hindbrain; (B) dorsal view and (C) angled left dorsolateral view. Abbreviations: fb, forebrain; nt, nasal turbinate; ob, olfactory bulb; pf, parietal foramen; uz, unossified zone.

The maxilla is a large bone that contributes the majority of the lateral surface of the snout. In SAM-PK-K11655, the palatal region of the maxilla is 12.91 mm in anteroposterior length, thus contributing

almost two thirds (61,89%) of the length of the secondary palate (Fig.15B). The palatal processes of the two maxillae do not contact each other in the midline ventrally. The apparent contact between the bones is the result of mediolateral compression of the skull during diagenesis causing the bones to overlap slightly. This phenomenon has been noted in other cynodonts including *Bolotridon* (Pusch *et al.* 2021) and *Galesaurus* (Pusch *et al.* 2019). The maxillary portion of the secondary palate extends posteriorly to the level of the fourth postcanine. A large paracanine fossa is visible anterior to the right upper canine. It is entirely enclosed within the maxilla, but unlike that of *Cistecynodon* (Fig. 6). Due to damage, only a single, small foramen is visible on the lateral surface of the right maxilla in lateral view (Fig. 14A). This foramen is above the first postcanine, at the level of the jugal. This foramen may be one of the many openings of the maxillary canal onto the surface of the maxilla (Benoit *et al.* 2016b).

The palatine of SAM-PK-K11655 sutures anteriorly and laterally with the maxilla (Fig. 15). The palatal process of the palatine contributes to the posterior end of the secondary palate and is 3.05 mm long. This is approximately 14,62% of the length of what is preserved of the secondary palate. This proportion of the palatine contribution to the secondary palate is a trait shared with basal cynodonts and the eucynodont *Cynognathus* (Pusch *et al.* 2019). The secondary palate is similar to that of *Cistecynodon* (Fig. 6B), *Thrinaxodon*, *Nythosaurus* and *Cynosaurus* in which there is still a space between the palatal processes of the maxilla and palatine (Jasinoski *et al.* 2015; Van den Brandt & Abdala 2018; Pusch *et al.* 2023). This morphology differs from eucynodonts, where the secondary palate is completely closed (Pusch *et al.* 2019, 2021 but see Estes 1961). Anteriorly, the transverse laminae of the palatine contribute the majority of the roof and lateral walls of the nasopharyngeal passage, with a small contribution to the floor of the passage. The maxilla contributes most of the floor of the nasal passage. Posteriorly, the palatal process of the palatine sutures with the pterygoid, and the transverse lamina of the palatine contacts the vomer in the midline, forming the secondary choanae (Fig. 15B).

The vomer is a single, elongated bone located along the midline of the cranium and dorsal to the secondary palate (Fig. 15). There is a vertical ridge that runs anteroposteriorly along the midline of the bone and extends vertically into the nasal passage, between the paired palatine bones, to form the vertical vomerine plate which is 1.96 mm tall. Anteriorly, the ridge becomes a long, mediolaterally narrow strip of bone that extends from the vomer along the dorsal surface of the premaxilla, terminating just before the anterior most point of the premaxillary plate. In SAM-PK-K11655 this ridge is damaged. Posteriorly, this ridge runs along the length of the dorsal surface of the vomer. This condition is seen in taxa such as *Thrinaxodon* and *Massetognathus* (Fourie 1974; Crompton *et al.* 2015) and *Cistecynodon* (Fig. 8). The vomer contacts the pterygoid posteromedially in ventral view (Fig. 15B). The posterior body of the vomer expands laterally into two 'wings', one on each side. These wings contact the transverse laminae of the palatine laterally, which contribute the roof of the choanae.

The pterygoid is a large, fused bone located posterior to the palate. In ventral view the pterygoid is somewhat butterfly shaped. In lateral view, the transverse flange of the pterygoid projects ventrally in an almost vertical orientation, with a slight posterior deflection (Fig. 14A). In ventral view, mediolaterally narrow interpterygoid vacuities are present between the processus cultriformis of the parabasisphenoid and the pterygoids as in *Cistecynodon* (Fig. 6). The pterygoid contacts the parabasisphenoid complex posteromedially. Posterolaterally, the quadrate ramus of the pterygoid is a long and thin process that extends toward the quadrate. The quadrate ramus lies ventral to the epipterygoid and is concave in dorsal view.

Like in *Cistecynodon*, the ectopterygoid is present as a small, roughly triangular bone in ventral view (Fig. 15). As in *Nythosaurus*, the ventral exposure of the ectopterygoid is larger than its internal (dorsal) exposure (Pusch *et al.* 2023). It is situated ventral to the posterolateral margin of the maxilla and the transverse flange of the pterygoid. It sits dorsolateral to the posterolateral side of the palatine. The ectopterygoid is present in epicynodonts such as *Galesaurus*, *Nythosaurus*, *Thrinaxodon*,

Platycraniellus, *Cynosaurus* (Parrington 1934; Van den Brandt & Abdala 2018; Pusch *et al.* 2019, 2023) but absent in eucynodonts such as *Cynognathus* and *Lumkuia* (Seeley 1895; Hopson & Kitching 2001).

Circumorbital region

Only the lateral surface of the right jugal is preserved (Fig. 14). The jugal contacts the maxilla anterolaterally, the lacrimal dorsomedially, the pterygoid ventrally and the ectopterygoid and palatine anteromedially. Small pieces of the left and right prefrontal bones are present thus it is not possible to determine whether the prefrontal would have contacted the postorbital.

The medial half of the left lacrimal and an almost complete right lacrimal are preserved in SAM-PK-K11655 (Figs. 14). The dorsal region of the right lacrimal bone is missing (Fig. 15C), but the anterior end of the large nasolacrimal canal is preserved and clearly visible. The nasolacrimal canal begins posteriorly as two foramina located intra-orbitally at the posterior surface of the lacrimal. The dorsal foramen is considerably smaller than the ventral foramen. The lacrimal contacts the pterygoid and ectopterygoid ventrally, jugal laterally, maxilla anteriorly, nasal anteromedially, and the prefrontal posteromedially.

Only two posterior fragments of the frontal are preserved. The anterolateral edges of the frontal fragments form a triangular process which extends between the prefrontal and the postorbital but does not contribute to the orbit (Fig. 15C). Fragments of the left and right postorbital are preserved. There is more of the left postorbital remaining, but neither fragment preserves any indication of the postorbital bar (Fig. 15C). A small piece of the left parietal and most of the lateral surface of the right parietal are present. Neither of the parietal bones provides any anatomical features for description, however they outline where the forebrain region of the endocast of SAM-PK-K11655 would have been (see description of the endocast, below).

Braincase and Occiput

The epipterygoid is a mediolaterally flat bone situated posterodorsally to the pterygoid. The bone is vertically oriented and the lateral surface of the epipterygoid is concave in dorsal view (Figs. 14B and 15). It forms most of the thin lateral wall of the braincase. The epipterygoid contacts the prootic posteriorly, the basioccipital medially, the postorbital anterodorsally and the parietal dorsally. The anteromedial region of the footplate of the epipterygoid contacts the dorsolateral margin of the pterygoid. The posterior process of the epipterygoid sits dorsally to the quadrate ramus of the pterygoid and extends posterolaterally toward the quadrate.

The prootic is located posteriorly to the epipterygoid and forms part of the lateral wall of the braincase (Fig. 17). It also forms the anterior margin of the inner ear and the anterior rim of the fenestra vestibuli ventrally. The prootic bones of SAM PK-K11655 are relatively well preserved, however, the medial and anteromedial portions of both the left and right prootic are damaged. Thus, the left and right pila antotica of the prootic bones are not preserved. Damage prevents observation of most of the sutures with other bones. The prootic is triangular in occipital view and concave on its medial surface (Fig. 17). Despite damage to the bones, the prootic and opisthotic appear separated, unlike in galesaurids and most eucynodonts, in which the prootic and opisthotic are almost completely fused (Pusch *et al.* 2019). The prootic sutures with the epipterygoid anteriorly and anterolaterally, the parabasisphenoid complex anteromedially, and the basioccipital posteromedially. Posteriorly, the prootic is in contact with the opisthotic and the squamosal posterolaterally. In other basal cynodonts, the prootic forms the anterior and anterolateral borders of the vestibule of the inner ear. The opisthotic forms the posterior and posterolateral border of the vestibule and the basioccipital forms the medial border (Pusch *et al.* 2019, 2023). Not enough of the prootic and opisthotic are preserved to enable reconstruction of the complete vestibule (Fig. 17). The anterodorsal and anterolateral portion of the prootic is partially preserved and allows for a partial reconstruction of sections of the semicircular canals of the inner ear (Fig. 18). The anterior semicircular canal is a very narrow tubular canal. What

remains of the canal is 2.59 mm long. Only the anterior half of the lateral semicircular canal is preserved and measures 2.8 mm. The lateral semicircular canal appears thicker and more bulbous than the other semicircular canals. This morphology may not be correct as the lateral semicircular canal lies within a region of the prootic that is damaged, thus making proper digital reconstruction of this canal difficult.

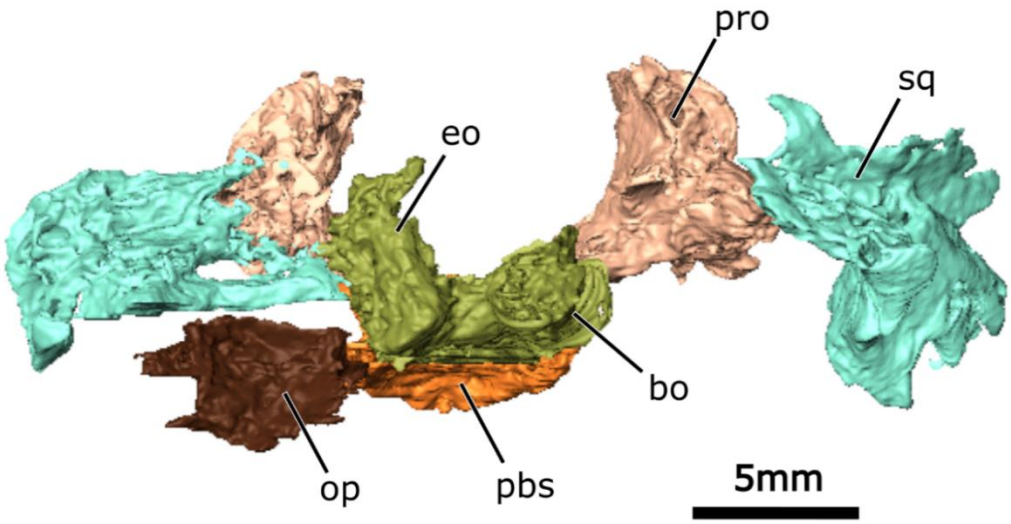

Figure 17: cranium of SAM-PK-K11655 in occipital view. Abbreviations: bo, basioccipital; eo, exoccipital; op, opisthotic; pbs, parabasisphenoid; pro, prootic; sq, squamosal.

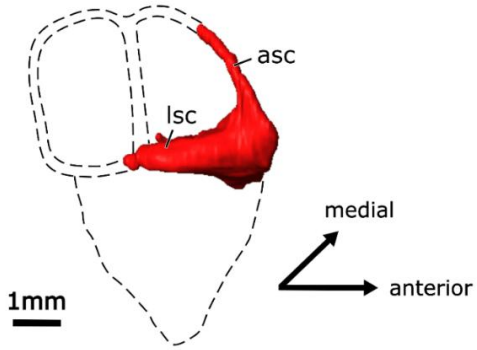

Figure 18: three-dimensional reconstruction of the right inner ear of SAM-PK-K11655 in right lateral view. Dotted black line indicates the hypothetical shape of the rest of the inner ear based on the inner

morphology seen in other basal cynodonts (see Pusch *et al.* 2024). Abbreviations: asc, anterior semicircular canal; lsc, lateral semicircular canal.

The basisphenoid and parasphenoid are fused to form the parabasisphenoid complex (Fig. 15). This structure forms the floor of the braincase. The processus cultriformis of the parasphenoid projects slightly dorsally from the anterior-most point of the parasphenoid in the sagittal plane and terminates abruptly at the posterior border of the pterygoid. This morphology is seen in specimens of *Progalesaurus* (Pusch *et al.* 2024) and differs from other cynodonts in which the processus cultriformis extends from the parasphenoid along the dorsal surface of the pterygoids and terminates just before the anteromedial portion of the pterygoids (i.e., *Galesaurus* (Pusch *et al.* 2019), *Cynosaurus*, *Nythosaurus* and *Nanictosaurus* (Pusch *et al.* 2024)). In SAM-PK-K11655, the posterodorsal surface of the parabasisphenoid is damaged and the sella turcica is only partially visible. A carotid foramen is present on either side of the sella turcica, as in all other epicynodonts, as well as *Lumkuia* (Hopson & Kitching 2001). In dorsal view the foramina are located in the middle of the anteroposterior length of the sella turcica. In ventral view, they are slightly posterior from the position noted on the dorsal surface. In ventral view, the posterior portion of the parabasisphenoid has lateral projections that extend posteriorly around the lateral margins of the basioccipital. These projections (lateral tubera) have an inverted U-shape that surrounds the anterior and lateral margins of the basioccipital. This U-shape is seen in other basal cynodonts such as *Thrinaxodon*, *Nythosaurus*, *Vetusodon*, *Cynosaurus* and *Progalesaurus* (Fourie 1974; Sidor & Smith 2004; Van den Brandt & Abdala 2018; Abdala 2019; Pusch *et al.* 2023). There are prominent crests that diverge from the point of the dorsum sellae and span the anteroposterior length of the lateral tubera. The posterior margin of the basisphenoid is concave in ventral view and is characterised by the dorsum sellae, a prominent notch that sits along the midline of the posterior margin of the basisphenoid. The unossified region is a space which separates the basisphenoid from the basioccipital (Pusch *et al.* 2019). In SAM-PK-K11655, this space is very small (Fig. 15A).

The dorsal region of the skull is weathered away and the orbitosphenoid is not preserved. The basioccipital forms the posterior floor of the braincase and contributes part of the occipital condyle (Figs. 15 and 17). The posterior portion of the basioccipital of SAM-PK-K11655 is dumbbell shaped in dorsal view and narrows into a U-shape at its anterior edge. Despite damage to both the ventral and dorsal surfaces, a slight depression is noted on the anterior half of the dorsal surface of the basioccipital (Fig. 15A). This depression would have housed the hindbrain region (Pusch *et al.* 2019). In occipital view, there are two condyles at the posterior margin of the basioccipital which contribute the ventral rim of the double occipital condyles of the foramen magnum.

The supraoccipital and most of the exoccipitals of SAM-PK-K11655 are not preserved (Fig. 17). Only a small fragment of the left exoccipital is preserved, but due to weathering, the suture line between the exoccipital and the dorsal margin of the basioccipital could not be distinguished. The exoccipital forms the lateral margin of the foramen magnum and most of the occipital condyle (Pusch *et al.* 2019).

Only a small portion of the left opisthotic is preserved in SAM-PK-K11655 and is ventrally displaced from its anatomical position (Fig. 17). The opisthotic contributes the posterior margin of the inner ear and contacts the prootic anteriorly. Due to damage, the fenestra vestibuli cannot be described. The paraoccipital process of the opisthotic is not preserved. The medial region of the opisthotic is missing; however, it would have sutured with the lateral margin of the basioccipital to form the anterior half of the jugular foramen (Pusch *et al.* 2019). The dorsal surface of the left opisthotic is damaged, and the ventral margin of the post-temporal foramen is not visible.

Both the left and right squamosal bones are preserved but damaged on the medial and anterior surfaces (Fig. 17). There is an anterolateral projection of the squamosal, ending in a narrow vertical rim which acts as the facet for articulation with the surangular. The post-temporal fenestra is usually enclosed by the tabular, with contributions from the squamosal to the lateral border (Pusch *et al.* 2019). Since the tabular and most of the squamosals are not preserved in SAM-PK-K11655, the post-temporal fenestra is not preserved.

The left and right quadrate are preserved but have been damaged by weathering (Figs. 14 and 19). It appears that only the trochlear portion of the quadrate is preserved, with the dorsal plate of the quadrate missing. The trochlear region of the quadrate is anteroposteriorly narrow and has a slight concavity on its anterior surface for articulation with the articular bone of the lower jaw (Fig. 19).

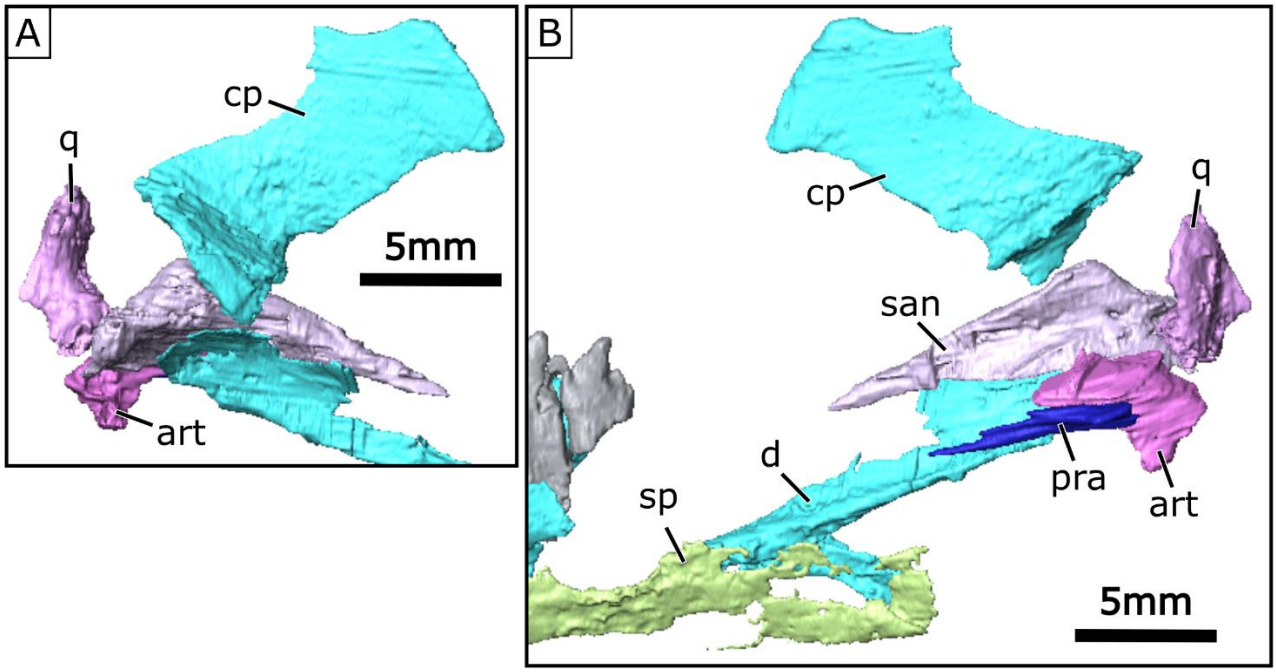

Figure 19: Magnification of the articulation bones of the right lower jaw of SAM-PK-K11655 in (A) right lateral and (B) right medial views. Abbreviations: art, articular; cp, coronoid process of the dentary; d, dentary; pra, prearticular; q, quadrate; sp, splenial; sur, surangular.

There is insufficient bone preservation to determine the entire morphology of the endocast. Therefore, observations are made from the mould of the endocast that are visible on the dorsal surface of the skull (Fig. 16). The olfactory bulbs are located at the anterior most part of the endocast. The olfactory bulbs are wider than the hemispheres (6.03 mm compared to 5.52 mm respectively). The bulbs are slightly anteroposteriorly convex in dorsal view (Fig. 16) and separated by a shallow depression running along the midline. Just posterior to the olfactory bulbs, there is a slight depression

identified as the forebrain. Based on the morphology of the partial frontal and parietal bones of SAM-PK-K11655, the forebrain would have been tubular. The surface of the endocast, apart from the presence of the cast of the parietal foramen, appears smooth, with no sulci or shallow depressions, aside from the very shallow depression extending anteroposteriorly along the midline of the endocast. This depression may be a possible cast of the sagittal suture of the parietal. Posterior to the pineal body there is an unossified region of the brain endocast. The posterior portion of the skull is missing therefore no observations can be made about the hindbrain and associated structures.

Lower jaw

Both the left and right dentaries of the lower jaw are preserved but damaged anteriorly (Fig. 20). The anterior region of the right dentary is better preserved than the left one. The right dentary preserves the tooth bearing portion of its ramus, and a portion of the coronoid process, and reflected lamina of the angular bone of the dentary. The posterior half of the left dentary is damaged, preserving only a small section of the reflected lamina. The dentary is mediolaterally thick at its anterior end, in dorsal view and narrows towards the posterior end until it is a thin sheet of bone (Fig. 20A). From anterior to posterior, the horizontal ramus of the dentary is concave along its dorsal surface and convex along its ventral surface. In lateral view, the dentary ramus extends to the level of the jugal, and the coronoid process extends from the level of the jugal to that of the parietal. There are eight alveoli in both the left and right dentary, all of which contain postcanines at varying degrees of damage, except for the penultimate left alveolus which has no tooth preserved. The left and right dentary are fused at the dentary symphysis. A fused dentary symphysis is considered a synapomorphy of eucynodonts (Hopson & Kitching 2001). However, there are exceptions, such as the Middle Triassic cynodont *Bolotridon frerensis*, a recently resurrected taxon considered stemward of eucynodonts (Pusch *et al.* 2021). A dentary foramen is present on the lateral side of the right dentary, at the level of the first postcanine (Fig. 20A). The left coronoid process of the dentary is not preserved in SAM-PK-K11655, but the right

coronoid process is preserved as a mould in the rock matrix (Fig. 14C). Where the coronoid would meet the dentary ramus, it has a height of 10.43 mm. The dorsal most point of the coronoid process is missing however the mould of this section is preserved. Both the left and right splenial are preserved but damaged at their posterior ends due to recent post-burial weathering (Fig. 20A and B). The splenial is a sheet-like piece of bone that extends along the length of the medial surface of the horizontal ramus of the dentary.

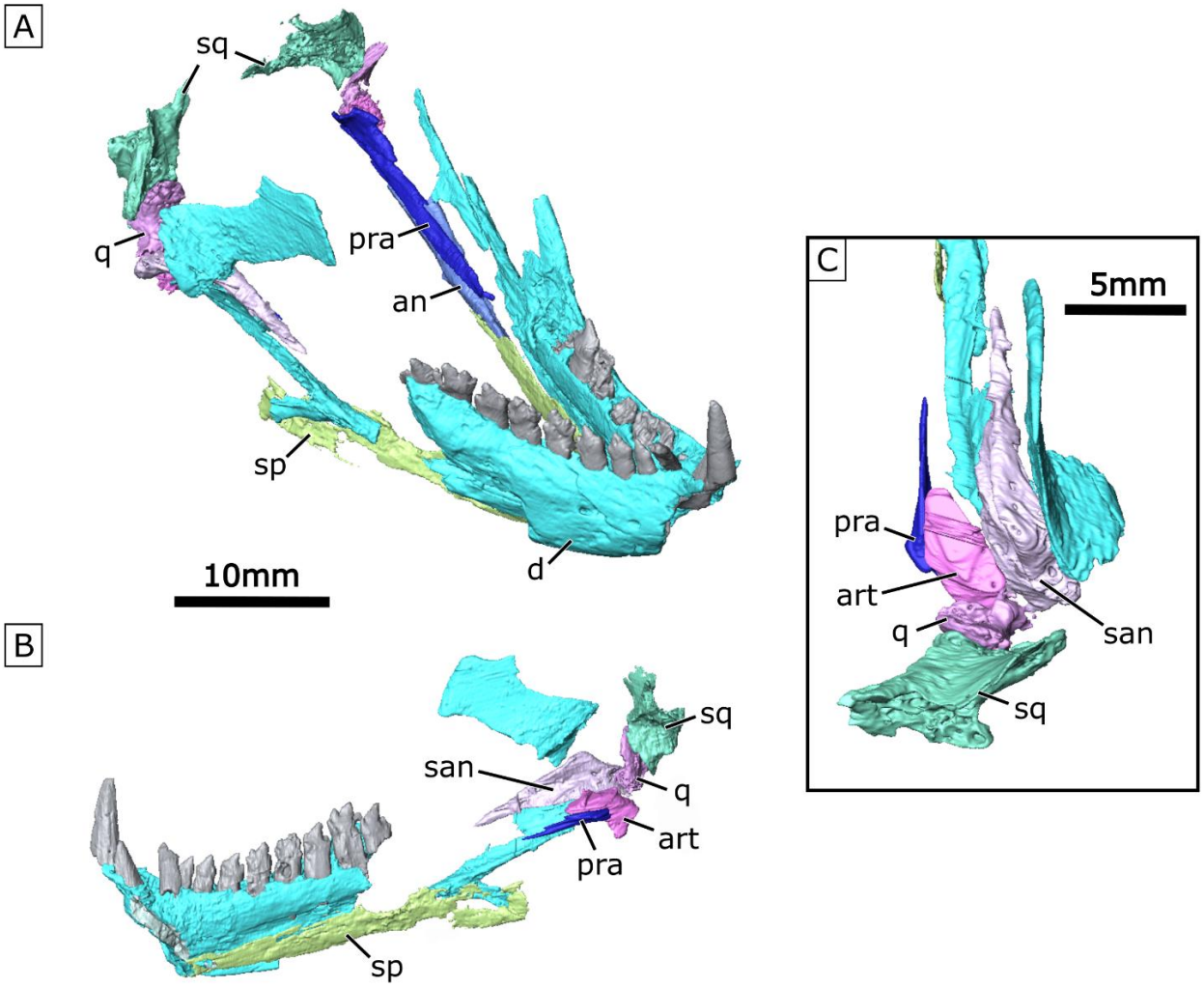

Figure 20: mandible of SAM-PK-K11655 in (A) angled right lateral view, (B) right lower jaw in medial view and (C) enlarged jaw articulation of SAM-PK-K11655 in dorsal view. Abbreviations: an, angular; art, articular; d, dentary; pra, prearticular; q, quadrate; san, surangular; sp, splenial; sq, squamosal.

Only the left angular is preserved (Fig 20A). The angular is a mediolaterally compressed, appearing plate-like, vertically oriented bone. It lies along the medial surface of the dentary, forming the ventral and posterolateral margins of the dentary. The posterior end of the angular is not preserved, therefore no observations of the reflected lamina can be made. Along the middle of the bone on the lateral surface, two ridges develop – one dorsal and one ventral – and branch away from each other as they extend further posteriorly. This creates a shallow V-shape on the lateral surface of the angular. The angular lies laterally to the surangular. The dorsal portion of the angular contacts the lateral surface of the prearticular.

The right surangular is preserved. The posterior end of the surangular is triangular in lateral view and is robust (Fig. 19). The articulation facet at the posterior end of the surangular is rounded on its dorsal surface and then slopes posteroventrally at almost 45° (Fig. 20B). This creates a platform for articulation with the squamosal. The anterior most point of the squamosal is damaged, however the placement of the squamosal in relation to the angular suggests a squamosal-surangular articulation (Fig. 20C).

Both articulars are poorly preserved but the left articular shows a clear articulation facet for the left quadrate (Fig. 19B). The facet is mediolaterally expanded and concave to correspond with the convex articular facet of the quadrate. The left and right prearticular are preserved. The prearticular lies medially to the articular and extends anteriorly (Fig. 20A and B). Where it is intact, the anterior elongation of the prearticular extends anteriorly and lies along the medial surface of the angular. Specimen SAM-PK-K11655, like *Cistecynodon*, preserves a double jaw articulation. However, in SAM-PK-K11655 the jaw articulation is articular-quadrate and surangular-squamosal (Fig. 20C), unlike in *Cistecynodon* in which the surangular articulates with the anterolateral rim of the quadrate (Fig. 12D).

Dentition

The anterior-most region of the snout is damaged therefore no upper or lower incisors are preserved. The right maxilla preserves one functional canine, a remnant root of the previous canine, a replacement canine and eight postcanines (Fig. 21B). The left maxilla only preserves six postcanines (Fig. 21A). The right mandibular series consists of the functional canine, and its replacement canine, with eight or nine postcanines in the right dentary (Fig. 21D) whereas the left only preserves a series of seven postcanines (Fig. 21C).

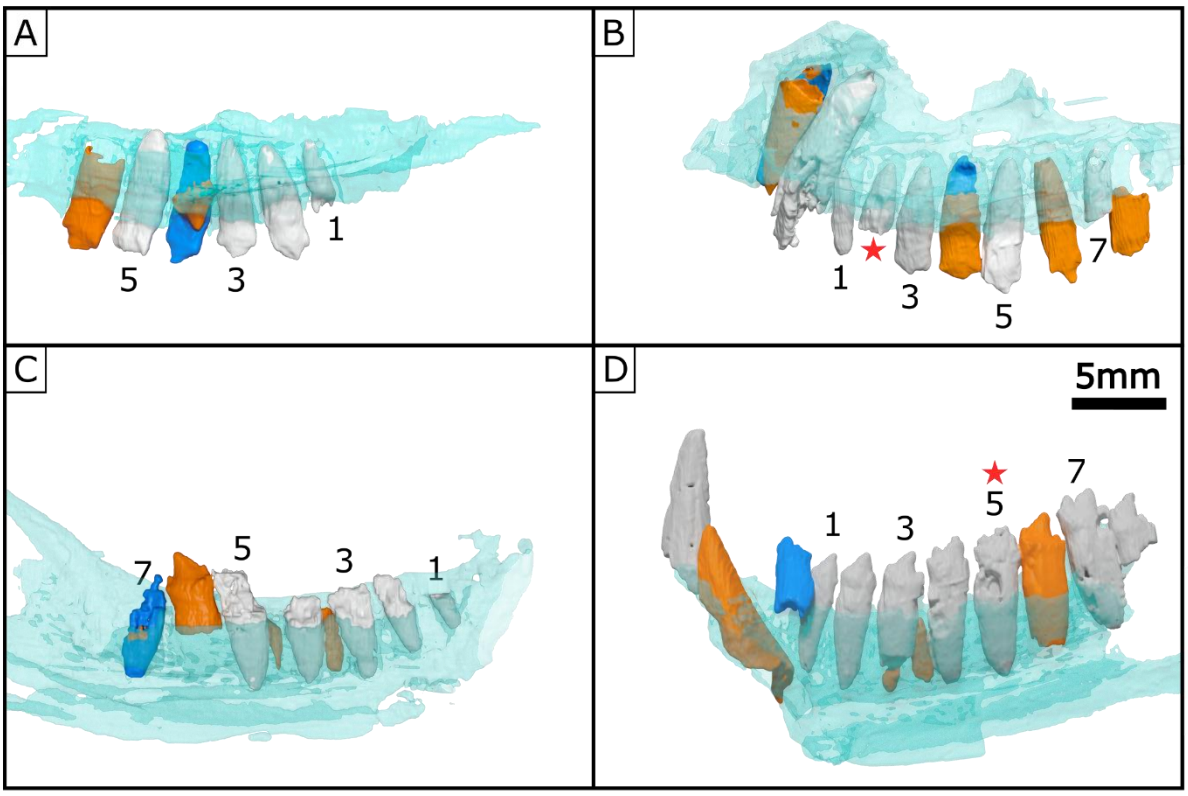

Figure 21: Dentition of SAM-PK-K11655 in lingual view. (A) Left upper dentition, (B) right upper dentition, (C) left lower dentition and (D) right lower dentition. Functional teeth appear in grey, replacement teeth in orange and remnant roots in blue. Red stars indicate postcanines which have resorption pits.

In the upper dentition, one functional canine, a replacement canine and the remnant root of the previous canine are preserved. The single right upper canine is conical and directed slightly rostrally, with a small opening at the tip of the root (Fig 21B). A replacement canine is located anteromedially to the erupted canine and has a large open root. Lateral to the replacement tooth is the remnant root of the previous functional canine. The root and crown of the remnant canine are in the process of being resorbed, leaving only the lateral side of the remnant tooth. The replacement canine is erupting into the space where the remnant canine was originally located. In the right mandibular series, there is one functional canine (Fig. 12D). It is conical and oriented almost vertically, like in *Cistecynodon* (Fig. 13) but unlike *Lumkuia* which is laterally compressed (Hopson & Kitching 2001). The replacement canine lies posteromedially to the functional canine and the root of the functional canine has been resorbed. The replacement tooth has an open root, indicating that this tooth was still in the process of developing and erupting. There are no serrations on the canines. The absence of canine serrations is a synapomorphy of Cynodontia (Pusch *et al.* 2024).

All upper and lower postcanines are mesiodistally elongated and lateromedially narrow, each with a gentle posterior recurve of the main cusp (Fig. 21). The recurve of the main cusp is not as distinct as what is seen on the dentition of *Galesaurus*, in which the main cusp is crescent moon-shaped (Pusch *et al.* 2019). Only the root of PC2, PC4, PC7 and the damaged crown of PC8 are preserved in the right maxilla (Fig. 21B). However, there is a resorption pit forming in the root of PC2 which is indicates that a replacement tooth was going to start developing (Norton *et al.* 2020). The roots of PC4 and PC6 are open, as these are replacement teeth that have erupted but are not yet completely closed at the root. The crown of PC1 is preserved but damaged at the anterior-most point of the crown, therefore no inferences can be made regarding crown morphology. PC5 and PC6 are tricuspid, each with a small anterior and posterior cusp and a slightly recurved main cusp (Fig. 21B). The crown of PC3 is slightly damaged but it appears that it would have also been tricuspid. There is a replacement tooth for PC4, which has a developed crown and has begun resorbing the root of the remnant tooth. The cusp count on PC4 cannot be assessed due to damage of the crown. Tooth PC7 preserves an open root only and

also has a small pit forming within the root of the remnant tooth. This may indicate evidence of resorption; however, it is possible that the crown of PC7 broke off at the point where the tooth is exposed out of the alveolus of the maxilla.

The upper left postcanines are poorly preserved, with only PC1-6 present (Fig. 21A). Tooth PC1 is damaged and the crown of PC5 is damaged, thus no inferences can be made on their morphology. There are open roots present at PC4, PC6 and PC8. Teeth PC2, PC3 and PC4 appear tricuspid, however there is slight erosion of the crowns which may affect the cusp count (Fig. 21A). The crown of PC6 is partially eroded, but there are remnants of cusps, suggesting at least 3 (possibly 4) cusps. There is a developing replacement tooth noted for PC4.

On the lower jaw, replacement teeth are present for pc1 in the right dentary and pc3 and pc5 in the left dentary. There are open roots on the left pc6 and on the right pc3 and pc6. The anteroposterior width of the postcanine teeth increases from anterior to posterior (Fig. 21C and D). In the right dentary, pc1 and pc2 have a single, slightly recurved main cusp, but there may be very small anterior and posterior cusps on pc2, indicating that it could be tricuspid (Fig. 21D). The third postcanine is tricuspid, with the main cusp slightly recurved, a small anterior cusp and a posterior cusp that is slightly larger than the anterior one. From pc4 to pc8, each tooth has a main cusp that is slightly more recurved than pc1 and pc2 but have variations in anterior and posterior cusp number and location. The pc4 is tetracuspid, with a main cusp, two small anterior cusps (one located more buccally/laterally and the other more lingually) and a small posterior cusp. The crown of pc5 is damaged, but there are remnants of cusps which indicate that it had possibly 4-5 cusps. There is also a resorption pit forming in the root of pc5 for a replacement tooth (Fig. 21D). The lower right pc6 is pentacuspid, with one large recurved main cusp, two small anterior and two small posterior cusps. and pc7 have a large main cusp, and two small anterior cusps. Two small posterior cusps are present in pc6, whereas pc7 only shows evidence of one posterior cusp, as the posterolingual region of the tooth is damaged. Lower pc8 has a large main cusp, one small anterior cusp that is located lingually, and two small posterior cusps. All

postcanines in the left dentary are damaged beyond possible description, except for pc6 (Fig. 21C). The sixth postcanine is pentacuspid and shares the same cusp morphology as the right pc6 (Fig. 21C and D).

Postcrania

Pectoral girdle

SAM-PK-K11655 preserves elements of the left pectoral girdle. The procoracoid, coracoid, clavicle and scapula are present but are disarticulated. Most of the clavicle is preserved (Fig. 22). The lateral end of the clavicle is rod-like, connected to the medial end by a twisted diaphysis. The medial half of the clavicle gradually expands mediolaterally into thin, spoon-shaped sheet of bone (Fig. 22A). The lateral end of the clavicle is missing but would have articulated with acromion process of the scapula.

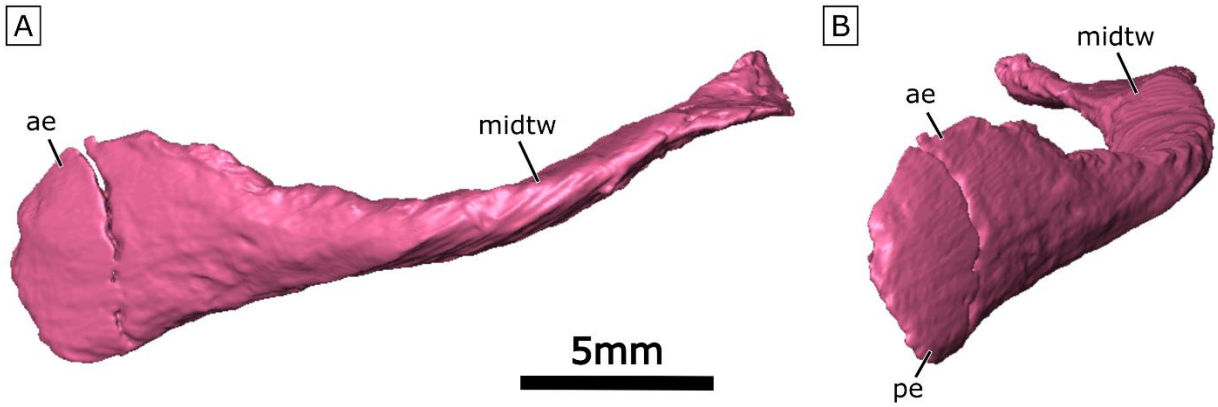

Figure 22: The left clavicle of SAM-PK-K11655 in (A) anterior and (B) medial view. Abbreviations: ae, anterior edge of the medial end of the clavicle; midtw, midlength twist of the clavicle; pe, posterior edge of the medial end of the clavicle.

The distal end of the scapula of SAM-PK-K11655 is preserved. The diaphysis and blade of the scapula are missing. In lateral and medial view, the neck of the scapula is narrower than the base (Fig. 23). The base of the scapula articulates with the coracoid and precoracoid. In SAM-PK-K11655 these elements remain separated, but this is possibly due to taphonomical processes. There are two articular surfaces. The anterior surface is large and bulbous (Fig. 23A), whilst the posterior articular surface is smaller, somewhat flatter, and slightly ovoid. The smaller articular surface is the glenoid buttress of the scapula which contributes to the glenoid cavity of the pectoral girdle. The larger articular surface articulates with the posterodorsal surface of the procoracoid anteriorly and with the anterodorsal surface of the coracoid posteriorly (Fig. 23). These surfaces are separated by a low, mediolaterally oriented ridge. On the anterior margin of the base of the scapula, there is a slight crest visible in lateral view. In more derived cynodonts, this crest is more pronounced, and is the acromion process of the scapula, but in basal cynodonts such as *Thrinaxodon*, *Galesaurus* and *Prosynosuchus*, this process is completely absent (Jenkins 1971; Kemp 1979; Butler *et al.* 2019). Due to damage to this surface in SAM-PK-K11655, it is not possible to determine whether an acromion process is present (Fig. 23).

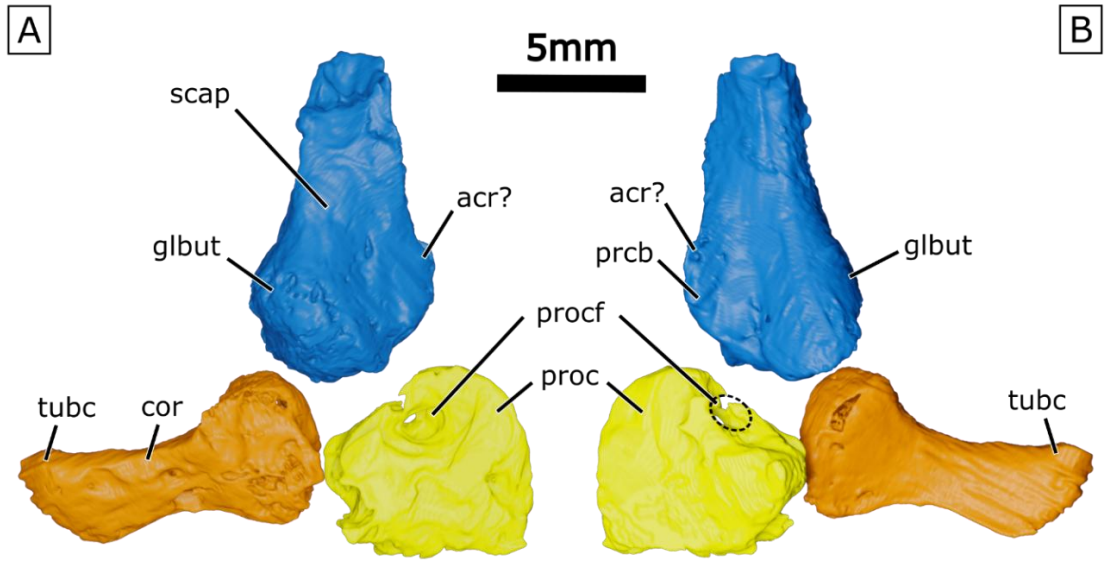

Figure 23: digitally reconstructed pectoral girdle of SAM-PK-K11655 in (A) medial and (B) lateral views. Abbreviations: acr?, acromion process; cor, coracoid; glbut, glenoid buttress; proc, procoracoid; procf, procoracoid foramen; prcb, procoracoid buttress; scap, scapula; tubc, tuber coracoideus.

The procoracoid is preserved as a small, anteroposteriorly compressed, rhomboidal bone (Fig. 23). It is damaged on the medio- and lateroventral edges but preserves the circular procoracoid foramen. The procoracoid is disarticulated from the coracoid. These elements are usually in close sutural contact with one another. In other cynodonts like *Thrinaxodon* and *Cynognathus* (Jenkins 1971), these elements are fused and in *Lumkuia* they are partially fused (Benoit *et al.* 2022a). Here, their unfused condition may be because the specimen is a juvenile (see discussion). In lateral and medial view, it appears that the procoracoid has a larger surface contact with the scapula than that of the coracoid with the scapula (Fig. 23). However these bones are damaged, so the full extent of the contact of either bone with the scapula cannot be confidently assessed. The procoracoid plate thickens slightly along its anterior edge. Normally, the procoracoid articulates with the scapula and coracoid via a lateral buttress (Benoit *et al.* 2022a), but in SAM-PK-K11655 this surface is damaged (Fig. 23). The procoracoid contributes to the glenoid cavity in cynodonts such as *Thrinaxodon* (Jenkins 1971), with less of a contribution seen in eucynodonts such as *Lumkuia* and *Cynognathus* (Jenkins 1971; Benoit *et*

al. 2022a). Due to the surface damage of the postcrania, this contribution is not able to be confidently assessed.

The coracoid of SAM-PK-K11655 is short and robust. In lateral view the bone is concave along its dorsal edge. The coracoid buttress is very large and bulbous. The coracoid buttress forms the majority of the glenoid cavity. The glenoid cavity is incomplete because of damage to the bones that contribute to it. In dorsal view, there is a prominent groove lateral to the coracoid buttress on the more posterior side of the bone. The ventromedial surface of the coracoid is missing.

Phylogenetic placement of BP/1/2520 and SAM-PK-K11655 within Cynodontia

Specimens BP/1/2520 and SAM-PK- K11655 were added to the data matrix used by Pusch *et al.* (2024). The analysis resulted in two most parsimonious trees, from which a strict consensus tree was generated (Fig. 24). The consensus tree has a length of 340 (CI = 0.56, RI = 0.75). *Abdalodon* and *Charassognathus* form a clade at the base of the cynodont tree. From this, BP/1/2520 and SAM-PK-K11655 branch in successive grades more derived than *Dvinia* and *Procynosuchus*, which makes them basal epicynodonts. Synapomorphies that support the inclusion of BP/1/2520 and SAM-PK-K11655 within Epicynodontia are: character 32 (Transverse lamina position - BP/1/2520 and SAM-PK-K11655 coded as (1) Anteriorly, just behind the palatal process of the maxilla), character 60 (Parabasisphenoid-basioccipital suture in ventral view - BP/1/2520 and SAM-PK-K11655 coded as (1) Inverted V- or U-shaped), character 63 (Prootic lateral exposure - BP/1/2520 and SAM-PK-K11655 coded as (0) Curved, extending anteroventrally to posterodorsally), character 85 (Mandibular symphysis - BP/1/2520 and SAM-PK-K11655 coded as (1) Fused), character 91 (Mandibular fenestra between dentary and angular - BP/1/2520 and SAM-PK-K11655 coded as (0) Absent). In this analysis, based on Hopson and Kitching's (2001) definition of Epicynodontia (Epicynodontia being the clade that includes Mammalia, but excludes *Procynosuchus*), SAM-PK- K11655 is recovered as the basal most epicynodont (Fig. 24). The placement of SAM-PK-K11655 as the basal-most epicynodont is supported by the following: character 61 (Posterior wings of basisphenoid/parasphenoid ala – SAM-PK-K11655 coded as (0) Form raised tubercles making up anterior half of the basal tubera), character 90 (Dentary coronoid process position in temporal fenestra – SAM-PK-K11655 coded as (0) Lateral), character 94 (Angular lateral surface with elongated crest – SAM-PK-K11655 coded as (1) Present) and character 112 (Postcanines main cusp – SAM-PK-K11655 coded as (1) Strongly recurved). Specimen SAM-PK-K11655 shares characters 61, 90, 94 and 112 with BP/1/2520. However, SAM-PK-K11655 separated from BP/1/2520 and the remaining epicynodonts by character 88 (Lateral crest of dentary). SAM-PK-K11655 is coded as 0 (lateral crest absent) and BP/1/2520 is coded as 1 (lateral crest incipient). The following synapomorphies separate BP/1/2520 from more derived the epicynodonts: character 18 (Lacrimal posteroventral flange -

BP/1/2520 coded as (1) Largely restricted to region below border of prefrontal), character 23 (Jugal anterior extent - BP/1/2520 coded as (0) Extends anteriorly beyond anterior margin of orbit), character 30 (Vomerine-pterygoid contact in ventral view - BP/1/2520 coded as (2) Posterior portion of vomer extending far posteriorly, almost reaching the basicranial girder and covering much of the ventral surface of the pterygoids), character 53 (Pterygoid quadrate ramus - BP/1/2520 coded as (1) Absent), character 56 (Epipterygoid quadrate ramus - BP/1/2520 coded as (1) Contacts the quadrate), character 68 (Squamosal medial process prootic contact - BP/1/2520 coded as (1) Present, enclosing pterygoparoccipital foramen), character 86 (Dentary symphysis morphology - BP/1/2520 coded as (1) Tall, steeply sloping, forming a distinct 'chin'), character 121 (Maxillary canal internal nasal and superior labial rami - BP/1/2520 coded as (1) reduced or absent), character 125 (Fenestra ovalis position - BP/1/2520 coded as (0) Distal or ventrolateral end of vestibule), character 142 (Internal carotid foramina on basisphenoid - BP/1/2520 coded as (1) Absent). Specimen BP/1/2520 is then separated from *Nythosaurus* by: character 11 (Ectopterygoid-maxillary contact - BP/1/2520 coded as (0) Present), character 62 (Parabasisphenoid ventromedian keel - BP/1/2520 coded as (1) Reduced to narrow process) and character 126 (Cochlear canal - BP/1/2520 coded as (0) Absent). The Permian taxa *Vetusodon*, *Nanictosaurus* and *Cynosaurus* are branched within a clade that also gathers all Triassic cynodonts, *Nythosaurus* being the most basal of them. The relationships within Epicynodontia more derived than *Nythosaurus* remains mostly similar to that in Pusch *et al*. (2024). The Probainognathia and Cynognathia clades are supported (Fig. 24).

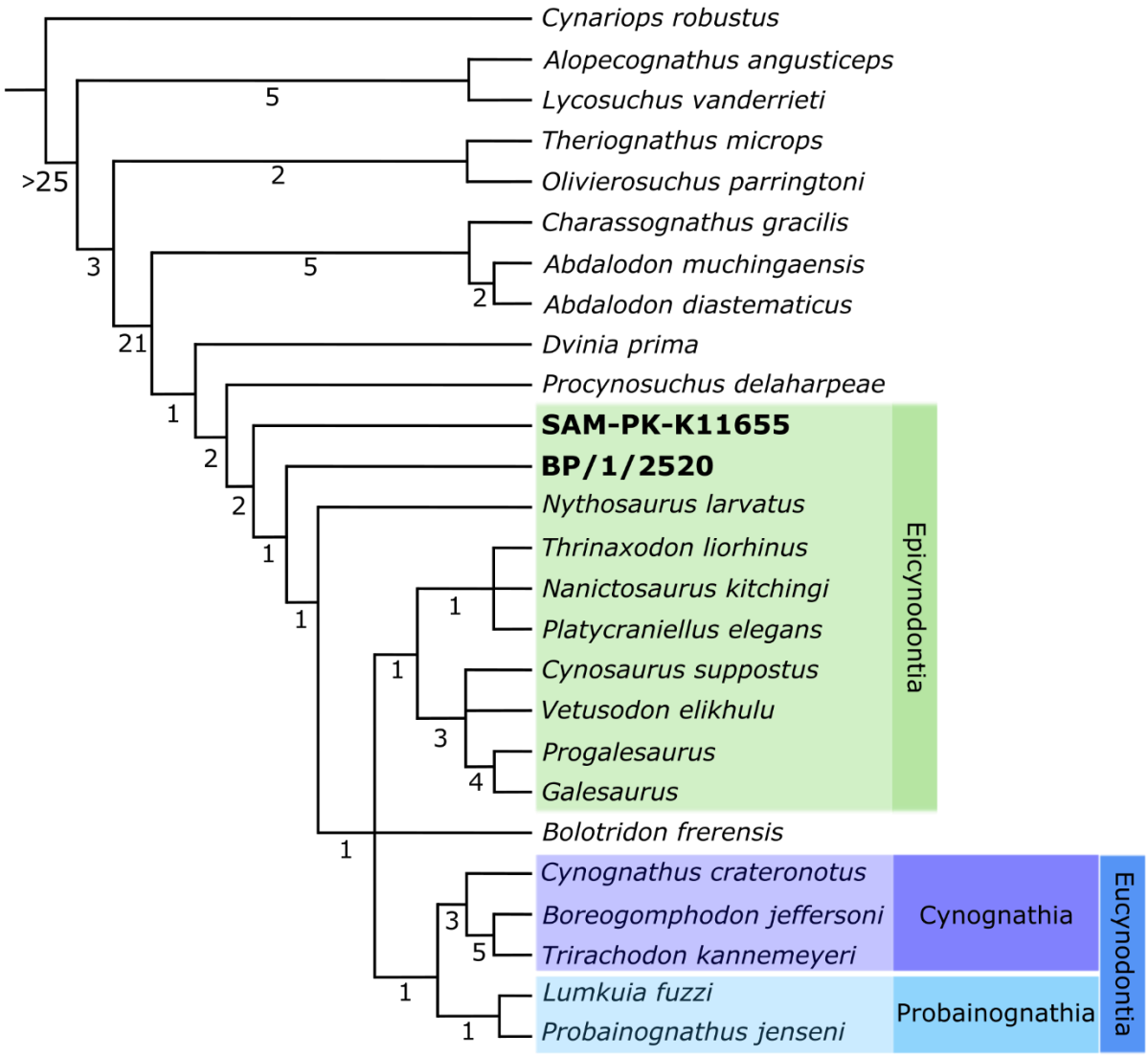

Figure 24: Strict consensus of the phylogenetic analysis of Cynodontia modified from Pusch *et al.* (2024). Tree length is 340, CI = 0.56, RI = 0.75. Numbers below the lines indicate the Bremer support values.

A second phylogenetic analysis was conducted using the matrix from Fonseca *et al.* (2024). The analysis resulted in one most parsimonious tree (Fig. 25). The tree length is 394, with a CI of 0.58 and RI of 0.75. The resulting tree topology is overall consistent with other analyses (i.e. Pusch *et al.* 2021, 2023; Benoit *et al.* 2022a). In this phylogeny, *Procynosuchus* is the most basal taxon, followed by the epicynodonts *Galesaurus* and *Thrinaxodon* branching in a pectinate sequence in this order. Just crownward to *Thrinaxodon*, BP/1/2520 and SAM-PK-K11655 form a clade with *Platycraniellus*. This

clade is supported by these synapomorphies: character 30 (Ectopterygoid – BP/1/2520, SAM-PK-K11655 and *Platycraniellus* coded as (1) Contacts the maxilla), character 31 (Interpterygoid vacuity in adults between pterygoid flanges – BP/1/2520 and *Platycraniellus* coded as (0) Present and SAM-PK-K11655 coded as ? because it is a juvenile (see discussion below)), character 72 (Size of the lateral trochlear condyle relative to the medial trochlear condyle on quadrate- BP/1/2520 and *Platycraniellus* coded as (1) The medial condyle equal or larger than the lateral condyle and SAM-PK-K11655 coded as ?. Two out of the three characters for the clade containing BP/1/2520, SAM-PK-K11655 and *Platycraniellus* are not able to be assessed in SAM-PK-K11655, therefore this clade is not well supported.

BP/1/2520 and SAM-PK-K11655 form a clade to the exclusion of *Platycraniellus*. This clade is supported by the synapomorphies: character 32 (Secondary palatal plate on maxilla reaches midline - coded as (0) Absent), character 33 (Secondary palatal plate on palatine reaches midline – coded as (0) Absent), character 59 (Pterygoparoccipital foramen – coded as (1) Squamosal contributes the enclosure of the foramen), character 118 (Upper tooth series posterior extension – coded as (0) Directed lateral to the subtemporal fossa).

The clade including *Platycraniellus*, BP/1/2520 and SAM-PK-K11655 is then sister to the Eucynodontia (as according to Hopson and Kitching's (2001) definition of the clade). The characters excluding BP/1/2520 and SAM-PK-K11655 from the Eucynodontia are: character 47 (Basisphenoid wing (parasphenoid ala) - BP/1/2520 and SAM-PK-K11655 coded as (0) Long, border the fenestra vestibuli), character 106 (Posterior postcanines with strongly curved main cusp - BP/1/2520 and SAM-PK-K11655 coded as (0) Absent) and character 121 (Morphology of upper postcanines for taxa with sectorial teeth - BP/1/2520 and SAM-PK-K11655 coded as (0) Symmetrical postcanines with main cusp A and small mesial and distal cusps). The clade Cynognathia and Probainognathia are supported, as in the most recent literature (i.e., Pusch *et al.* 2021, 2023; Benoit *et al.* 2022a).

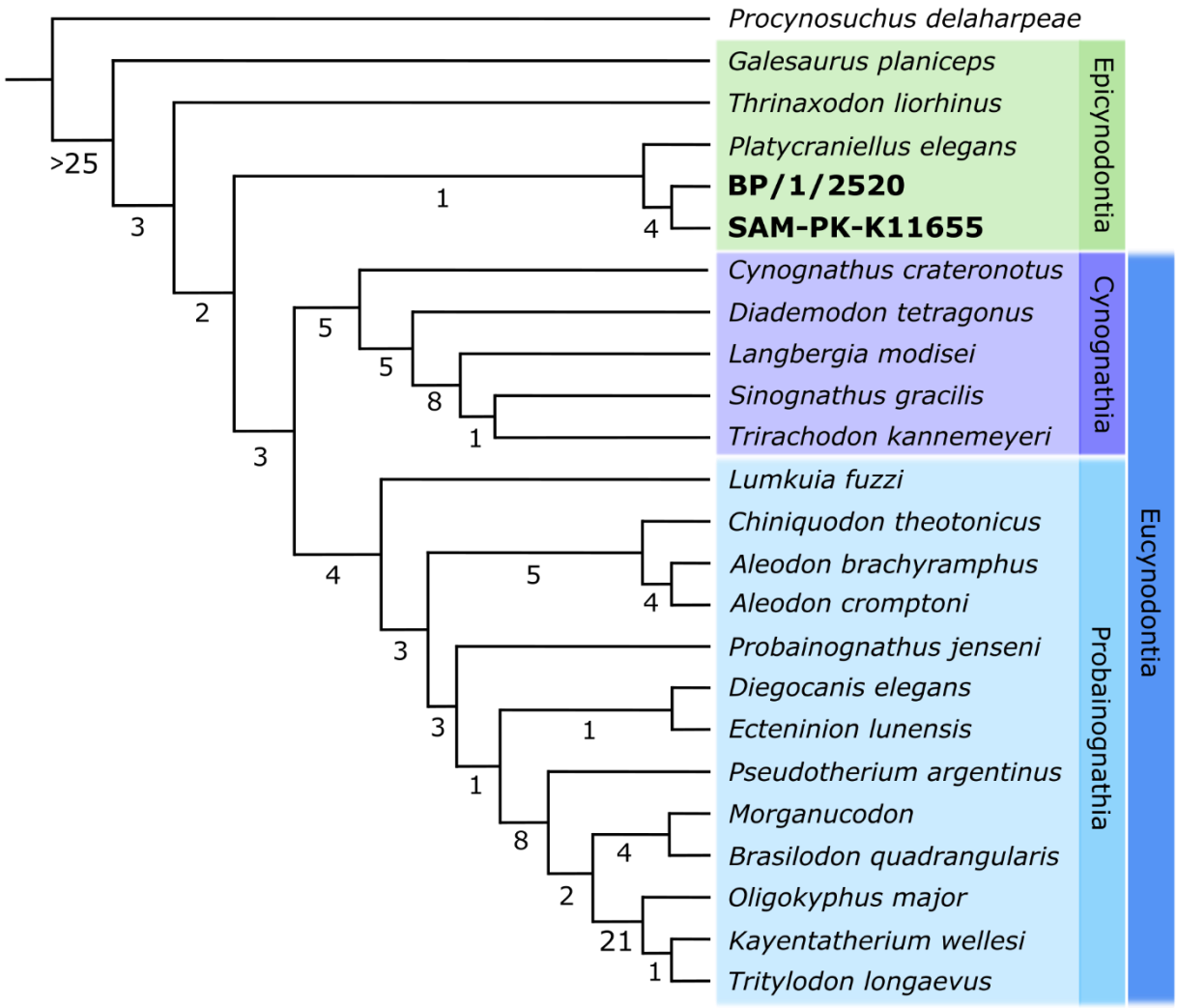

Figure 25: Maximum parsimony strict consensus phylogeny of Cynodontia from Fonseca *et al*. (2024).

Tree length is 394, CI = 0.58, RI = 0.75. Numbers below the lines indicate the Bremer support values.

Discussion

Growth status of BP/1/2520 and SAM-PK-K11655

Specimen BP/1/2520 (*Cistecynodon parvus*) was referred to as a juvenile *Cynognathus* by Hopson and Kitching (1972). However, Brink and Kitching (1953) noted that there is no space after the penultimate upper postcanine for the development of an additional tooth which, in contrast, is suggestive of complete dentition and proximity to adulthood (see also Bonaparte and Barberena 2001). Here, in support to the latter observation, the 3D reconstruction of the dentition of BP/1/2520 shows no evidence of space behind the penultimate postcanine in the upper or lower dentition (Figs. 6B and 12A). In addition, there are open roots on the canines and postcanines , and no replacement teeth for any of these teeth (see Fig. 13). Open roots are associated with the largest, most mature specimens in the basal epicynodont *Galesaurus* (Norton *et al.* 2020). In *Thrinaxodon*, the presence of the open roots on the canines and postcanines, with no replacement teeth present is a characteristic feature noted in subadults, in which the final set of teeth have emerged and are in the process of having the roots close (Abdala *et al.* 2013). Replacement teeth are noted in other basal cynodonts such as *Galesaurus* (Norton *et al.* 2020) and *Cynosaurus* (Norton *et al.* 2021). Interestingly, BP/1/2520 shows similar dental morphology to *Lumkuia fuzzi* (BP/1/2669, a specimen which also has no replacement teeth and open roots on some of the canines and postcanines), an inferred subadult specimen (Benoit *et al.* 2022a). Additional dental evidence for the subadult-early adult age of BP/1/2520 is the considerable wear noted on the postcanine crowns (Fig. 13). Wear on the crowns of the upper postcanines could be attributed to taphonomical processes during fossilisation, or weathering of the specimen thereafter. However, the lower postcanines are medial to (and thus protected from erosion by) the upper dentition, yet these teeth also show considerable wear. This wear may then have been caused by extended use of the teeth during the individual's life.

Specimen BP/1/2520 also displays cranial morphology indicative of a subadult or adult age. These include signs of advanced suture closure on the skull (including both parietals fused together, as well

as the bones of the occiput and periotic that are fused (Fig. 7A)). The parietal fuses behind the parietal foramen in adult *Cynosaurus* (Van den Brandt & Abdala 2018), *Thrinaxodon* (Fourie 1974), *Galesaurus* (Pusch *et al.* 2019) and *Progalesaurus* (Sidor & Smith 2004). Subadult specimens of *Galesaurus* also begin to show signs of fusion of the parietals behind the parietal foramen (Pusch *et al.* 2019), thus supporting this feature in BP/1/2520 as a subadult or adult trait. Specimen BP/1/2520 has two narrow, elongated interpterygoid vacuities (Fig. 6), similar in morphology to that seen in either juvenile and/or subadult specimens of *Thrinaxodon* (Estes 1961) and *Lumkuia* (Hopson & Kitching 2001); however, interpterygoid vacuities are present in adult specimens of basal cynodonts such as *Procynosuchus* (Kemp 1979). Thus, this morphology is considered plesiomorphic in cynodonts (Hopson & Kitching 2001) and is reconstructed as such for *Cistecynodon* in the phylogenetic analyses (Figs. 24 and 25). In conclusion, the evidence points towards a subadult or early adult age for the holotype of *Cistecynodon*.

The age category of SAM-PK-K11655 was not assessed by Wolvaardt *et al.* (2023), however digital segmentation of this specimen indicates that it displays clear signs of juvenility. All of the cranial sutures are wide open and on the extensive evidence for intense dental replacement. There are replacement teeth for both the canines and postcanines on the upper and lower dentition (Fig. 21). The pattern of tooth replacement in SAM-PK-K11655 is similar to that seen in *Thrinaxodon*, *Galesaurus* and *Cynosaurus*, in which there is an alternating pattern of tooth replacement of the postcanines (Abdala *et al.* 2013; Norton *et al.* 2020, 2021).

In SAM-PK-K11655, there is some evidence for the same alternating pattern in the upper dentition. In the upper right dentition, PC4, PC6 and PC8 are replacement teeth (Fig. 21B). However, this alternating pattern is disrupted by the presence of a replacement tooth for PC7. An alternating replacement pattern is noted in the upper left dentition with PC4 and PC6 present as replacement teeth (Fig. 21A). It appears that the first three postcanines in the upper dentition of SAM-PK-K11655 have not undergone replacement or are in the process of developing replacement teeth. In *Thrinaxodon*,

juvenile specimens appear to have replacements for PC2, thus suggesting that the lack of a replacement tooth for the PC2 of SAM-PK-K11655 may indicate that it is not a very young juvenile (Abdala *et al.* 2013). It may be a slightly older juvenile, bordering on progressing into its subadult stage. In subadults of *Thrinaxodon*, the replacement PC2 is more erupted – this may also be the case for SAM-PK-K11655, suggesting that it is somewhere between a juvenile and a subadult age. In terms of the canines, the replacement pattern is the same as that noted in juveniles and subadults of *Thrinaxodon*, in which the replacement canine erupts anteromedially to the functional canine (Abdala *et al.* 2013). This results in the remnant root of the previous canine being pushed anterolateral to the functional canine. Further evidence of the juvenility of SAM-PK-K11655 is the complexity of the cusps. In subadults and juveniles, the lower postcanines (particularly postcanines 5 – 8) tend to be multicusped, and have a lingual cingulum, whereas in adults, the postcanines have reverted back to the simpler tricuspid morphology (Abdala *et al.* 2013).

Specimen SAM-PK-K11655 also has interpterygoid vacuities (Fig. 15A and B). As previously stated, this morphology is considered a plesiomorphic condition in cynodonts (Hopson & Kitching 2001). However, it is also often used as an indicator of juvenility, as it is only present in juveniles or subadults of taxa such as *Thrinaxodon* (Estes 1961; Fourie 1974; Jasinoski *et al.* 2015), *Nanictosaurus* (van Heerden & Rubidge 1990), *Cynosaurus* (Van den Brandt & Abdala 2018) and *Lumkuia* (Hopson & Kitching 2001). As a result, this character trait could not be coded for in the phylogenetic analyses. Therefore, the presence of these vacuities in SAM-PK-K11655 in combination with the complex dental morphology and replacement teeth supports its status as a juvenile.

Taxonomic validity and phylogenetic position of *Cistecynodon parvus*

Since its discovery, *Cistecynodon* (BP/1/2520) has been referred to two different clades of therapsids, these being Therocephalia (Watson and Romer, 1956) and Cynodontia (Brink & Kitching, 1953; Lehman, 1961; Hopson & Kitching, 1972; Tatarinov, 1974; Battail 1991a; Abdala, 1995, 1996). Watson

and Romer (1956) referred *Cistecynodon* to the Bauriomorpha, but it lacks the suborbital vacuities of therocephalians, and the presence of multicusped postcanine teeth, a narrow supraoccipital, and the presence of a double occipital condyle are diagnostic of cynodonts. The updated phylogenies indicate that BP/1/2520 is best placed well within Cynodontia (Figs. 24 and 25).

Within Cynodontia, *Cistecynodon* has been referred to multiple taxa, from basal non-eucynodonts through to the more derived Probainognathia and Cynognathia (see Table 1). Lehman (1961) and Hopson and Kitching (1972) considered *Cistecynodon* as being a possible cynognathid. Hopson and Kitching (1972) synonymised *Cistecynodon* with *Cynognathus crateronotus*, concluding that it was a juvenile representative of the species. BP/1/2520 does possess some characters which would be consistent with this conclusion, including the presence of a jugal arch that is dorsoventrally deep (Fig. 5), the absence of internal carotid foramina on the ventral surface of the basisphenoid (Fig. 6B), a tricuspid dentition with a slightly recurved main cusp (Fig. 13D) and a prominent anteroventral dentary resulting in a distinct 'chin' (Fig. 5C) (Seeley 1895; Reichel *et al.* 2009). However, the phylogenetic analyses performed here do not support this hypothesis (Figs. 24 and 25). The absence of internal carotid foramina on the ventral surface of the basisphenoid is usually recovered as a synapomorphy shared with the Cynognathia (Hopson & Kitching 2001) and distinguishes BP/1/2520 from most other basal cynodonts in this analysis, with the exception of *Dvinia* and *Platycraniellus* (Gaetano *et al.* 2022). This implies a certain degree of convergent evolution of this character among early cynodonts. The dentition of BP/1/2520 appears similar to that of *Cynognathus*, with a prominent curved main cusp and one anterior and one posterior accessory cusp which are not as prominent as the main cusp (Fig. 13D). However, the surface of each tooth in BP/1/2520 is smooth, which differs from that of *Cynognathus* which has slight serrations on the canines, and along the main and accessory cusps of the postcanines (Seeley 1895). Additionally, BP/1/2520 is an adult or subadult specimen, which excludes it as a possible juvenile *Cynognathus* (contra Hopson & Kitching 1972). Similarly, *Cistecynodon* cannot be referred to Probainognathia because of the presence of a parietal foramen, a medially open secondary palate, and the fact that the secondary palate does not extend posteriorly

to the level of the orbit (Figs. 6 and 7). Additionally, the phylogenetic analyses updated from both Fonseca *et al.* (2024) and Pusch *et al.* (2024) support that it is not a probainognathian (Figs. 24 and 25).

Finally, Tatarinov (1974) placed *Cistecynodon* into the family Galesauridae in its own subfamily Cistecynodontinae. This subfamily would include *Cistecynodon* and *Sinognathus*. Tatarinov (1974) separates *Cistecynodon* from other galesaurids based on the short snout with the sharp expansion of the orbital and occipital regions from the posterior end of the snout and very prominent coronoid process of the dentary. However, Tatarinov (1974) also mentions that the presence of a notch on the occipital surface may suggest a closer relation of *Cistecynodon* to cynognathids, thus the placement of *Cistecynodon* into the 'Cistecynodontinae' subfamily was tentative. In the phylogenetic analysis modified from Fonseca *et al*. (2024), *Sinognathus* is recovered as a Cynognathia, not a Galesauridae. This is consistent with its usual placement in other cynodont phylogenies (Ruta *et al.* 2013; Abdala 2019), while *Cistecynodon* is placed more stemward as a basal Epicynodontia (Figs. 24 and 25). The clade Cistecynodontinae (sensu Tatarinov 1974) is thus not supported. However, *Cistecynodon* is indeed recovered as a basal epicynodont, like *Galesaurus*.

Brink and Kitching (1953) also suggested that *Cistecynodon* may represent its own new family of cynodont because of two features: the absence of palatine contribution to the secondary palate and absence of a parietal foramen. Here, the new CT data indicates that *Cistecynodon* does have both a palatine contribution to the secondary palate and a parietal foramen (Figs. 6 and 7), thus rendering Brink and Kitching's definition incorrect. The hereby proposed phylogenies modified from Pusch *et al*. (2024) and Fonseca *et al*. (2024) both consistently place BP/1/2520 as a basal non-eucynodont epicynodont (Figs. 24 and 25). This is consistent with Abdala (1995, 1996), who hypothesised *Cistecynodon* to be a non-eucynodont (neither cynognathian nor probainognathian).

Regardless of the slight differences in the placement of *Cistecynodon* in the cynodont phylogenetic trees (Figs. 24 and 25), BP/1/2520 displays a number of unique derived characters that sets it apart as

a separate and valid genus and species of cynodont. The inflated vestibule of the inner ear is unique to *Cistecynodon* among epicynodonts and within Cynodontia in general, with the cynognathian *Boreogomphodon* being one of the only other cynodonts known to display this type of morphology (Pusch *et al.* 2024). The maxillary canal is rather featureless compared to other basal cynodonts, which tend to be more branched (Pusch *et al.* 2024). *Cistecynodon* also lacks the superior labial, and internal nasal canals present in other cynodonts (Benoit *et al.* 2024a). The parietal foramen of *Cistecynodon* is small and pinched (Fig. 7), whereas in other basal cynodonts this foramen is relatively larger (i.e., *Galesaurus* (Pusch *et al.* 2019), *Thrinaxodon* (Fourie 1974), *Procynosuchus* (Kemp 1979) and *Platycraniellus* (Abdala 2007)). The ascending ramus of the jugal of *Cistecynodon* is oriented diagonally (Fig. 5) and, as a result, the orbits are facing upwards (the socket is more horizontal relative to the skull compared to other cynodonts (i.e. *Galesaurus* (Pusch *et al.* 2019) and *Thrinaxodon* (Fourie 1974; Hopson & Kitching 2001)). *Cistecynodon* also lacks carotid foramina, a synapomorphy of cynognathians (Hopson & Kitching 2001). The floccular fossa of BP/1/2520 is shallow which results in a floccular lobe that is neither well-defined nor prominent (Fig. 10) whereas among cynodonts the floccular lobe is always very prominent (Kielan-Jaworowska *et al.* 2004; Rodrigues *et al.* 2014; Benoit 2023; Pusch *et al.* 2024). Even in specimens in which the floccular lobes are comparatively short (i.e. *Nythosaurus*), the plane defined by the anterior semicircular canal is perforated by the lobe (Pusch *et al.* 2023), whereas this is not the case in *Cistecynodon* (Fig 10) or in *Boreogomphodon* (Pusch *et al*. 2024).

Additionally, among non-eucynodonts, *Cistecynodon* displays characters that are supposed to be synapomorphies of the Eucynodontia and contributes the unique mosaic of traits that diagnoses it, such as: the absence of the quadrate ramus of the pterygoid and a fused dentary symphysis (Hopson & Kitching 2001). As such it is safe to conclude that *Cistecynodon parvus* is a valid genus of non-eucynodont epicynodont.

Systematic Palaeontology

THERAPSIDA Broom, 1905

CYNODONTIA Owen, 1861

EPICYNODONTIA Hopson and Kitching, 2001

CISTECYNODON PARVUS Brink & Kitching 1953

Emended diagnosis for *Cistecynodon parvus*

Small to medium-sized basal cynodont (epicynodont) with the following autapomorphies: absence of carotid foramina in the basisphenoid; reduced and pinched parietal foramen; short, broad snout relative to the skull length; dorsal oriented orbits; inflated vestibule of the inner ear. Dental formula is I4/i3, C1/c1, PC6/pc7. Combines the following plesiomorphic features: secondary palate open in the midline; palatine contribution to the secondary palate; postcanines that are mostly tricuspid; with the following derived (eucynodont) features: absence of the quadrate ramus of the pterygoid; fused dentary symphysis; double jaw articulation (quadrate-articular and quadrate-surangular).

Adaptations to fossoriality in *Cistecynodon*

Modern fossorial vertebrates display a combination of derived traits to assist with their subterranean lifestyles. These can include different degrees of reduction in orbit size (e.g., Quilliam 1966a, 1966b; Nevo 1999; Francescoli 2000; Borghi *et al.* 2002), a well-developed sense of smell (Burda *et al.* 1990; Francescoli 2000) and fusion (or tight sutural contact) of the cranial bones such the parietals with the surrounding cranial bones (Strong *et al.* 2021). The underground environment also has a reduced ability for medium and high frequency sound propagation; therefore, many fossorial animals have evolved a sensitivity to low-frequency sounds, particularly seismic waves (e.g., Fleischer 1978; Heth *et al.* 1986; Burda *et al.* 1990; Nevo 1999; Begall *et al.* 2007).

CT scanning has enabled the reconstruction of the inner ear and trigeminal canal of *Cistecynodon*. This data shows the unique morphology of the presence of an inflated vestibule of the inner ear of *Cistecynodon* (Fig. 11), which is indicative of enhanced low-frequency hearing capability (Benoit et al 2024). This type of morphology is commonly encountered in modern fossorial squamates (Palci *et al.* 2016; Benoit *et al.* 2022b). An inflated vestibule is interpreted as an adaptation for low frequency hearing (Laaß 2014), as it increases the distance between the proximal region of the basilar membrane and the stapedial footplate (Meng & Wyss 1995; Fox & Meng 1997). As a result, low frequencies are then only perceived at the distal region of the basilar membrane. *Cistecynodon* shares the trait of an inflated inner ear vestibule with other interpreted fossorial fossil taxa such as *Kawingasaurus fossilis* (Laaß 2014) and with inferred fossorial taxa like *Boreogomphodon* (Pusch *et al.* 2024). *Boreogomphodon* has been found around many burrows and has postcrania which is adapted for burrowing (Liu *et al.* 2017).

Further assessment of the fossorial capability can be made by assessing the morphology of the footplate of the stapes (Laaß, 2014), but the stapes of BP/1/2520 is not preserved. Based on the fenestra vestibuli, (Benoit *et al.* 2024a) inferred that BP/1/2520 would have had a stapedial footplate with a surface area of roughly 30 mm^2. The size of the footplate relative to the skull length suggests that the stapedial footplate of BP/1/2520 was as large as that of *Kawingasaurus*, an inferred obligate burrowing dicynodont (Benoit *et al.* 2024a). Moreover, another indication of fossoriality is the morphology of the paraflocculus. As mentioned, the floccular fossa of BP/1/2520 is shallow and not well defined. This suggests a poor gaze stabilization in BP/1/2520 and is consistent with the relatively reduced semicircular canals and indistinct ampullae of the inner ear seen in the specimen (Benoit *et al.* 2024).

Additionally, the cranial morphology of *Cistecynodon* indicates some adaptation for burrowing, as the parietals are fused along the midline, most of the bones of the occipital region of the skull are fused or have very tight suture between the bones, and the prootic and opisthotic are fused (Figs. 7A and

9). Fusion of the prootic and opisthotic may be an adaptation for strengthening the chamber that houses the inner ear, for protection of this element during burrowing. However, there is no reduction in the orbit size of *Cistecynodon* (Fig. 5), which is suggested as possible adaptation for underground living based on extant animals (e.g., Quilliam 1966a, 1966b; Burda *et al.* 1990; Nevo 1999; Francescoli 2000; Borghi *et al.* 2002).

Overall, *Cistecynodon* displays a number of features which are suggestive of a fossorial lifestyle, which is especially relevant as it is often believed to have been a key behavioural adaptation to account for how cynodonts survived repeated mass extinction events through the Mesozoic (Damiani *et al.* 2003; Fernandez *et al.* 2013).

Taxonomic identification and phylogeny of SAM-PK-PK11655

Both phylogenetic analyses of SAM-PK-K11655 support that it is a non-eucynodont epicynodont, like *Cistecynodon* (Figs. 24 and 25). This is consistent with its palatal morphology. In the analysis modified from Pusch *et al.* (2024), SAM-PK-K11655 is on its own branch, but in the one modified from Fonseca *et al.* (2024), it forms a clade with *Cistecynodon* (Fig. 25). The characters that support this clade are the secondary palate, which is open along the midline (Fig. 15), a pterygoparoccipital foramen in which the squamosal contributes to the enclosure of the foramen (Fig. 15A and B), and the upper tooth series directed lateral to the subtemporal fossa. The morphology of the secondary palate is a well-known and crucial phylogenetic character within Cynodontia, thus making it a valid and heavily weighted character within cynodont phylogeny. However, given the juvenile status of SAM-PK-K11655, it is not possible to determine whether the secondary palate would close in adulthood, as the secondary palate is open in epicynodonts but closes with ontogenetic growth (Estes 1961). The squamosal contribution to the enclosure of the pterygoparoccipital foramen is coded for 20 out of the 24 cynodont specimens included in the analysis from Fonseca *et al*. (2024) and is strongly supported as a trait present in epicynodonts and cynognathians. The final trait, the axis of the posterior tooth row is

coded for every taxon in the phylogeny, although this feature may be subject to distortion during taphonomical processes. Therefore, especially in taxa where there is only the holotype specimen as a representative of the taxon, this can be a misleading character and should be considered with caution. The possibility that BP/1/2520 and SAMP-PK-K11655 form a clade may thus be seriously considered and discussed.

Since SAM-PK-K11655 is most likely a juvenile, this leaves open the possibility that it is a juvenile *Cistecynodon*. However, it is unlikely that SAM-PK-K11655 would be a juvenile of *Cistecynodon* due to the presence of carotid foramina in SAM-PK-K11655 (Fig. 15) whereas they are absent in BP/1/2520 (Fig. 6); the presence of the quadrate ramus of the pterygoid in SAM-PK-K11655 (Fig. 15) whereas they are absent in BP/1/2520 (Fig. 6); the absence of a lateral crest on the dentary of SAM-PK-K11655 (Fig. 20) where BP/1/2520 has a salient lateral crest (Fig. 12). Additionally, SAM-PK-K11655 possesses none of the autapomorphies listed above in the emended diagnosis for *Cistecynodon*. Therefore, it can be safely concluded that SAM-PK-K11655 should not be assigned to *Cistecynodon* despite them forming a clade in one of the two phylogenetic analyses proposed here.

SAM-PK-K11655 can also be excluded from other sectorial-toothed cynodonts from the Burgersdorp Formation. The specimen was referred to *Lumkuia* but differs in that the secondary palate is shorter (Fig. 15; Hopson & Kitching 2001), a parietal foramen is present and the postcanines are not hooked (strongly recurved) unlike in *Lumkuia* (Hopson & Kitching 2001; Benoit *et al.* 2022a). Based on these features and the phylogenetic analyses, SAM-PK-K11655 is therefore excluded from the Probainognathia, including *Lumkuia*. It is distinguished from *Bolotridon* by a shorter secondary palate, the absence of hooked cusps on the postcanines, the absence of lingual cingula on the lower postcanines and the fewer number of postcanines (eleven in *Bolotridon* compared to seven to eight postcanines in SAM-PK-K11655) (Fig. 21; Pusch *et al.* 2021; Wolvaardt *et al.* 2023). SAM-PK-K11655 is excluded from Cynognathia based on the presence of carotid foramina in the parabasisphenoid (Hopson & Kitching 2001). Therefore, it cannot be considered as a juvenile *Cynognathus* or

Diademodon (the last of which only has sectorial teeth as a juvenile (Hopson 2005)). Further features distinguishing SAM-PK-K11655 from *Cynognathus* and *Diademodon* are the difference in secondary palate length (shorter in SAM-PK-K11655 than in the latter genera) and cranial length of SAM-PK-K11655, which is much smaller than in recorded juveniles of *Cynognathus* and *Diademodon* (Seeley 1895; Grine 1978). Finally, and although this bone is imperfectly preserved, there is no indication that the posterolateral corner of the squamosal formed a prominent flange like see in the cynognathians (Seeley 1985).

Specimen SAM-PK-K11655 shares many characters that are generalised among early epicynodonts, such as the presence of internal carotid foramina in the basisphenoid, the presence of interpterygoid vacuities as well as the presence of an ectopterygoid, and the upper postcanines have no more than three cusps (Abdala *et al.* 2013; Pusch *et al.* 2019, 2023). For these reasons, it may match *Nythosaurus*, which was recently re-assigned to the *Cynognathus* Assemblage Zone (Benoit *et al.* 2024b). SAM-PK-K11655 is distinguished from *Nythosaurus*, however, by its tricuspid right upper PC5, whereas PC5 in *Nythosaurus* has 5 cusps and a distinct cingulum (Pusch *et al.* 2023). SAM-PK-K11655 and *Nythosaurus* also do not form a clade in either of the phylogenetic analyses (Figs. 24 and 25).

To conclude, SAM-PK-K11655 cannot be safely referred to any of the sectorial toothed taxa from the Burgersdorp Formation. It is probably the juvenile of a new genus and species (as supported by the phylogenetic analysis from Fonseca *et al.* (2024)). However, naming a new taxon based on juvenile material is not scientifically sound. Therefore, until a more mature specimen of this taxon is found it should be referred to as Cynodontia nov. sp.

Conclusion

Cynodonts are an important clade of non-mammaliaform therapsid that ultimately gave rise to modern mammals. Thus, the systematics of this clade is a focal point for researchers. Over the past century *Cistecynodon* has been variously referred to different clades of non-mammalian cynodont without any emerging consensus. The data from this research firmly supports that *Cistecynodon parvus* is a valid taxon of basal non-eucynodont Cynodontia. Its position is supported by the secondary palate, which is open along the midline, despite it being a sub-adult to adult age specimen. Lastly, its unique inner ear anatomy and fused cranial bones supports the hypothesis that *Cistecynodon* was a fossorial animal. The new specimen from Lemoenfontein, SAM-PK-K11655, is found to be closely related, but clearly distinct from *Cistecynodon*, and thus likely represents a new genus and species. Both taxa are reconstructed as basal lineages of cynodonts surviving past the Permian-Triassic boundary into the *Cynognathus* AZ, thus supporting the persistence of a relict fauna of cynodonts in Southern Africa during the Early and early Middle Triassic (Benoit *et al.*, 2024b).

Acknowledgements

I would like to thank my supervisors, Prof. Julien Benoit, Prof. Roger Smith and Dr. Frederik Wolvaardt for their expertise, patience, and incredible guidance over the course of my dissertation. This dissertation would also not have been possible without the generous support from GENUS-DSI-NRF Centre of Excellence and PAST who funded my studies. I would like to thank the Evolutionary Studies Institute at the University of the Witwatersrand for providing access to specimen BP/1/2520 and for the use of their CT scanning and computer facilities to conduct my research; NECSA for CT scanning specimen SAM-PK-K11655; Iziko South African Museum for access to specimen SAM-PK-K11655 and Dr. Wolvaardt for the palaeontological work he conducts on Lemoenfontein, without whom SAM-PK-K11655 would not have been discovered. I extend my grateful thanks to Morgan Hopf for the beautiful palaeontological reconstruction of *Cistecynodon parvus*, Atashni Moopen for assistance with photographing my specimens, and to my colleagues and friends at the ESI for their continuous support (in particular to Andrew Bolton for insisting that I take lunch breaks and remain sociable at the ESI). Lastly, I would like to thank my partner, Damian Dowie for his endless support, care, and encouragement throughout the course of my dissertation.

References

ABDALA, F. 1995. The family Chiniquodontidae and its relationships among eucynodonts. *Journal of Vertebrate Palaeontology* **Abstracts of papers, Fifty-fifth Annual Meeting, Society of Vertebrate Paleontology**, 16a.

ABDALA, F. 1996. Redescripción del cráneo y reconsideración de la validez de *Cynognathus minor* (Eucynodontia - Cynognathidae) del Triásico Inferior de Mendoza. *Ameghiniana* **33**, 115–126.

ABDALA, F. 2007. Redescription of *Platycraniellus elegans* (Therapsida, Cynodontia) from the Lower Triassic of South Africa, and the cladistic relationships of eutheriodonts. *Palaeontology* **50**, 591–618.

ABDALA, F. 2019. Permo-Jurassic cynodonts: the early road to mammalness. **In**: Alderton, D. & Elias, S.A. (eds), *Encyclopedia of Geology*, 206–226 (Second Edition). United Kingdom, Academic Press. Online at: https://doi.org/10.1016/B978-0-12-409548-9.12020-2 (accessed 2019)

ABDALA, F., GAETANO, L.C., SMITH, R.M.H. & RUBIDGE, B.S. 2019. A new large cynodont from the Late Permian (Lopingian) of the South African Karoo Basin and its phylogenetic significance. *Zoological Journal of the Linnean Society* **186**, 983–1005.

ABDALA, F., JASINOSKI, S.C. & FERNANDEZ, V. 2013. Ontogeny of the Early Triassic cynodont *Thrinaxodon liorhinus* (Therapsida): dental morphology and replacement. *Journal of Vertebrate Paleontology* **33**, 1408–1431.

ABDALA, F. & RIBEIRO, A.M. 2010. Distribution and diversity patterns of Triassic cynodonts (Therapsida, Cynodontia) in Gondwana. *Palaeogeography, Palaeoclimatology, Palaeoecology* **286**, 202–217.

BATTAIL, B. 1991a. Les cynodontes (Reptilia, Therapsida): une phylogénie. *Bulletin du Muséum national d'histoire naturelle, Section C: Sciences de la terre, paléontologie, géologie, minéralogie* **13**, 17–105.

BATTAIL, B. 1991b. A reassessment on the biogeography of the Triassic. 5-6. *Fifth Symposium on the Mesozoic Terrestrial Ecosystems and Biota, Extended Abstracts. Kielan-Jaworowksa, Z., Heintz, H. and Narken, H.A. (Eds).*, 1–72. University of Oslo.

BATTAIL, B. 2001. A short review of studies on cynodonts. *Publicación Electrónica de la Asociación Paleontológica Argentina* **7**, 29–38.

BEGALL, S., LANGE, S., SCHLEICH, C.E. & BURDA, H. 2007. 2007. Acoustics, Audition and Auditory System. *Subterranean Rodents: News from Underground*, 97–111 (Begall, S., Burda, H., Schleich, C.E., Eds.). New York: Springer.

BENOIT, J. 2023. Synchrotron scanning reveals the deep evolutionary root of the mammalian brain: the surprisingly advanced endocast morphology of *Lumkuia fuzzi* (Cynodontia: Probainognathia). *Palaeontologia africana* **56**, 103–110.

BENOIT, J., ARAUJO, R., LUND, E.S., BOLTON, A., LAFFERTY, T., MACUNGO, Z. & FERNANDEZ, V. 2024a. Early synapsids neurosensory diversity revealed by CT and synchrotron scanning. *The Anatomical Record*, 1–18.

BENOIT, J., DOLLMAN, K.N., SMITH, R.M.H. & MANGER, P.R. 2022b. At the root of the mammalian mind: The sensory organs, brain, and behaviour of pre-mammalian synapsids. *Progress in Brain Research* **275**, 25–72.

BENOIT, J., JASINOSKI, S.C., FERNANDEZ, V. & ABDALA, F. 2017a. The mystery of a missing bone: revealing the orbitosphenoid in basal Epicynodontia (Cynodontia, Therapsida) through computed tomography. *The Science of Nature* **104**, 7–8.

BENOIT, J., JIRAH, S., LUND, E.S., LAFFERTY, T., BUFFA, V. & NORTON, L.A. 2024b. Re-assessing the age of the type locality of *Nythosaurus larvatus* (Therapsida, Cynodontia) and implications on the

evolutionary dynamics of cynodonts. *Proceedings of the Geologists' Association.* Online at: https://doi.org/10.1016/j.pgeola.2024.08.007 (accessed 2024)

BENOIT, J., MANGER, P.R., FERNANDEZ, V. & RUBIDGE, B.S. 2017b. The bony labyrinth of late Permian Biarmosuchia: palaeobiology and diversity in non-mammalian Therapsida. *Palaeontologia africana* **52**, 58–77.

BENOIT, J., MANGER, P.R. & RUBIDGE, B.S. 2016. Palaeoneurological clues to the evolution of defining mammalian soft tissue traits. *Scientific Reports* **6.**

BENOIT, J., NXUMALO, M., NORTON, L.A., FERNANDEZ, V., GAETANO, L.C., RUBIDGE, B. & ABDALA, F. 2022a. Synchrotron scanning sheds new light on *Lumkuia fuzzi* (Therapsida, Cynodontia) from the Middle Triassic of South Africa and its phylogenetic placement. *Journal of African Earth Sciences* **196**, 104689.

BENOIT, J., RUF, I., MIYAMAE, J.A., FERNANDEZ, V. & RUBIDGE, B.S. 2019. The Evolution of the Maxillary Canal in Probainognathia (Cynodontia, Synapsida): Reassessment of the Homology of the Infraorbital Foramen in Mammalian Ancestors. *Journal of Mammalian Evolution* **27**, 329–348.

BONAPARTE, J.F. & BARBERENA, M.C. 2001. On two advanced carnivorous cynodonts from the Late Triassic of southern Brazil. *Bulletin of the Museum of Comparative Zoology* **156**, 59–80.

BORGHI, C.E., GIANNONI, S.M. & ROIG, V.G. 2002. Eye reduction in subterranean mammals and eye protective behaviour in *Ctenomys*. *Mastozoologia Neotropical* **9**, 123–134.

BOTHA, J., ABDALA, F. & SMITH, R. 2007. The oldest cynodont: new clues on the origin and early diversification of the Cynodontia. *Zoological Journal of the Linnean Society* **149**, 477–492.

BRACK, P., RIEBER, H., NICORA, A. & MUNDIL, R. 2005. The Global Boundary Stratotype Section and Point (GSSP) of the Ladinian Stage (Middle Triassic) at Bagolino (Southern Alps, Northern Italy) and its implications for the Triassic time scale. *Episodes* **28**, 233–244.

BRINK, A.S. 1954. *Thrinaxodon* and some other *Lystrosaurus* Zone cynodonts in the collection of the National Museum, Bloemfontein. *Navorsinge van die Nasionale Museum Bloemfontein* **1**, 115–125.

BRINK, A.S. & KITCHING, J.W. 1953. On some new *Cynognathus* Zone specimens. *Palaeontologia africana* **01**, 29–48.

BURDA, H., BRUNS, V. & MÜLLER, M. 1990. Sensory adaptations in subterranean mammals. *Evolution of Subterranean Mammals at the Organismal and Molecular Levels*, 269–293 (Nevo, E., Reig, O.A., Eds.). New York: Wiley-Liss.

BUTLER, E., ABDALA, F. & BOTHA-BRINK, J. 2019. Postcranial morphology of the Early Triassic epicynodont *Galesaurus planiceps* (Owen) from the Karoo Basin, South Africa. *Papers in Palaeontology* **5**, 1–32.

CROMPTON, A.W., MUSINSKY, C. & OWERKOWICZ, T. 2015. Evolution of the mammalian nose. **In**: Dial, K.P., Shubin, N. & Brainerd, E.L. (eds), *Great Transformations in Vertebrate Evolution*, 189–203. Chicago, University of Chicago Press. Online at: https://doi.org/10.7208/9780226268392-012 (accessed 2024).

CROMPTON, A.W., OWERKOWICZ, T., BHULLAR, B.-A.S. & MUSINSKY, C. 2017. Structure of the nasal region of non-mammalian cynodonts and mammaliaforms: speculations on the evolution of mammalian endothermy. *Journal of Vertebrate Paleontology* **37**, e1269116.

DAMIANI, R., MODESTO, S., YATES, A. & NEVELING, J. 2003. Earliest evidence of cynodont burrowing. *Proceedings of the Royal Society of London B* **270**, 1747–1751.

ESTES, R. 1961. Cranial anatomy of the cynodont reptile *Thrinaxodon liorhinus*. *Bulletin of the Museum of Comparative Zoology* **125**, 165–180.

FERNANDEZ, V., ABDALA, F., CARLSON, K.J., COOK, D.C., RUBIDGE, B.S., YATES, A. & TAFFOREAU, P. 2013. Synchrotron reveals Early Triassic odd couple: injured amphibian and aestivating therapsid share burrow. *PLOS ONE* **8**, e64978.

FLEISCHER, G. 1978. Evolutionary principles of the mammalian middle ear. *Advances in Anatomy, Embryology and Cell Biology* **55**, 1–70.

FONSECA, P.H.M., MARTINELLI, A.G., GILL, P.G., RAYFIELD, E.J., SCHULTZ, C.L., KERBER, L., RIBEIRO, A.M. & SOARES, M.B. 2024. Anatomy of the maxillary canal of *Riograndia guaibensis* (Cynodontia, Probainognathia) - A prozostrodont from the Late Triassic of southern Brazil. *The Anatomical Record*, 1–17.

FOURIE, S. 1974. The cranial morphology of *Thrinaxodon liorhinus* Seeley. *Annals of the South African Museum* **65**, 337–400.

FOX, R.C. & MENG, J. 1997. An X-radiographic and SEM study of the osseous inner ear of multituberculates and monotremes (Mammalia): Implications for mammalian phylogeny and evolution of hearing. *Zoological Journal of the Linnean Society* **121**.

FRANCESCOLI, G. 2000. Sensory capabilities and communication in subterranean rodents. *Life Underground: The Biology of Subterranean Rodents.*, 111–144 (Lacey, E.A., Patton, J.L., Cameron, G.N., eds.). Chicago: The University of Chicago Press.

FRÖBISCH, J. 2007. The cranial anatomy of *Kombuisia frerensis* Hotton (Synapsida, Dicynodontia) and a new phylogeny of anomodont therapsids. *Zoological Journal of the Linnean Society* **150**, 117–144.

GAETANO, L.C., ABDALA, F., SEOANE, F.D., TARTAGLIONE, A., SCHULZ, M., OTERO, A., LEARDI, J.M., APALDETTI, C., KRAPOVICKAS, V. & STEINBACH, E. 2022. A new cynodont from the Upper Triassic Los Colorados Formation (Argentina, South America) reveals a novel paleobiogeographic context for mammalian ancestors. *Scientific Reports* **12**, 6451.

GRADSTEIN, F.M., OGG, J.G., SMITH, A.G., BLEEKER, W. & LOURENS, L.J. 2004. A new Geologic Time Scale, with special reference to Precambrian and Neogene. *Episodes* **27**, 83–100.

GRINE, F.E. 1978. Notes on a specimen of *Diademodon* previously referred to *Cyclogomphodon*. *Palaeontologia africana* **21**, 167–174.

HANCOX, P.J. 1998. Stratigraphic, sedimentological and palaeoenvironmental synthesis of the Beaufort-Molteno contact in the Karoo Basin. Doctoral dissertation, University of the Witwatersrand, Department of Geology/Palaeontology.

HANCOX, P.J., NEVELING, J. & RUBIDGE, B.S. 2020. Biostratigraphy of the *Cynognathus* Assemblage Zone (Beaufort Group, Karoo Supergroup), South Africa. *South African Journal of Geology* **123**, 217–238.

VAN HEERDEN, J. & RUBIDGE, B.S. 1990. The affinities of the early cynodont reptile, *Nanictosaurus*. *Palaeontologia africana* **27**, 41–44.

HETH, G., FRANKENBURG, E. & NEVO, E. 1986. Adaptive optimal sound for vocal communication in tunnels of a subterranean mammal (*Spalax ehrenbergi*). *Experientia* **42**, 1287–1289.

HILLENIUS, W.J. 1994. Turbinates in therapsids: evidence for Late Permian origins of mammalian endothermy. *Evolution* **48**, 207–229.

HILLENIUS, W.J. 2000. Septomaxilla of nonmammalian synapsids: soft tissue correlates and a new functional interpretation. *Journal of Morphology* **245**, 29–50.

HOFFMAN, J.W. & DE BEER, F.C. 2012, April 16. Characteristics of the Micro-Focus X-ray Tomography Facility (MIXRAD) at Necsa in South Africa. Hoffman, J.W., & De Beer, F.C., 2012. 18th World Conference on Nondestructive Testing.

HOPSON, J.A. 1991. Systematics of nonmammalian Synapsida and implications for patterns of evolution in Synapsida. **In**: Schulze, H.-P. & Trueb, L. (eds), *Origins of the Higher Groups of Tetrapods: Controversy and Consensus*, 635–693. Ithaca, NY, Cornell University Press.

HOPSON, J.A. 2005. A juvenile gomphodont cynodont specimen from the *Cynognathus* Assemblage Zone of South Africa: implications for the origin of gomphodont postcanine morphology. *Palaeontologia africana* **41**, 53–66.

HOPSON, J.A. & KITCHING, J.W. 1972. A revised classification of the cynodonts (Reptilia, Therapsida). *Palaeontologia africana* **14**, 71–85.

HOPSON, J.A. & KITCHING, J.W. 2001. A probainognathian cynodont from South Africa and the phylogeny of nonmammalian cynodonts. *Bulletin of the Museum of Comparative Zoology* **156**, 5–35.

HUTTENLOCKER, A.K. & SIDOR, C.A. 2020. A basal non-mammaliaform cynodont from the Permian of Zambia and the origins of mammalian endocranial and postcranial anatomy. *Journal of Vertebrate Palaeontology* **40**, e1827413.

IVAKHNENKO, M.F. 2013. Cranial morphology of *Dvinia prima* Amalitzky (Cynodontia, Thermomorpha). *Journal of Paleontology* **47**, 210–222.

JASINOSKI, S.C. & ABDALA, F. 2017. Cranial ontogeny of the Early Triassic basal cynodont *Galesaurus planiceps*. *The Anatomical Record* **300**, 353–381.

JASINOSKI, S.C., ABDALA, F. & FERNANDEZ, V. 2015. Ontogeny of the Early Triassic cynodont *Thrinaxodon liorhinus* (Therapsida): cranial morphology. *The Anatomical Record* **298**, 1440–1464.

JENKINS, F.A. 1971. The postcranial skeleton of African cynodonts: problems in the early evolution of the mammalian postcranial skeleton. *Bulletin of the Peabody Museum of Natural History, Yale University* **36**, 1–216.

JOHNSON, M.R., VAN VUUREN, C.J., VISSER, J.N.J., COLE, D.I., WICKENS, H. DE V., CHRISTIE, A.D.M., ROBERTS, D.L. & BRANDL, G. 2006. Sedimentary rocks of the Karoo Supergroup. *The Geology of South Africa*, 461–499 (Johnson, M.R., Anhaeusser, C.R., Thomas, R.J. (Eds.)). Geological Society of South Africa and Council for Geoscience.

KAMMERER, C.F. 2016. A new taxon of cynodont from the *Tropidostoma* Assemblage Zone (Upper Permian) of South Africa, and the early evolution of Cynodontia. *Papers in Palaeontology* **2**, 387–397.

KEMP, T.S. 1979. The primitive cynodont *Procynosuchus*: functional anatomy of the skull and relationships. *Philosophical Transactions of the Royal Society of London. B* **285**, 73–122.

KEMP, T.S. 1982. *Mammal-like Reptiles and the Origin of Mammals*. London, Academic Press Inc.

KIELAN-JAWOROWSKA, Z., CIFELLI, R.L. & LUO, Z.-X. 2004. *Mammals from the Age of Dinosaurs: Origins, Evolution, and Structure*. New York, Columbia University Press. Online at: https://doi.org/10.7312/kiel11918 (accessed 2024).

KITCHING, J.W. 1977. *The Distribution of the Karoo Vertebrate Fauna*. University of the Witwatersrand, Bernard Price Institute for Palaeontological Research.

LAAß, M. 2014. Bone-conduction hearing and seismic sensitivity of the late Permian anomodont *Kawingasaurus fossilis*. *Journal of Morphology* **276**, 121–143.

LEHMAN, J. 1961. Cynodontia. *En: J. Piveteau (Ed.). Traité de Paléontologie* **6**, 1–131.

LIU, J., SCHNEIDER, V.P. & OLSEN, P. 2017. The postcranial skeleton of *Boreogomphodon* (Cynodontia: Traversodontidae) from the Upper Triassic of North Carolina, USA, and the comparison with other traversodontids. *PeerJ* **5**, e3521.

LUKIC-WALTHER, M., BROCKELHURST, N., KAMMERER, C.F. & FRÖBISCH, J. 2019. Diversity patterns of nonmammalian cynodonts (Synapsida, Therapsida) and the impact of. *Palaeobiology* **45**, 56–69.

LUO, Z. 1994. Sister-group relationships of mammals and transformations of diagnostic mammalian characters. **In**: Fraser, N.C. & Sues, H.-D. (eds), *In the Shadow of the Dinosaurs: Early Mesozoic Tetrapods*, 98–128. Cambridge, Cambridge University Press.

LUO, Z.-X., RUF, I., SCHULTZ, J.A. & MARTINELLI, T. 2011. Fossil evidence on evolution of inner ear cochlea in Jurassic mammals. *Proceedings of the Royal Society of London B*, 28–34.

MARTINELLI, A. & SOARES, M. 2016. Evolution of South American cynodonts. *Contribuciones del Museo Argentino de Ciencias Naturales "Bernardino Rivadavia"* **6**, 183–197.

MENG, J. & WYSS, A.R. 1995. Monotreme affinities and low frequency hearing suggested by multituberculate ear. *Nature* **377**, 141–144.

MILLER, C.S. & BARANYI, V. 2021. Triassic Climates. *Encyclopedia of Geology*, 514–523 (2nd edition). Elsevier. Online at: https://doi.org/10.1016/B978-0-12-409548-9.12070-6 (accessed 2024).

NEVELING, J. 2004. Stratigraphic and sedimentological investigation of the contact between the *Lystrosaurus* and the *Cynognathus* Assemblage Zones (Beaufort Group: Karoo Supergroup). *Council for Geoscience Bulletin* **137**, 1–164.

NEVO, E. 1999. *Mosaic Evolution of Subterranean Mammals: Regression, Progression and Global Convergence.* New York: Oxford University Press.

NORTON, L.A., ABDALA, F., RUBIDGE, B.S. & BOTHA, J. 2020. Tooth replacement patterns in the Early Triassic epicynodont *Galesaurus planiceps* (Therapsida, Cynodontia). *PLoS ONE* **15**, e0243985.

NORTON, L.A., ABDALA, F., RUBIDGE, B.S. & BOTHA, J. 2021. Tooth replacement in the non-mammalian cynodont *Cynosaurus suppostus* (Therapsida) from the late Permian of South Africa. *Journal of Vertebrate Palaeontology* **41**, e2001650.

PALCI, A., LEE, M.S.Y. & HUTCHINSON, M.N. 2016. Patterns of postnatal ontogeny of the skull and lower jaw of snakes as revealed by micro- CT scan data and three-dimensional geometric morphometrics. *Journal of Anatomy* **229**, 723–754.

PARRINGTON, F.R. 1934. On the cynodont genus *Galesaurus*, with a note on the functional significance of the changes in the evolution of the Theriodont skull. *Annals and Magazine of Natural History* **13**, 38–67.

PUSCH, L., KAMMERER, C.F. & FERNANDEZ, V. 2023. Cranial anatomy of Nythosaurus larvatus Owen, 1876, an Early Triassic cynodont preserving a natural endocast. *Journal of Vertebrate Palaeontology*

PUSCH, L., KAMMERER, C.F. & FRÖBISCH, J. 2019. Cranial anatomy of the early cynodont *Galesaurus planiceps* and the origin of mammalian endocranial characters. *Journal of Anatomy* **234**, 592–621.

PUSCH, L., KAMMERER, C.F. & FRÖBISCH, J. 2021. Cranial anatomy of *Bolotridon frerensis*, an enigmatic cynodont from the Middle Triassic of South Africa, and its phylogenetic significance. *PeerJ* **9** Online at: e11542. https://doi.org/10.7717/peerj.11542 (accessed 2024).

PUSCH, L., KAMMERER, C.F. & FRÖBISCH, J. 2024. The origin and evolution of Cynodontia (Synapsida, Therapsida): Reassessment of the phylogeny and systematics of the earliest members of this clade using 3D-imaging technologies. *The Anatomical Record*, 1–97.

QUILLIAM, T.A. 1966a. The mole's sensory apparatus. *Journal of Zoology* **149**.

QUILLIAM, T.A. 1966b. The problem of vision in the ecology of *Talpa* europaea. *Experimental Eye Research* **5**, 63–78.

REICHEL, M., SCHULTZ, C.L. & SOARES, M.B. 2009. A new traversodontid cynodont (Therapsida, Eucynodontia) from the Middle Triassic Santa Maria Formation of Rio Grande do Sul, Brazil. *Palaeontology* **52**, 229–250.

RODRIGUES, P.G., RUF, I. & SCHULTZ, C.L. 2014. Study of a digital cranial endocast of the non-mammaliaform cynodont *Brasilitherium riograndensis* (Late Triassic, Brazil) and its relevance to the evolution of the mammalian brain. *Paläontologische Zeitschrift* **88**, 329–352.

RUBIDGE, B.S. & SIDOR, C.A. 2001. Evolutionary patterns among Permo-Triassic therapsids. *Annual Review of Ecology and Systematics* **32**, 449–480.

RUTA, M., BOTHA-BRINK, J., MITCHELL, S.A. & BENTON, M.J. 2013. The radiation of cynodonts and the ground plan of mammalian diversity. *Proceedings of the Royal Society of London B* **280**, 20131865.

SEELEY, H.G. 1895. Researches on the structure, organisation, and classification of the fossil Reptilia. Part IX., Section 5. On the Skeleton in New Cynodontia from the Karoo Rocks. *Philosophical Transactions of the Royal Society of London. B* **185**, 59–148.

SIDOR, C.A. & SMITH, R.M.H. 2004. A new galesaurid (Therapsida: Cynodontia) from the Lower Triassic of South Africa. Palaeontology 47, 535–556. *Palaeontology* **47**, 535–556.

SMITH, R.M.H., RUBIDGE, B.S., DAY, M.O. & BOTHA, J. 2020. Introduction to the tetrapod biozonation of the Karoo Supergroup. *South African Journal of Geology* **123**, 131–140.

STRONG, M., PALCI, A. & CALDWELL, M.W. 2021. Insights into skull evolution in fossorial snakes, as revealed by the cranial morphology of *Atractaspis irregularis* (Serpentes: Colubroidea). *Journal of Anatomy* **238**, 146–172.

TATARINOV, L.P. 1974. Theriodont of the USSR. *Trudy Paleontology Institute* **143**, 5–250.

VAN DEN BRANDT, M.J. & ABDALA, F. 2018. Cranial morphology and phylogenetic analysis of *Cynosaurus suppostus* (Therapsida, Cynodontia) from the upper Permian of the Karoo Basin, South Africa. *Palaeontologia africana* **52**, 201–221.

WATSON, D.M.S. & ROMER, A.S. 1956. A classification of therapsid reptiles. *Bulletin of the Museum of Comparative Zoology* **114**, 37–89.

WOLVAARDT, F.P., HANCOX, P.J., BROWNING, C. & STRONG, M. 2023. Biostratigraphic and palaeoenvironmental significance of a rich tetrapod fossil accumulation in the Lower to Middle Burgersdorp Formation of the Karoo Basin. *Journal of African Earth Sciences* **198**.